Nd:YAG laser in urogenital surgery of the dog and cat

Bas van Nimwegen

Nd:YAG laser in urogenital surgery of the dog and cat

Nd:YAG laser in de urogenitale chirurgie van de hond en kat

(met een samenvatting in het Nederlands)

Proefschrift

ter verkrijging van de graad van doctor aan de Universiteit Utrecht
op gezag van de rector magnificus, prof.dr. J.C. Stoof,
ingevolge het besluit van het college voor promoties in het openbaar
te verdedigen op donderdag 17 april 2008, des middags te 12.45 uur

door

Sebastiaan Alexander van Nimwegen

geboren op 18 augustus 1977 te Eindhoven

Promotoren: Prof.dr. F.J. Van Sluijs

Prof.dr. J. Kirpensteijn

Co-promotor: Dr.ir. A.I. Rem

Contents

Aims of the thesis

The Nd:YAG laser has generally been used for incisional surgery, simultaneously conducting hemostasis. Furthermore, it is also known for its ability to induce relatively deep tissue coagulation. The use of a thin flexible optical fiber makes the application of laser energy an attractive option in minimally invasive surgery.

It was hypothesized that the Nd:YAG laser with its incisional and hemostatic action, could be useful for meticulous tissue dissection in a subcapsular partial prostatectomy in dogs (*Chapter 4*), and in laparoscopic surgery (*Chapters 5, 6 and 7*). In order to gain knowledge of Nd:YAG laser-induced changes in prostate tissue prior to clinical use, its action was investigated in a tissue model (*Chapter 2*) and in *ex vivo* canine prostate tissue (*Chapter 3*).

Thesis outline

Chapter 1   Introduction

Chapter 1 describes the principles of laser surgery and laser tissue interaction, with special emphasis on the Nd:YAG laser and canine prostate tissue. Furthermore, modeling of laser-induced tissue damage for in vitro damage evaluation is discussed. The use of laser for prostate surgery and laparoscopic procedures is introduced and its advantages hypothesized.

Chapter 2   Dynamic color schlieren imaging of Nd:YAG laser-induced temperature distribution in a tissue model: a pilot study

Visualization of spatial temperature distribution in tissue is complicated. Schlieren imaging is an optical technique to visualize temperature gradients in transparent media. A transparent polyacrylamide gel may serve as a model for laser tissue interaction. Spatial distribution of Nd:YAG laser-induced temperature distribution is investigated in a polyacrylamide gel using a dynamic color schlieren technique, comparing contact and free beam laser exposure. An attempt is made to calibrate the gel for canine prostate tissue.

Chapter 3   **Nd:YAG surgical laser effects in canine prostate tissue: Temperature and damage distribution**

In order to investigate the amount of thermal tissue damage inflicted by laser surgery, this chapter deals with in vitro temperature measurement of laser-irradiated prostate tissue. Laser-induced tissue damage is assessed through the use of an Arrhenius damage prediction formula, and through histological examination. Results are compared and discussed. A threshold temperature for acute laser-induced prostate tissue damage is determined, and expected safety margins for prostate surgery are outlined.

In addition (**appendix**), an attempt is made to relate the tissue damage described in this chapter to the schlieren model of Chapter 2, in order to validate the model for canine prostate tissue.

Chapter 4   **Partial prostatectomy using Nd:YAG laser for the management of canine prostate carcinoma**

The Nd:YAG surgical laser is used for a subtotal prostatectomy in a pilot study on 4 normal dogs and a clinical trial of 8 patients with prostate carcinoma (PCA). Prostate tissue is resected, preserving prostate capsule, urethra, and dorsal portion of the prostate containing important nerves and vessels, aiming to maintain urinary continence. Additional treatment of patients with PCA consists of local administration of IL-2 and systemic treatment with meloxicam.

      Appendix: In order to support findings in Chapter 3, histological evaluation is performed on the prostate and laser-resected tissue parts after *in vivo* subcapsular laser prostatectomy of the normal dog.

Chapter 5   **Neodymium:Yttrium-Aluminium-Garnet surgical laser versus bipolar electrocoagulation for laparoscopic ovariectomy in dogs**

The Nd:YAG surgical laser is introduced in laparoscopy and is investigated through comparison with bipolar electrocoagulaion (BEC) in laparoscopic ovariectomy (lapOVE) in healthy dogs, comparing use, complications, hemostasis, and recovery.

Chapter 6   **Comparison of Nd:YAG surgical laser and Remorgida bipolar electrosurgery forceps in canine laparoscopic ovariectomy**

The Remorgida BEC forceps combines two instruments in one: BEC forceps and sharp resection by an independently moveable knife blade. It is compared to the Nd:YAG surgical laser in lapOVE. Because of its dual function, the Remorgida device is expected to enhance laparoscopic surgery and reduce surgery duration.

Chapter 7   **Laparoscopic ovariectomy in cats: Comparison of laser and bipolar electrocoagulation**

Laparoscopic surgery in cats is not well described. In chapter 6, lapOVE is introduced in cats, using both laser and BEC, aiming to evaluate overall technique and compare instruments, with emphasis on ease of surgery, intra- and postoperative complications, hemostasis, and recovery.

Chapter 8   **Discussion**

Chapter 8 evaluates, compares and draws conclusions from the studies on laser-tissue interaction and the use of the Nd:YAG laser as a tool in urogenital surgery, and as an alternative in laparoscopic surgery.

1

Chapter 1

Introduction: Lasers and laser-tissue interaction

Sebastiaan A. van Nimwegen

The introduction describes the principles of laser surgery and laser-tissue interaction, with special emphasis on the Nd:YAG laser and prostate tissue. Furthermore, a widely-used model of laser-induced tissue damage is reviewed. The use of the Nd:YAG laser for prostate surgery and laparoscopic procedures is presented and its advantages hypothesized. Where applicable, subjects directly related to other chapters in the thesis are outlined.

1 Basic laser physics

"LASER" stands for: Light Amplification by Stimulated Emission of Radiation. In a laser, an external energy source excites atoms in the laser-medium so electrons acquire a higher energy-status: $E_0 \rightarrow E_1$ (electrons move to a next orbit (i.e. energy level) around the atom nucleus). This is called a metastable state, which exists only in specific atoms. If the electron falls back to its ground-state E_0, a photon is emitted. This photon has a specific wavelength because the energy-states of selected orbits around a nucleus are predetermined for each matter, and:

$$E_1 - E_0 = hf \tag{1}$$

in which h is Planck's constant ($6.626*10^{-34}$ J s) and f is the frequency of the emitted photon. The wavelength (λ) of the emitted photon is:

$$\lambda = \frac{c}{f} \tag{2}$$

in which c is the velocity of light ($2.998*10^8$ m s^{-1}).

This photon is emitted in a random direction. If a photon of resonant energy $hf = E_1 - E_0$ passes by an atom in excited state E_1, it stimulates the atom to drop to the lower state E_0. In this process, the atom releases a photon of the same energy, direction, phase and polarization as that of the photon passing by. Consequently, there are now two identical photons instead of one and the intensity of the incident "beam" has increased. This is the principle of 'stimulated emission' (Einstein 1917) which enables the amplification of light in lasers (Figure 1).
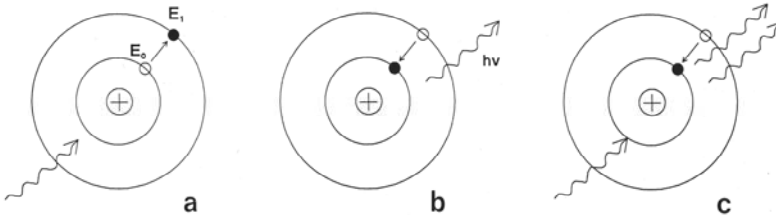
Figure 1: Schematic representation of an atom in the laser medium. a) Absorption of a photon (from an external energy-source) induces a higher energy-state (E_1) of the electron. b) Spontaneous emission. c) Stimulated emission. (Hillegersberg 1993).

In a laser, the external power-source (or pump) creates a situation called 'population inversion' in which more atoms in the laser-medium are in the excited state E_1 than in ground-state E_0. Thus, a spontaneous emitted photon can stimulate the emission of many more photons. To create a collimated beam, the light is reflected in an optical cavity or resonator which consists of two opposing mirrors directing the beam back and forth through the laser- (amplifying) medium. One mirror has a reflectivity of <100% to allow part of the resonating beam to escape and become useful as laser beam (Figure2).
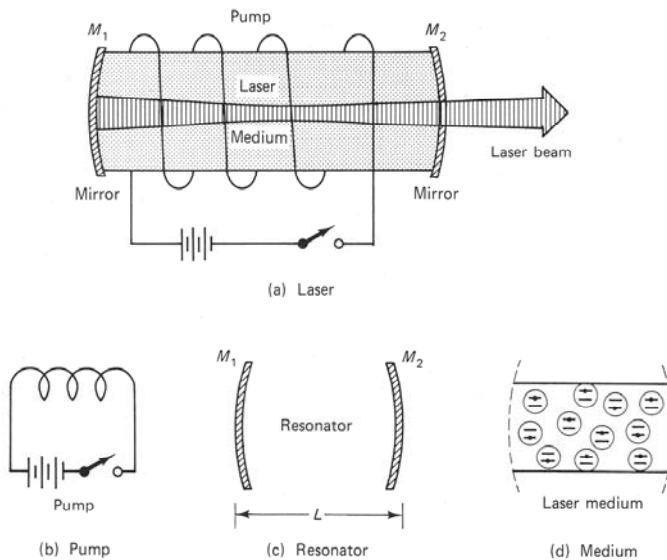
Figure 2: General working mechanism of a laser. (Pedrotti and Pedrotti 1996)

A high-power monochromatic beam with minimum angular spread (divergence) is created, able to deliver high power at a relatively small spot. Furthermore, the laser beam is

monochromatic and coherent. Useful in laser surgery are monochromaticity (because absorption of light by specific molecules is wavelength-dependent), the high power density (W/m^2) that can be achieved, and the fact that most laser light can be applied through flexible optical fibers, making it a versatile instrument for minimally invasive procedures. The laser-medium can be various sorts of matter (gas, liquid, solid or a special case: semiconductor (diode)) all with specific emitted wavelengths.

In the Nd:YAG laser (1064 nm wavelength) a synthetic Yttrium-Aluminium-Garnet (YAG) crystal serves as laser-host-medium supporting Neodymium (Nd) laser-atoms. A xenon lamp serves as the laser pump. A distinction is made between pulsed lasers and Continuous Wave (CW) surgical lasers, delivering a constant power laser beam (typically 1-100 W). This thesis will deal with near infrared CW lasers, in particular the Nd:YAG laser. In contrast, the high power pulsed lasers, which emit 'modest' energies (0.01-10 J) in very short pulses (10^{-12}-10^{-5} s) with accompanying very high powers (10^3-10^{10} W) creating explosive tissue effects (i.e. lithotripsy) are beyond the scope of this thesis.

2   Laser-tissue interaction

Effects of laser irradiation in tissues can be divided in 3 basic actions (Jacques 1992) (although many variations to these terms and sub-divisions exist; some are given in parentheses):

- *Photothermal effect*: Laser energy is transformed into heat upon absorption by tissue molecules. This is by far the most utilized effect of lasers in surgery, ranging from rapid vaporization (ablation) of tissue to slow heating in interstitial thermotherapy (photocoagulation).
- *Photochemical effect*: An important example of photochemical reaction is photodynamic therapy (PDT, a form of light-induced chemotherapy). Photons react with molecular chromophores (endogenous or exogenous) by exciting them to a higher energy state. The excited molecules can subsequently participate in a chemical reaction. In PDT, this reaction usually implies the formation of oxygen radicals, as a means to (selectively) destroy cancer cells.
- *Photomechanical effect*: Because of the relatively high laser power demand, pulsed lasers are typically used to achieve photomechanical effects (photodisruptive, photoionizing). High laser power can cause stress (force/unit area) through:
  - sudden thermoelastic expansion of tissue

- sudden expansion secondary to phase change:
  - explosive phase changes (like rapid formation of water vapour which bursts out of the tissue
  - creation of plasma, which rapidly expands, creating a stress wave.

This thesis will mainly deal with the photothermal effect of CW surgical lasers.

The complete extent of laser-tissue interaction depends on three phenomena:

1. Light distribution in tissue
2. Transformation of laser energy into heat and the distribution of heat in tissue
3. The biological response of the tissue to increased temperature

These events are dependent on laser characteristics (wavelength, beam size, power density of the delivered beam and exposure time) and on optical and thermal properties of the tissue.

2.1 *Light distribution in tissue*

When light or a laser beam is aimed at tissue, the interaction with the tissue is characterized by four events (Figure 3):
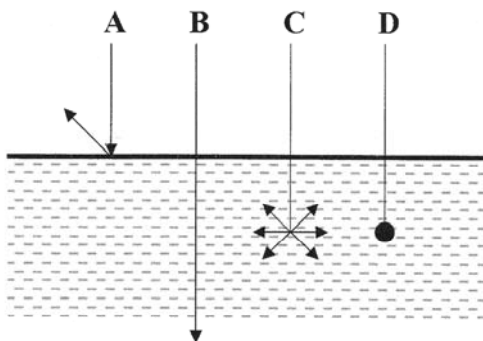
Figure 3: Laser-light interaction with biological tissue. From: G. M. Peavy (Peavy 2002).

A. Reflection: part of the beam is reflected at the tissue surface
B. Transmission: Part of the beam travels through the tissue
C. Scattering: the light is scattered throughout the tissue in multiple directions before being absorbed
D. Absorption: photons are absorbed by tissue molecules which results in production of heat or the initiation of photochemical reactions.

The degree in which these events occur differs for different tissues and wavelengths.

Optical properties of tissue can be described in physical terms as:

- ***Absorption coefficient*** μ_a (cm^{-1}); the proportionality constant describing the amount of light attenuated by absorption (the mean free path before absorption = $1/\mu_a$).

- ***Scattering coefficient*** μ_s (cm^{-1}); describing the attenuation of light due to scattering away from the direction of propagation (the mean free path between scattering events = $1/\mu_s$)

- ***Anisotropy factor g*** is the average cosine of the scattering angle in anisotropic media. Describing the fraction of light scattered into any given direction. *g* is usually around 0.9 for visible and near-infrared wavelengths (indicating the forward scattering nature of tissue).

- ***Reduced scattering coefficient*** $\mu_s' = \mu_s(1\text{-}g)$ is used to describe scattering in anisotropic materials ($1/\mu_s'$ = the mean free path before a photon's trajectory has become randomized) (Jacques 1992).

μ_s, μ_a and *g* can be measured experimentally *in vitro* using spectrophotometry.

Important light-absorbing substances in tissue are water and hemoglobin (Hb) and in skin and retina also melanin. The light-absorption (μ_a) of these tissue constituents varies with wavelength (Figure 4). This explains why tissue effects of different laser wavelengths can vary considerably.

Figure 4: Absorption (log scale) of water, (oxi-) hemoglobin (Hb (ox)) and melanin for several laser wavelengths. SHG: second harmonic generation. (Teichmann *et al* 2007).

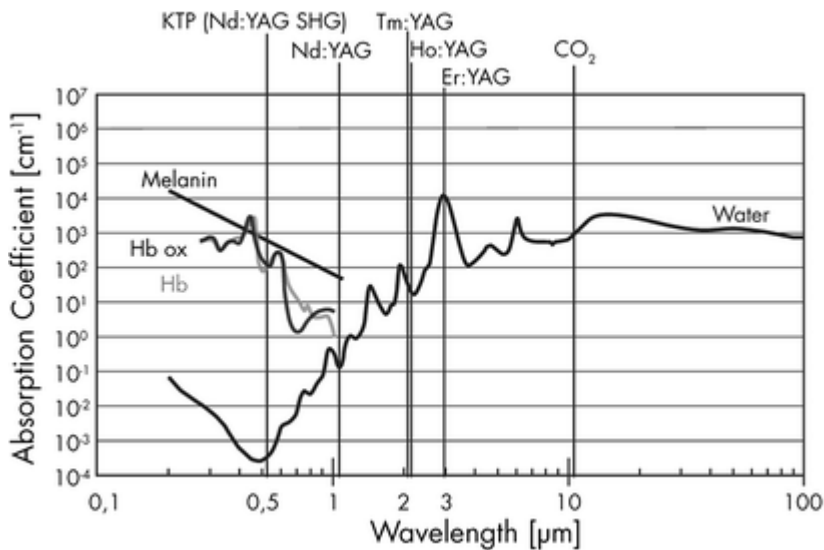As an example, CO_2 laser light (10600 nm) is strongly absorbed by water and therefore has a very shallow penetration depth in tissue. All irradiation energy is superficially absorbed and transferred into heat causing superficial tissue temperature to rise rapidly leading to carbonization and subsequent vaporization of tissue. The near infrared laser wavelengths, such as the Nd:YAG wavelength (1064 nm) and the diode laser wavelengths (805-980 nm) are less well absorbed by water and hemoglobin and therefore have a relatively deep (up to 10 mm) penetration depth in tissues, enabling formation of relatively deep tissue coagulation. In fact, the near infrared lasers show the deepest optical penetration in tissue compared to other surgical lasers. These lasers are therefore commonly used in laser-induced thermotherapy for tumor coagulation. Near infrared wavelengths are relatively better absorbed by hemoglobin and melanin than by water. This difference in absorption can be utilized for selective photocoagulation (or photothermolysis) of superficially located pigment-containing structures (such as hemangiomas, birthmarks, pigmented dermal lesions and hair follicles). Several lasers commonly used in soft tissue surgery are presented in Table 1.

Tissue effects of Nd:YAG and diode lasers are in many cases comparable (Judy *et al* 1993, Nikfarjam *et al* 2005). However, since the Nd:YAG wavelength is relatively better absorbed by water and less by haemoglobin compared to diode laser (this difference increases with shorter diode wavelengths, Figure 4), differences in penetration depth and temperature distribution in tissues can be expected due to haemoglobin content and perfusion rate. Penetration depth of diode laser irradiation is therefore usually somewhat less compared to Nd:YAG laser, causing more rapid heating of a smaller volume. This does not necessarily imply smaller lesions, depending on exposure time and on cooling by blood perfusion, which can have a greater effect on Nd:YAG laser-induced slow heating (Jiang and Zhang 2005, Nikfarjam *et al* 2005).

Type of laser	λ (nm)	Water μ_a	Hb μ_a	Penetration depth δ (mm)	Tissue effects	Clinical use examples
CO₂	10600	800	-	~ 0.3	Vaporization	Incision/vaporization
Er:YAG (erbium) (not fiberguided)	2940	12000	-	~ 0.03	Vaporization	Lithotripsy Incision/vaporization
Ho:YAG (holmium)	2100	27	-	~ 0.4	Vaporization Coagulation	Lithotripsy Prostate ablation
Tm:YAG (thulium)	2000		-	~ 0.25	Vaporization	Incision/vaporization
Nd:Yag (neodymium)	1064	0.120	-	3-10*	Coagulation Vaporization with contact tip	Prostate ablation LITT/Tumor coagulation Incision/vaporization
Diode	980	0.430	2	2-8*	Coagulation Vaporization with contact tip	LITT Coagulation Tissue welding Incision/vaporization
	910	0.073	4			
	830	0.029	4			
	810	0.023	4			
KTP frequency-doubled Nd:YAG	532	0.004	203	0.3-1.0	Vaporization	Prostate ablation

Table 1: Lasers used in soft tissue surgery. LITT=Laser Induced (or Interstitial) ThermoTherapy, μ_a=absorption coefficient, Hb=hemoglobin. λ= wavelength. Penetration depth is the theoretical depth in an average tissue at which the intensity of irradiation is attenuated by a factor 1/e (63.2%). *Penetration depth (δ) of near infrared wavelengths varies considerably between tissues due to differences in absorption and scattering. (Peavy 2002, Tan and Gilling 2003, Pierre and Albala 2007, Teichmann *et al* 2007).

2.2   *Light fluence and penetration depth in tissue*

This section presents a simple method to estimate laser light distribution in tissue in one dimension (1D). Methods to estimate spatial light distribution are beyond the scope of this thesis. The given 1D estimation methods are derived for a broad beam situation: δ<<beam diameter.

Light distribution inside tissue is dependent on absorption and scattering, which are both wavelength dependent. If a tissue would not scatter, penetration of collimated (laser) light would be accurately estimated using Beer's law:

$$\phi(z) = (1-R)E_0 e^{-\mu_a z} \tag{3}$$

in which $\Phi(z)$ is the fluence rate (W/cm^2) at a distance z from the tissue surface and E_0 is the delivered irradiance (W/cm^2) of the laser beam at the surface. R is the specular reflection term (the fraction of laser irradiation reflected at the surface, $R=(n_1-n_2)^2/(n_1+n_2)^2 \approx 0.024$ for a refractive index $n_{tissue}=1.37$ and a beam perpendicular to the surface) (Wright *et al* 2002). This formula can also be used in scattering media (replace μ_a with $(\mu_a+\mu_s)$), but it then represents the penetration of *collimated* light only, disregarding the scattered/diffuse light. In turbid media (such as tissue), light is scattered in all directions. However, in tissue, forward scattering is usually predominant (g is usually around 0.9), so penetration depth is larger compared to that of only collimated light. In turbid media, when $\mu_s \gg \mu_a$ (as with near infrared light in most tissues), penetration depth can be estimated using:

$$\delta = \frac{1}{\sqrt{3\mu_a(\mu_a + (1-g)\mu_s)}} = \frac{1}{\mu_{eff}} \tag{4}$$

Equation 4 is derived from diffusion theory (Jacques 1992, Wright *et al* 2002), in which δ is the penetration depth (cm) (63.2% attenuation of the incident irradiance) and μ_{eff} is the effective attenuation coefficient.

Several experimentally derived optical properties of canine prostate tissue for 1064 nm are displayed in Table 2. Note the differences in values due to different methods.

μ_a [cm^{-1}]	μ_s [cm^{-1}]	μ_s' [cm^{-1}]	μ_{eff} [cm^{-1}]	g	δ [mm]	Method	Reference
0.36		9.64		0.9*	3.03	-	(Anvari *et al* 1994)
0.27	30.6	17.6		0.45	(2.63)	Spectrometry**	(Nau *et al* 1999)
0.09		6.3	1.3		(7.7)	Acoustic theory***	(Oraevsky *et al* 1997)
0.04		13.0	1.25		(8.0)	Acoustic theory	(Cheong 1995)

Table 2: Experimentally determined optical properties of canine prostate tissue for 1064 nm wavelength. Values within parentheses are calculated from the experimental data. *g=0.9 assumed by authors (Anvari *et al* 1994). **Double integrating sphere spectrometry. ***Calculated from laser-induced stress waves.

Because light is scattered in all directions (including backscattering), the total fluence rate $\Phi(z)$ (W/cm^2) just underneath the tissue surface is usually higher than the irradiance E_0 of the incident laser beam (Figure 5): laser energy piles up near the surface. The fluence rate in scattering media (tissue) can be estimated (for $z>\delta$) using:

$$\phi(z) = (1 - R)E_0be^{-z/\delta} \tag{5}$$

in which b is a constant that accounts for the accumulation of backscattered light, which can be estimated using: $b=3+5.1R_d-2\exp(-9.7R_d)$, in which R_d is the diffuse reflectance (amount of diffusely reflected light) which can be estimated using: $R_d \approx \exp(-8\mu_a\delta)$ (Jacques 1992).

Canine prostate tissue shows relatively high scattering compared to most tissues. As an example: μ_s' = 13.0 (dog prostate) compared to 6.4 (human prostate), 4.8 (canine myocardium), 9.1 (rat skin), 2.4 (canine bladder), 10.1 cm^{-1} (porcine liver) at 1064 nm (Cheong 1995). For canine prostate μ_s' (17.6 ± 1.3 cm^{-1}), μ_s (30.6 ± 2.6 cm^{-1}), μ_a (0.27 ± 0.03 cm^{-1}) and g (0.45 ± 0.03) have been measured in native (non-coagulated) canine prostate tissue for 1064 nm wavelength using a double integrating sphere spectrometer (Nau *et al* 1999). These values were used here to estimate penetration depth (δ=2.63 mm, Equation 4) and fluence rate $\Phi(z)$ (W/cm^2) inside canine prostate tissue using Equation 5 (Figure 5). The fluence rate is also calculated for an 'imaginary' tissue in which μ_s=0, and only μ_a accounts for attenuation of the laser light (using Equation 4, Figure 5), to show the effect of scattering on energy distribution.

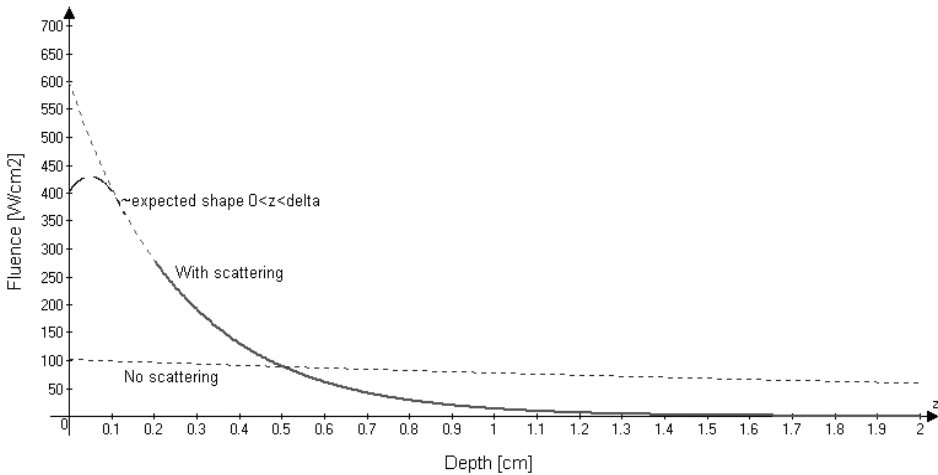**Figure 5**: Estimation of fluence rate (W/cm^2) in canine prostate tissue irradiated with E_0=102W/cm^2, as with 20W laser power and 0.2 cm^2 spot-size. Also, an example is given of fluence decay when scattering does not exist and light attenuation is only dependent on absorption. An arbitrary indication is given of the expected fluence maximum at $0<z<\delta$.

The estimation of $\Phi(z)$ in Figure 5 is accurate for $z>\delta$, and the actual fluence rate will peak somewhere near the surface ($0<z<\delta$). The initial heating of the tissue will be linear related to the fluence distribution, but will change in time due to conduction and diffusion.

In Chapter 2, a transparent polyacrylamide gel is used as a tissue model to visualize laser-induced temperature distribution. This gel shows approximately no scattering, and gel-absorption and diameter of the laser beam have to be configured in a way as to mimic an energy distribution comparable to that in tissue. The fluence rate calculations presented in this Section are applied in Chapter 2 to calibrate the model for canine prostate tissue.

2.3   Heat distribution in tissue

Upon absorption of light by tissue molecules heat is produced which causes a rise in temperature. This heat will spread through conduction and diffusion, depending on tissue thermal properties, anatomy (blood flow) and exposure time. Light is instantaneously distributed in the tissue, whereas heating and heat-spreading takes time.

2.4   Biological response of tissue to heat

Thermal damage of tissue is mainly governed by protein denaturation (He *et al* 2004, Bischof and He 2005) and is described as being dependent on both temperature and the duration of increased temperature (thermal history). Throughout the literature, threshold temperatures of 40 - 60°C are given for tissue damage to occur, measured in experiments using various exposure times (seconds to hours). Many studies assumed a single value of around 60°C to be the threshold temperature for acute (instantaneous) irreversible tissue damage. Table 3 shows known experimental temperature-damage relations, as reported in several publications. Moritz and Henriques (1947) already stated in their thermal injury studies, that describing threshold temperatures for tissue damage is only valuable for others if the relevant exposure times are also reported. They recorded the onset of burn wounds at several temperatures and exposure times in skin and plotted the threshold temperature for 1st degree and 2nd degree skin burns in pigs and humans against accompanying exposure time (logarithmic scale) to find a linear relation. They formulated the Arrhenius damage integral to describe this relation, which became a very valuable tool to describe the temperature and time dependence of tissue damage, as discussed in section 4.

Tissue Temperature	Biological Effect	Exposure time
40 - 45°C	Reversible damage due to inactivation of enzymes, protein denaturation, edema, hyperaemia, irreversible damage with sufficient exposure time	Minutes/hours
45 - 60°C	Protein denaturation, coagulation, loss of birefringence from collagen, cell shrinkage and hyperchromasia, irreversible damage after sufficient exposure time	Minutes
60 – 100°C	Protein coagulation, loss of birefringence from collagen, cell shrinkage and hyperchromasia, irreversible damage.	Minutes/seconds
100°C	Vaporization of tissue water, extracellular vacuole formation, 'popcorn' effect (rupture of tissue from steam expansion)	Seconds
>250°C	Carbonization	<1s
> 300°C	Vaporization of tissue	<1s

Table 3: Temperature-damage relations for biological tissue, modified from Thomsen (1991) and Pearce and Thomsen (1995).

2.5   *Histological changes in laser-irradiated tissue*

Immediate effects of *non-lethal* thermal injury are not visible on histology. Delayed effects can be seen in the form of cellular edema and hyperemia. Low temperature *non-coagulative lethal* injury, in which vital enzymes (for energy production and cellular repair mechanisms) are destroyed, is also not visible on short-term histological examination, except for severe damage seen with long exposure times (Thomsen 1991, Pearce and Thomsen 1995). However, cell death will ultimately lead to the development of tissue necrosis within 1 – 3 days, which is readily detectable on histology. Higher temperature and/or longer exposure to increased temperature will lead to denaturation and conformational changes of the more heat-stable tissue structural proteins, a process called *thermal coagulation* of tissue (the term coagulation necrosis, a pathologic process not necessarily inflicted by heat, is also commonly used). Coagulation is immediately visible as a macroscopic whitening of tissue. Still, low temperature-induced coagulation can be subtle and difficult to interpret using light microscopy. High temperature-induced tissue

coagulation leads to more distinct histological changes in tissue. Cells and nuclei undergo conformational changes and loose their normal internal structure caused by denaturation of structural and cytolasmic proteins and organelles. Hematoxylin & eosin (HE) stained tissue shows hyperchromasia of cytoplasm (eosinophilic) and nucleus (basophilic). Denatured/coagulated collagen can also show changes in staining. However, these histological changes can sometimes be hard to distinguish from technical artifacts or poor staining techniques. Another important histological change is the temperature-induced loss of birefringence of fibrillar collagen and regular arrangement of fibrillar proteins, which is best appreciated in collagen rich tissues or highly fibrillar structured tissues such as striated muscle (Thomsen *et al* 1989) and cornea (Rem *et al* 2001). When the temperature further increases, evaporation of water becomes an important factor. Dehydration of tissue and cells further increases hyperchromasia and conformational changes. When reaching 100°C, water vapor can cause formation of gas bubbles within the tissue (vacuolization). Heating >100°C can cause explosive vapor formation and subsequent rupture of tissue ('popcorn' effect (Verdaasdonk *et al* 1990)). Further heating of tissue eventually causes caramelization and carbonization.

3   Application modes of near infrared lasers

3.1   *Dynamics of laser-tissue interaction*

During heating, the optical and thermal properties of tissue change. During coagulation of tissue (macroscopically visible as whitening of tissue), scattering increases considerably and subsequently the penetration-depth of laser irradiation decreases (Nau *et al* 1999, Skinner *et al* 2000, Ritz *et al* 2001). As water-content of the tissue decreases (evaporation), the thermal conductivity decreases. These changes cause a redistribution of applied laser energy, leading to a more rapid superficial temperature increase. Changes in absorption are small during coagulation of tissue (Nau *et al* 1999). As carbonization occurs, the heat-distribution changes dramatically because the black carbonized tissue strongly absorbs laser irradiation. Charring of the tissue strongly blocks tissue-penetration of laser irradiation leading to further heating of the carbonized tissue which can cause subsequent vaporization of tissue. With carbonization, further heat-distribution in the underlying tissue is mainly dependent on conduction and diffusion of the heat produced at the carbonized site. Other important factors in tissue heating are water evaporation which acts as a heat-sink at 100°C, and blood perfusion. Blood perfusion has a significant cooling effect with increasing exposure time (see also Section 4.2) (Anvari *et al* 1994, Sturesson *et al* 1997).

Temperature-induced changes in optical and thermal properties explain that the extent of tissue damage in laser irradiation procedures is more dependent on power density (W/cm^2) of the beam and irradiation time and not solely on the amount of energy applied. High power density causes relatively rapid superficial tissue alterations resulting in increased scattering due to coagulation or char formation which blocks further light-penetration. The use of lower power densities, avoiding such superficial alterations of tissue, permits deeper light-penetration and subsequent larger coagulated volumes (Anvari *et al* 1994, Motamedi *et al* 1995, Orihuela *et al* 1995, Lippert *et al* 2003).

3.2 *Contact mode versus non-contact mode*

The difference in tissue interaction of near infrared irradiation due to changes in power density at the laser-irradiated tissue surface can be demonstrated by looking at two ways of using a Nd:YAG (1064 nm) or diode laser (805-980 nm).

In surgery, laser energy is preferably applied by means of a flexible optical fiber. A laser beam leaving a bare-end fiber is typically more or less divergent. This implicates that the power density decreases with distance from the fiber tip. A bare-end fiber can therefore be used in two ways (Philipp *et al* 1995, Brown 2000, Peavy 2002, Janda *et al* 2003):

- *Contact mode:* The fiber tip is in contact with the tissue. High power density at the fiber tip causes tissue to rapidly carbonize and subsequently vaporize. This way, the fiber tip can be used to cut through tissue (i.e. 'laser-scalpel'). During 'incision', the produced heat and scattered irradiation causes coagulation of the cut-surface and small blood vessels are effectively sealed. Since near infrared laser absorption by tissue is relatively weak, a clean fiber tip usually does not instantaneously cause carbonization and vaporization, and irradiation spreads inside the tissue. The first carbonization can be slow (1- >20s). However, after that, carbonized particles adhere to the tip (i.e. a 'dirty' tip) and will be heated instantaneously at subsequent laser firing and tissue vaporization is very effective (Verdaasdonk *et al* 1991).

- *Non-contact mode or free beam:* The fiber tip is held at some distance from the tissue. The diverging laser beam hits the tissue with a much lower power density and no carbonization occurs. Laser irradiation penetrates the tissue and spreads (penetration, scattering) over a certain volume of tissue which is heated (absorption) and eventually coagulated, depending on temperature rise and exposure time.

Theoretically, in contact mode most of the laser light is blocked and absorbed superficially during carbonization and vaporization of tissue and less heat-spread occurs deeper into the

tissue, being mainly dependent on conduction and diffusion. Figure 6 shows the theoretical differences between contact and non contact mode use of a fiber tip.
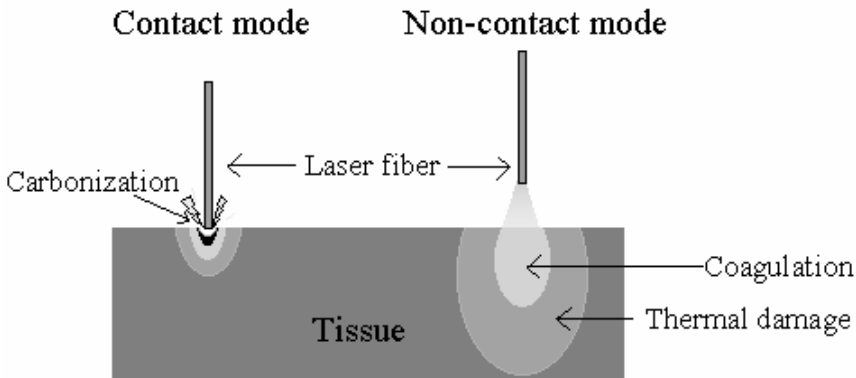

Figure 6: Theoretical difference of non-contact (free beam) versus contact mode laser application.

The terms *contact* versus *non-contact* originate from the fact that the Nd:YAG laser was one of the first lasers to be extensively used in medical applications. Because of the relatively low absorption in tissue, the fiber tip had to be brought in contact with the tissue to achieve vaporization of tissue. *Free beam* transurethral vaporization of prostate tissue using a Nd:YAG laser up to 90 W was less adequate than *contact* mode Nd:YAG prostatectomy (Kabalin *et al* 1995, Kuntzman *et al* 1996). However, if vaporization of considerable amounts of tissue is aimed for, a Nd:YAG laser might not be the laser of choice, considering the relatively high penetration depth of 1064 nm wavelength. Longer wavelengths (Holmium:YAG (2.0 μm), CO_2 (10.6 μm)), being strongly absorbed by water molecules, or shorter wavelengths (KTP (532 nm) being absorbed by haemoglobin, are more effective (free beam) tissue vaporizers (Kuntzman *et al* 1997). In contrast, Nd:YAG laser irradiation produces excellent tissue coagulation, and is preferably used for coagulation treatment strategies such as non-contact treatment of tumors and bleeding lesions, transurethral coagulation of the prostate for Benign Prostatic Hyperplasia (BPH) (Kabalin 1998) and Laser Interstitial ThermoTherapy (LITT): Fibers with diffusing tips are placed inside tissues and are used to (photo-) coagulate considerable tissue volumes, using relatively low power and relatively long exposure (10-20 or more minutes) (Heisterkamp *et al* 1999). Applications of LITT are the treatment of BPH (Perlmutter and Muschter 1998) and photocoagulation of non-resectable tumors. In LITT of non-resectable liver tumors (primary or colorectal metastasis) successful coagulation of tumors up to 4 cm in diameter is induced using a single fiber, and tumors of 8 – 10 cm using multiple fibers (Nikfarjam and Christophi 2003, Veenendaal *et al* 2006). During transurethral coagulation of the

prostate, depth of tissue coagulation typically reached 10-14 mm (Cromeens *et al* 1994, Orihuela *et al* 1995, Cromeens *et al* 1996, Kuntzman *et al* 1996), showing the photocoagulative ability of the free beam.

In Chapter 2, the effect of contact and free beam exposure is visualized, using color schlieren imaging in a transparent tissue model.

4   A model of temperature-induced tissue damage

4.1   *The Arrhenius accumulated damage model*

Generally, in all scientific fields, a description of a physical, chemical or biological process by means of a mathematical model can serve to predict the behavior of the process and help to further understand the process. Furthermore, modeling of laser-tissue interaction can help in determining conditions concerning laser dosimetry and treatment planning. As mentioned in Section 2, thermal tissue injury is found to be dependent on both increased temperature and exposure time and can not be adequately described if one of these parameters is unknown. The most extensively-used empirical model to describe time-dependent temperature-induced tissue damage is derived from the temperature dependence of molecular reaction rates described by the Arrhenius equation. It can be comprehensively used to understand and predict tissue damage as a function of temperature and time.

The rate of a reaction may be found to be proportional to the molar concentrations of two reactants X and Y, in which case the reaction rate (v) can be written as:

$$v = k[X][Y] \tag{6}$$

The rate constant k is independent of the concentrations but depends on temperature.

It is found experimentally that for many reactions $\ln k$ varies linear with $1/T$. This relation is mathematically expressed as the Arrhenius equation:

$$\ln k = \ln A - \frac{E_a}{RT} \qquad \text{or} \qquad k = Ae^{-E_a/RT} \tag{7}$$

in which A and E_a are the Arrhenius parameters. E_a represents the activation energy needed for reactants to form products. The exponential factor $e^{-E_a/RT}$ can be interpreted as the fraction of collisions between molecules that have enough kinetic energy to lead to reaction (described by Boltzman for gas phase reactions). A is the frequency factor and is a measure of the rate at which collisions occur, independent of their energy. Hence, Equation 7 gives the rate of 'successful' collisions (Atkins 1998).

This temperature relation for reaction speed was used by Henriques (1947) to formulate the Arrhenius accumulated damage integral:

$$\Omega = \ln\left(\frac{C(0)}{C(\tau)}\right) = A\int_0^\tau e^{-E_a/RT(t)}dt \qquad (8)$$

in which Ω represents the logarithm of the ratio of the original concentration $C(0)$ of native state tissue constituent to the remaining concentration $C(\tau)$ after a time τ. For instance, $\Omega=1$ means that 63% of the tissue-molecules are damaged (which is assumed to produce coagulation necrosis). A is the frequency factor (s^{-1}), E_a the activation energy barrier (J mol^{-1}) for tissue molecules to denature, R the universal gas constant (8.31 J mol^{-1} K^{-1}) and $T(t)$ the tissue temperature in time. In this formulation, the process of tissue denaturation is assumed to be governed by an Arrhenius rate relation (Equation 7). At moderate temperatures, the process is slow and thus damage accumulates slowly. With increasing temperature, the process gradually becomes faster (k increases) but rises steeply beyond a certain breaking point (also called 'critical temperature', where $d\Omega/dt=1$) (Figure 7) (Pearce and Thomsen 1995).
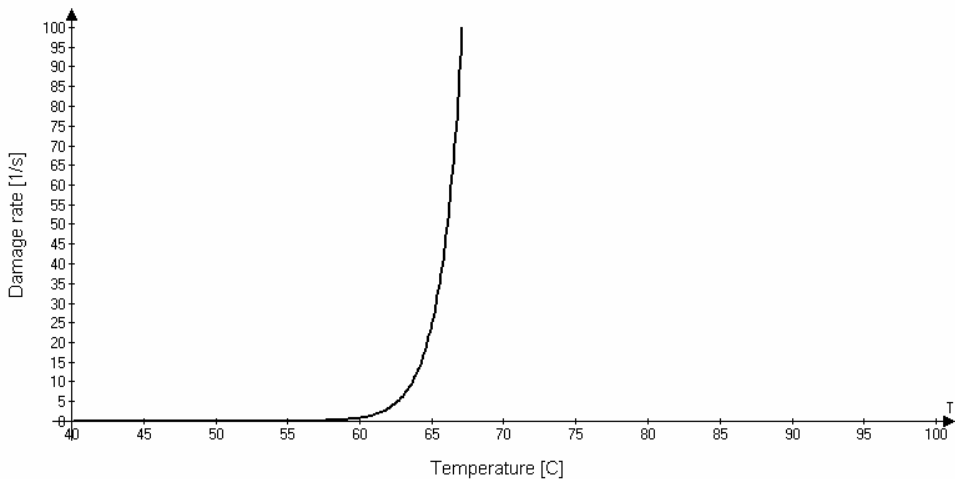
Figure 7: Damage rate ($d\Omega/dt$) as a function of temperature (T) for the Arrhenius equation using the rate parameters A and E_a derived by Henriques (Henriques 1947): $d\Omega/dt=3.1E98e^{6.28E5/RT}$.

The Arrhenius damage model assumes that the damage process (denaturation of tissue molecules) behaves as a single first order rate process. This is an oversimplified situation, since tissue is made up of various molecules which probably obey different rate processes at different temperatures. However, although the molecular basis of the model was never

proven for tissues, it has been successfully used to describe temperature and exposure thresholds for irreversible tissue damage in several tissues, cells and proteins (Henriques 1947, Pearce and Thomsen 1995, Bischof and He 2005).

The Arrhenius parameters A and E_a are tissue-dependent and can be determined by fitting the Arrhenius equation to experimentally determined damage thresholds (end points) at various temperatures and exposure times (Pearce and Thomsen 1995). This is usually achieved by assuming a *static temperature in time*, so Equation 8 can be written as:

$$\Omega = A\,\tau e^{-E_a/RT} \tag{9}$$

When assuming $\Omega=1$ for irreversible damage, equation 9 is transformed into:

$$T_{damage} = \frac{E_a}{R(\ln \tau + \ln A)} \tag{10}$$

or:

$$\ln \tau = \frac{E_a}{R}\frac{1}{T_{damage}} - \ln A \tag{11}$$

Equation 10 describes the (static) threshold temperature (T_{damage}) that induces irreversible tissue damage after a certain exposure time (τ) (Figure 8). Several Arrhenius parameters concerning prostate tissue and the classic rate parameters for 2nd degree burns in pig skin are given in Table 4 and plotted (Equation 10) in Figure 8. Such graphics give an appreciable impression of the time and temperature dependence of temperature induced tissue injury.

Tissue	Damage end-point	E_a (J mol^{-1})	A (s^{-1})	Reference
Skin	2nd degree burn	$6.28*10^5$	$3.1*10^{98}$	(Henriques 1947)
Human BPH tissue	Viability dye uptake, 90% cell death	$160.8*10^3$	$7.78*10^{22}$	(Bhowmick *et al* 2004)
Rat AT-1 prostate tumor cells	Overall protein denaturation via FTIR	$141.5*10^3$	$6.8*10^{19}$	(He *et al* 2004)
Rat prostate tissue	Rate of change of μ_s	$7.18*10^4$	$3.14*10^8$	(Skinner *et al* 2000)

Table 4: Arrhenius parameters for skin and prostate. FTIR=Fourier Transform Infrared Spectroscopy. μ_s=scattering coefficient.
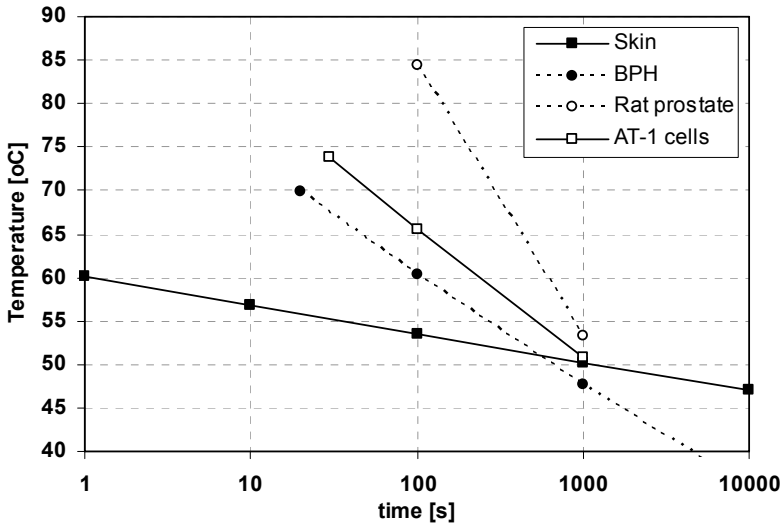
Figure 8: Static threshold temperature versus exposure time for experimentally derived Arrhenius parameters for pig skin, rat prostate, Dunning rat AT-1 prostate tumor cells and human BPH tissue as given in Table 4.

The Arrhenius damage relation is an empirical model describing experimental damage end points. The rate parameters are retrieved by fitting the Arrhenius equation to tissue damage end points as determined by the observer, which can be the onset of tissue coagulation, loss of birefringence of collagen, amount of dye uptake by dead cells, changes in scattering, etc. In general, the determined damage end points are assigned to represent the situation wherein Ω=1, and do not necessarily imply 63% damaged molecules or cells. Therefore, apart from being tissue specific, the Arrhenius parameters are also dependent on the used methods and the determined damage end points. Furthermore, Arrhenius parameters seem to be dependent on the temperature range in which they were measured (He *et al* 2004, Bischof and He 2005) and the damage relation within a certain temperature range can not always be defined by one set of rate parameters.

The Arrhenius rate parameters are usually determined from Equation 11, by plotting $\ln \tau$ against $1/T_{damage}$ for various measures of τ at various static temperatures T_{damage} and retrieving a linear fit. In order to obtain accurate values of E_a and A, exposure times of several orders of magnitude are necessary (Pearce and Thomsen 1995). Determining the Arrhenius rate parameters for very short durations (seconds) is difficult: Since time to achieve irreversible tissue damage is measured at static temperatures, the time to heat the tissue specimen to the desired constant temperature ('calibration time') must be negligible compared to the damage threshold exposure time. This assumption is applicable to long

exposure times. Nevertheless, for short exposures at accompanying high temperatures, measurements will be influenced by this calibration time because the temperature history during calibration time can no longer be neglected. This can cause inaccurate values of E_a and A. Neglectance of calibration time is probably one of the reasons, apart from tissue specificity, that the Arrhenius relation for rat prostate (Skinner *et al* 2000) differs so much from the other prostate relations in Figure 8, for a calibration time of > 90 s was neglected. The threshold temperature for thermal tissue damage was therefore probably overestimated, especially in the short exposure/high temperature range. Another difficulty is to accurately determine the desired end point at high temperatures. Using transient temperatures to determine the Arrhenius rate parameters yields even larger uncertainties because of the temperature-sensitivity of the Arrhenius equation (Figure 7) (Diller and Pearce 1999).

4.2   *Modeling of laser-induced damage using ex vivo prostate tissue*

When Arrhenius parameters of a certain tissue are known, one can predict the onset of irreversible tissue damage from the temperature history of the tissue. Likewise, the Arrhenius integral can be used to model tissue damage *in vitro*. This can be done purely mathematical by modeling light distribution and subsequent temperature increase in time, which requires several tissue-specific (temperature-dependent) parameters to be known or estimated (i.e. scattering, absorption, heat conductivity, specific heat, etc.). Especially scattering and absorption can vary between tissues. The use of *ex vivo* tissue as a model surpasses this problem, but only works for short exposure times since blood perfusion is excluded. As an example: during 20 s laser exposure, using a basal blood perfusion rate in canine prostate tissue of 0.34 ± 0.22 ml/min/g (Xu *et al* 1998) and tissue density of 1.045 kg/m^3 (Anvari *et al* 1994), blood perfusion is 0.07 ml blood/ml tissue. This could account for approximately 7% heat-loss, assuming linear temperature increase in time. However, the area of highest temperature increase is where coagulation takes place and thus blood perfusion diminishes, and the actual heat-loss will be much less than 7%.

In Chapter 3 the Arrhenius accumulated damage integral is used to both describe thermal damage in ex vivo tissue using measured temperature history, and to describe tissue damage behavior with increasing temperatures during short laser exposure as to determine a single threshold temperature for acute irreversible thermal damage in canine prostate tissue.

5   Nd:YAG laser in incisional surgery and laparoscopy

5.1   Laser compared to other energy devices for incisional surgery

Like all fiber-guided lasers, Nd:YAG laser energy is applied through a flexible optical fiber of typically 0.3-1.0 mm diameter, making it an attractive energy source in endoscopic and laparoscopic surgery. As a consequence, advances in laser surgery for a great deal parallel advances in minimally invasive surgery.

As a surgical tool, the Nd:YAG laser is appreciated for its dual use: the ability to coagulate tissue more extensively than any other surgical laser, while in contact mode use precise tissue dissection is possible with proper hemostasis. Tissue damage underneath a contact mode fiber tip or specially designed contact probe has been investigated in the acute stage for several tissues, displayed in Table 5. Generally, depth of tissue injury is less than 1.0 mm (Sultan and Boulnois 1989), and progression of injury in time (i.e. non-coagulation damage, Section 2.5) is minimal for contact mode incisions (see also Section 5.3).

Tissue	Damage depth [mm]	Exposure	Source
Turkey muscle, *ex vivo*	< 0.63	Moving fiber, 20W	(Janda *et al* 2003)
Canine trachea, *in vivo*	0.84	Probe, 35W, 165J	(Shapshay 1987)*
Human gastric wall, *ex vivo*	< 0.95	Probe, 5-30W , 5-150J	(Wyman *et al* 1991)
Bovine oral tissue, *ex vivo*	0.27 – 0.62	Moving probe, 3-10W	(Perry *et al* 1997)
Human aorta, *ex vivo*	0.25	Fiber, 5W, 5s	(Weber *et al* 1991)
Rat liver, uterus, *in vivo*	< 0.7	Probe incision, 10W	(Mecke *et al* 1991)**
Rabbit liver, *in vivo*	0.79-1.22	Probe incision, 12W	(Judy *et al* 1993)

Table 5: Depth of tissue damage underneath the contact mode ablated surface, of *ex vivo* or acute in vivo lesions. *Included electron microscopic evaluation. **Included ATPase and alkaline phosphatase viability staining.

In early stage laser surgery research, the use of *non-contact* Nd:YAG laser for tissue ablation and resection has been evaluated and compared to other energy devices such as thermocauters, electrosurgery forceps and ultrasonic shears, and always resulted in more extensive tissue damage compared to these other devices, as can be expected from the deep tissue penetration of the free beam and the relatively high powers used to achieve free beam incisions. The free beam as a tool for resection surgery will not be discussed, since it is not to be used for this purpose.

Several studies have compared the action of *contact mode* Nd:YAG laser with other energy sources for tissue dissection and hemostasis. A distinct difference from electrosurgery is the absence of muscle-twitching during laser dissection of muscle tissue, while obtaining excellent hemostasis. In many cases, contact Nd:YAG laser is comparable to CO_2 laser incisions in gross tissue effects, although hemostasis, microscopic findings and wound healing can differ between the two. Compared to the CO_2 laser, the Nd:YAG laser in contact mode produced less charring (carbonization) and less coagulation under the surface, which resulted in faster healing of lesions in canine (endoscopic study) and rabbit trachea (Shapshay 1987, Laranne *et al* 1997a). Less carbonization compared to CO_2 laser was also observed in excised soft palate during uvulopalatopharyngoplasty in humans (Laranne *et al* 1997b). CO_2 laser was equally effective for soft palate resection and resulted in similar tissue injury compared to the Ligasure® bipolar forceps in dogs (Brdecka *et al* 2007). Many studies show more extensive lateral spread of thermal damage using monopolar electrosurgery devices compared to the smoother and better defined wound margins when contact Nd:YAG laser (Schurr *et al* 1994) or CO_2 laser (Chinali *et al* 1983, Bellina *et al* 1984, Tulikangas *et al* 2001) are used in abdominal surgery. CO_2 laser caused less tissue injury compared to bipolar or monopolar electrosurgery and ultrasonic aspirator in abdominal tissues in pigs (Tulikangas *et al* 2001). Contact Nd:YAG laser yielded good results in experimental laparoscopic colon resection in dogs (Bohm *et al* 1994a, Bohm *et al* 1995), and facilitated better hemostasis compared to electrosurgery. There were no differences in healing or complications. Furthermore, the laser enabled more precise dissection near mesenteric vessels and was used as a stand-alone device, while electrocoagulation was combined with endoscopic scissors (Bohm *et al* 1994b). Contact mode Nd:YAG laser achieved better hemostasis in surgery of the liver and pancreas in rats, and compared favorably to CO_2 laser and electrosurgery in rats and dogs (Schroder *et al* 1987b, Schroder *et al* 1987a, Schroder *et al* 1988). Furthermore, contact Nd:YAG laser has been demonstrated to be as safe and precise as conventional pancreatectomy techniques in dogs (Schroder and Ramo 1989). Contact Nd:YAG surgery was considered useful for non-anatomic liver resection, produced good hemostasis, created a margin of approximately 0.5 mm tissue necrosis (Joffe 1989), and was equally effective compared with an ultrasonic dissector (Schroder *et al* 1987c). Others mention a risk of hemorrhage, because vessels in the 2 mm range were incised rather than coagulated (Schneider 1992).

As for parenchymatous tissues, Nd:YAG contact mode surgery has been applied in clinical settings for partial resection of the liver, pancreas, spleen and kidney in humans (Joffe 1989, Mason 1989, Schmittenbecher 1990, Litwin and Kirpitchev 1991).

An additional explanation for the suitability of contact mode laser for precise surgery compared to other energy devices is the relatively small contact-area of the fiber tip as

dissection instrument (300-600 μm). As a comparison, the contact area of monopolar or bipolar electrosurgery forceps and ultrasonic shears is generally >10x1 mm. Furthermore, the metal parts of these energy devices can build up relatively high temperatures: ultrasonic shears up to 150°C in 10-30s, electrosurgery up to >350°C within seconds (Kinoshita *et al* 1999, Owaki *et al* 2002, Emam and Cuschieri 2003). The dimensions of these shears or forceps and high temperatures can enhance coagulation of large blood vessels, but can also cause subsequent damage to surrounding tissues which may be a disadvantage in or close to delicate tissues such as nerves (Owaki *et al* 2002).

5.2   *Examples of laparoscopic and endoscopic laser applications*

A fiber-guided free beam Nd:YAG laser technique is commonly used in the endoscopic treatment of bleeding lesions, such as chronic epistaxis (Mahoney and Shapshay 2005) and bleeding from radiation therapy induced proctocolitis (Ventrucci *et al* 2001). Furthermore, the Nd:YAG laser (contact and free beam) was equally effective as bipolar electrocoagulation in the endoscopic treatment of upper gastrointestinal bleeding lesions (Goff 1986, Hui *et al* 1991) and as monopolar electrosurgery of the endometrium (Phillips 1994) in women. Laser surgery has been applied in laparoscopic cholecystectomy (Lane and Lathrop 1993, Evangelou *et al* 1996, Kostewicz and Hara 1996) with varying results, but is not widely used because of the relatively large blood vessels that can not be properly transected using a laser. Lasers are still under investigation in the development of a laparoscopic partial nephrectomy technique (Ogan *et al* 2002, Anderson *et al* 2007).

The use of Nd:YAG and CO_2 lasers is relatively widespread in otolaryngology, head and neck surgery and tracheobronchoscopic surgery (Brown 2000, Janda *et al* 2001, Oswal and Remacle 2002, Mair *et al* 2003, McQueen and Cullen 2003, Price *et al* 2007), and in laparoscopic gynecology (Takkar and Sinha 2002) for the treatment of endometriosis (Kristensen and Kjer 2007, Slack *et al* 2007) and adhesiolysis (Stratton *et al* 2002, Parker *et al* 2005), myomectomy (Kaseki *et al* 2001), hysterectomy (Karaman *et al* 2007), fallopian tube transaction (Erian *et al* 2005) and fetal surgery (Bussey *et al* 2004, Hecher *et al* 2006). Endoscopic laser surgery has several applications in urology (Pietrow and Smith 2001, Gurdal *et al* 2003) and is a common treatment for benign prostatic hyperplasia (BPH) in men (Tan and Gilling 2003, Tan and Gilling 2005).

5.3   *Wound healing*

Wound healing after laser surgery and electrosurgery mainly depends on the amount of inflicted tissue injury and char formation (Shapshay 1987, Laranne *et al* 1997a, Sinha and Gallagher 2003), and will therefore typically be slower compared to scalpel wounds. Swelling and edema have been mentioned to be less in contact laser surgery incisions

compared to scalpel wounds, due to minimal deep tissue damage and coagulation of small capillaries and lymphatics (Fankhauser and Kwasniewska 2002, Lucroy and Bartels 2003). In a primary cutaneous wound-healing model in rats, contact-laser incisions showed increased numbers of inflammatory cells and delayed fibroblast invasion compared to scalpel wounds up to 14 days and reduced tensile strength up to 21 days (Taylor *et al* 1997). On the other hand, it was shown that skin wound healing depended on the amount of thermal damage and that wound healing occurred within normal duration (i.e. about 9 days) using adequate power density and speed of incising (Sultan and Boulnois 1989). A study of contact mode incisions in rabbit liver showed good hemostasis and relatively shallow acute tissue damage surrounding the incision (~1.0 mm, hyperemic zone included) which did not increase in the next 48 hours (~1.0 mm necrosis, surrounded by inflammatory cells), indicating that tissue damage extent did not exceed the initial visible damage in the acute stage. By 21 days, fibrous tissue lined the incisions and no inflammatory cells were present (Judy *et al* 1993). As a comparison, long duration exposure in LITT (10-20 minutes) can cause delayed necrosis which develops during the following 1-3 days. This delayed necrosis is caused by prolonged supraphysiological temperatures, leading to both sub-lethal damage and lethal (non-coagulative) cell death, which is not surprising since development of tissue damage generally obeys an Arrhenius-like relation of temperature and exposure time (Section 4).

It is concluded from Section 5.1 and 5.3 that surgical technique is a key factor in controlling tissue damage. An incorrect laser-incision technique can cause unacceptable thermal damage and charring and non-contact exposure can lead to extensive necrosis and delayed healing of tissues (Shapshay 1987, Laranne *et al* 1997a). Depending on the desired effect, the same standards should be considered as in general surgery regarding tissue handling, when using laser surgery for precise dissection of delicate tissues. Off course, a compromise is made in order to obtain hemostasis. Nevertheless, carbonization should be minimized and coagulation controlled at the required level (i.e. hemostasis). Power density, used for contact mode cutting is determined by tip-size and laser power. In contact mode, damage depth will increase with increasing laser power (Sultan and Boulnois 1989) but increasing power will not necessarily improve cutting and may increase char formation and the risk of unintended non-contact coagulation damage. Furthermore, a smaller tip causes less spread of thermal damage in contact mode incisions (Judy *et al* 1993) and can be used for more precise cutting.

Different strategies are used in coagulation and ablation procedures for bleeding lesions and tumors, in which carbonization does not have to be a problem, such as in secondary wound healing with sloughing of necrotized tissue.

6   The Nd:YAG laser for prostate surgery in dogs

Prostate surgery in dogs mainly concerns (para-) prostatic cysts and abscesses. Most indications do not require a total prostatectomy but are properly dealt with by draining, omentalization, or partial lobectomy. A problem arises however, with the occurrence of prostate carcinoma (PCA), a very aggressive, infiltrative, malignant tumor showing a high metastatic rate (Bell *et al* 1991, Cornell *et al* 2000). In the early stage, a total prostatectomy would be preferred, combined with an adjuvant anti-tumor treatment. Unfortunately, the incidence of urinary incontinence after total prostatectomy of diseased prostates is unacceptably high in dogs (Hardie *et al* 1984, Basinger *et al* 1989, Goldsmid and Bellenger 1991). It is unclear if this is caused by injury to the neurovascular supply of the prostate and proximal urethra (Figure 10), removal of the prostatic urethra, the underlying disease process or a combination of these factors. However, the incidence of urinary incontinence is seemingly not a problem after prostatectomy in normal dogs (Basinger *et al* 1987). This suggests that the primary disease plays a role in the pathogenesis of urinary incontinence in dogs with prostate carcinoma. In contrast, urinary incontinence is rare after total prostatectomy for prostate carcinoma in humans (~6-8%) (Cespedes and Swanson 1998, Catalona *et al* 1999, Burkhard *et al* 2006, Pierorazio *et al* 2007), although relatively high incontinence rates are also observed (Cambio and Evans 2006). The mechanism responsible for postoperative incontinence in humans is uncertain (Cambio and Evans 2006, Majoros *et al* 2006), but the importance of the urethral sphincter mechanism, which also involves the prostatic urethra, is generally emphasized and attempts are made to spare the prostatic urethra to a maximum (Vashi and Oesterling 1998, Gaker and Steel 2004).

A recent clinical study in men indicated that preoperative sphincter weakness might be a predisposing factor for postoperative incontinence (Majoros *et al* 2006). Furthermore, Burkhard *et al* (2006) (Kessler *et al* 2007) found that nerve sparing radical prostatectomy in men, in which the neurovascular supply of the corpora cavernosa is spared to maintain erectile function, also improved postoperative continence. Recent investigations of neurovascular anatomy and function in men have lead to new insights in the continence mechanism and the origin of incontinence after radical prostatectomy in men (Kessler *et al* 2007). Autonomic nerve fibres from the pelvic plexus, both afferent and efferent fibres, innervate the rectum and the urogenital tract and end as the *paraprostatic neurovascular bundle* before supplying the urogenital diaphragm, sphincter, and corpora cavernosa (Figure 9). Somatic fibers in an intra- and extra-pelvic branch of the pudendal nerve innervate the external urethral sphincter. Additional intrapelvic extrapudendal nerve fibres from S2–S3 pass lateral to the pelvic plexus and then continue along the dorsolateral

surface of the rectum until they disappear into the levator ani muscle and terminate in the external urethral sphincter (Akita *et al* 2003). Autonomic nerve branches of the pelvic plexus innervate the smooth muscle of the bladder neck and urethra sphincter mechanism. Stimulation of the neurovascular bundle has been shown to increase urethral pressure (Nelson *et al* 2003). A third group of important nerves are afferent fibers of the membranous urethra which sense the presence of urine in the proximal urethra and initiate urethral sphincter closure (either conscious or by a spinal reflex). These nerve fibers are thought to join branches of the pelvic plexus or intrapelvic pudendus, which are both prone to injury during radical prostatectomy (Kessler *et al* 2007) (Figure 9).
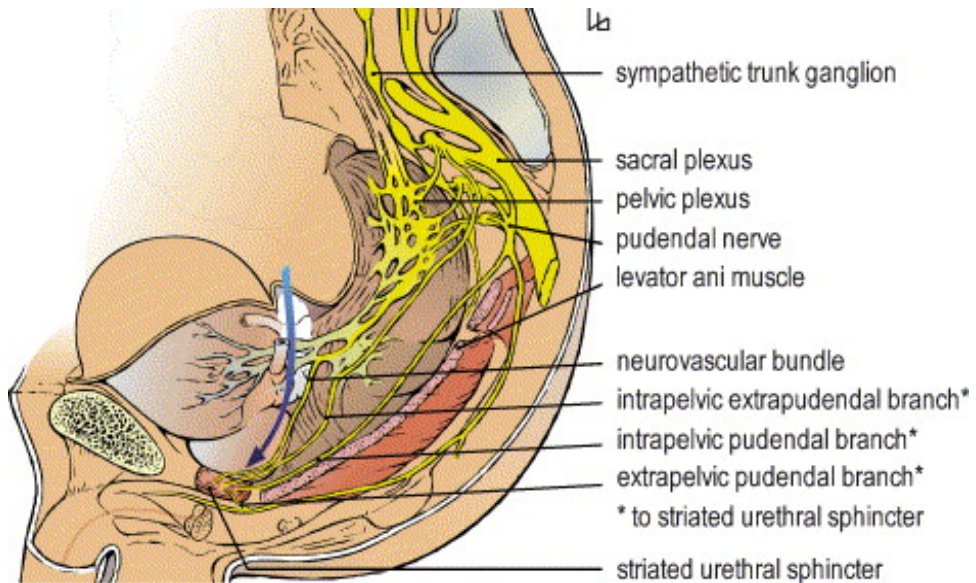
Figure 9: Nerve supply of pelvic structures in men. The arrow indicates the line of dissection when performing nerve-sparing radical prostatectomy (Kessler *et al* 2005).

Because of these findings nerve sparing prostatectomy is currently performed whenever possible with prostate carcinoma (i.e. no tumor involvement). The neurovascular bundles are meticulously separated from the dorsolateral prostatic capsule. Electrosurgery or ultrasonic energy should be avoided (Kessler *et al* 2007). In an experimental study in dogs (Ong *et al* 2004) and a clinical trial in men (Gill and Ukimura 2007), the use of electrosurgery and ultrasonic energy for hemostasis during dissection of the neurovascular bundle resulted in major disturbances of erectile function compared to conventional subtle blunt separation with ligation of vessels entering the prostate (see also Section 5.1). Figure

10 shows the nerve supply to the canine pelvic structures. Because of the anatomical similarity of the pelvic structures in dog and man, comparable considerations should probably be taken into account in order to preserve continence after prostatectomy in dogs.
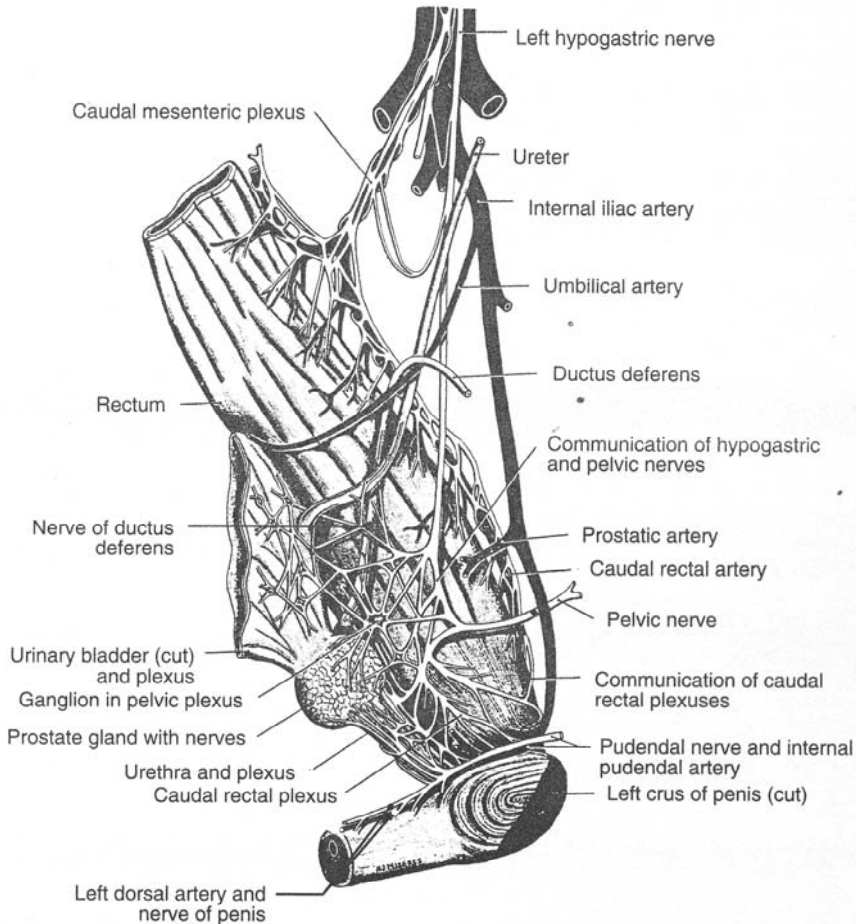
Figure 10: Nerve supply of the canine prostate, bladder neck and urethra (Anderson W. D. and G. 1994).

Attempts are made to treat canine prostate carcinoma, but results tend to be disappointing and a definitive therapy is not at hand (Fan and Lorimier 2007). In order to maintain continence in dogs with severe, but benign, disease of the prostate such as cystic enlargement and abscesses, a partial prostatectomy technique with preservation of the dorsolateral capsule and prostatic urethra was developed. This technique resulted in resolution of disease without major postoperative incontinence problems (Rawlings *et al* 1997).

In dogs with prostate carcinoma, partial prostatectomy with preservation of the prostatic urethra and dorsolateral capsule with associated neurovascular supply may help to maintain normal urinary tract function postoperatively (Figure 11). This procedure may be used as a palliative treatment for otherwise untreatable dogs. Furthermore, it could be part of a multi-modal anti-tumor treatment in which removal of as much diseased tissue as possible (debulking) is combined with adjuvant cancer therapy to destroy remaining neoplastic cells. Meticulous resection of prostate tissue adjacent to delicate tissue structures (neurovascular structures and urethra) is indicated in order to facilitate maximal clinical results in such a combined treatment.
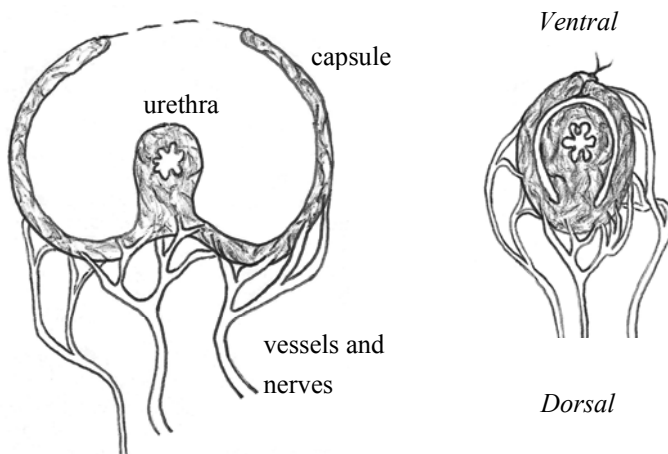
Figure 11: Subcapsular partial prostatectomy. Schematic cross section through the canine prostate (dog in dorsal recumbency). The major part of parenchyma has been resected using a ventral approach, leaving urethra and prostate capsule with associated neurovascular structures intact (left figure). Excess of ventral capsule is resected and the capsule is sutured together over the urethra (right figure).

Because the Nd:YAG laser is capable of relatively precise incisional surgery in parenchymatous tissues while maintaining appropriate hemostasis (Section 5.1), it is hypothesized that it can be successfully used in subcapsular partial prostatectomy in dogs.
Prior to a clinical study of subcapsular partial prostatectomy in dogs using the Nd:YAG surgical laser in Chapter 4, the effects of Nd:YAG laser in ex vivo prostate tissue are described in Chapter 3, evaluating the level of tissue damage in contact and non-contact mode to provide guidelines in clinical practice. Color schlieren imaging is used in Chapter 2 to obtain initial understanding of these laser-tissue effects, which are not directly visible in tissues during laser surgery and an attempt is made to use the schlieren technique as a model for laser-tissue interaction.

7   The Nd:YAG laser in laparoscopy of dogs and cats

In order to improve clinical outcomes, reduce patient morbidity and surgical duration and shorten recovery period, minimally invasive operating techniques are developed. Laparoscopy is nowadays an established approach for many surgical and diagnostic procedures in human medicine, and has become the method of choice for several standard operations such as cholecystectomy (Perissat 1995) and nephrectomy (Ono *et al* 2005). In veterinary medicine, laparoscopy is an emerging technique, which is applied in a growing number of diagnostic and surgical procedures in dogs (Freeman 1999, Monnet and Twedt 2003), such as exploratory laparoscopy to observe organs and obtain biopsies of tissues, cryptorchidectomy, ovari(ohyster)ectomy, gastrointestinal foreign body removal, placement of jejunostomy feeding tubes (Hewitt *et al* 2004), gastropexy (Rawlings *et al* 2001), cholecystectomy (Murphy *et al* 2007) and adrenalectomy. Also emerging in veterinary surgery are thoracoscopic procedures, such as pericardectomy (Dupre *et al* 2001), ductus thoracicus ligation (Radlinsky *et al* 2002), closure of persistent ductus arteriosus (Borenstein *et al* 2004) and lung surgery (Brissot *et al* 2003, Lansdowne *et al* 2005). Furthermore, the dog is used as a model for laparoscopic approaches in human medicine. In contrast to the dog, laparoscopy in cats is not commonly practiced and is generally limited to diagnostic use and cryptorchidectomy (Vannozzi *et al* 2002, Miller *et al* 2004).

The minimally-invasive nature of these and other procedures consequently limits the range of suitable instruments, being applied through trocars of limited diameter. In laparoscopic and endoscopic surgery, there is a high demand for instruments able to conduct hemostasis without the need for ligatures. Furthermore, tissue resection is preferably performed in a hemostatic manner to avoid complications due to blood loss and to maintain a clean and clear surgical field. Several laparoscopic instruments are utilized for sole hemostatic purpose: ligature and loop devices, endoscopic vascular clips and staplers and bipolar forceps. Monopolar devices can also facilitate dissection. Endoscopic electrosurgical devices greatly improve hemostasis in laparoscopy. However, monopolar electrosurgery has been associated with alternate site burns (Hunter 1992) and generally induces more collateral tissue damage and poor hemostasis compared to other hemostatic devices (Lantis *et al* 1998) (see also Section 5.1). Nowadays, capacitive coupling, insulation failure and patient-grounding failure are mostly detected by the electrosurgery unit, and alternate site burns are mainly induced by making contact with metal instruments which conduct energy to tissues in contact (often not in the camera field), and with surgery of thin or pedicle-like tissue structures in which relatively high temperature (read: high current density) can develop away from the contact site (Hunter 1992, Odell 1995). In laparoscopic ovariectomy

in dogs, monopolar electrocoagulation increased surgery time and intraoperative bleeding compared to bipolar electrocoagulation (Van Goethem *et al* 2003). Because of its incisional, hemostatic and coagulating abilities and its delivery through a flexible optical fiber, the Nd:YAG laser is perfectly suited to be used in companion animal laparoscopic surgery, but its application in clinical cases has not yet been described.

In Chapters 5, 6 and 7the Nd:YAG laser is evaluated in a clinical setting for laparoscopic ovariectomy in dogs and cats. It was hypothesized that the laser could further improve the procedure through enhanced hemostatic excision of the ovaries and increased ease and speed of surgery. Furthermore, laser laparoscopic ovariectomy is introduced in cats in Chapter 7.In Chapters 5 and 7, the Nd:YAG laser is compared to the standard technique using bipolar forceps and endoscopic scissors. In Chapter 6 a new bipolar device is introduced which combines electrocoagulation and sharp incision in one instrument.

References

Akita K, Sakamoto H and Sato T (2003) Origins and courses of the nervous branches to the male urethral sphincter *Surg Radiol Anat* **25** 387-92

Anderson J K, Baker M R, Lindberg G and Cadeddu J A (2007) Large-volume laparoscopic partial nephrectomy using the potassium-titanyl-phosphate (KTP) laser in a survival porcine model *Eur Urol* **51** 749-54

Anderson W. D. and G. A B (1994). Atlas of canine anatomy. Philadelphia, Lea & Febiger.

Anvari B, Rastegar S and Motamedi M (1994) Modeling of intraluminal heating of biological tissue: implications for treatment of benign prostatic hyperplasia *IEEE Trans Biomed Eng* **41** 854-64

Atkins P W (1998). Physical Chemistry, 6th ed. Oxford, Oxford University Press.

Basinger R R, Rawlings C A and Barsanti J A (1989) Urodynamic Alterations Associated with Clinical Prostatic Diseases and Prostatic Surgery *J Am Anim Hosp Assoc* **25** 385-92

Basinger R R, Rawlings C A, Barsanti J A, Oliver J E, Jr. and Crowell W A (1987) Urodynamic alterations after prostatectomy in dogs without clinical prostatic disease *Vet Surg* **16** 405-10

Bell F W, Klausner J S, Hayden D W, Feeney D A and Johnston S D (1991) Clinical and pathologic features of prostatic adenocarcinoma in sexually intact and castrated dogs: 31 cases (1970-1987) *J Am Vet Med Assoc* **199** 1623-30

Bellina J H, Hemmings R, Voros J I and Ross L F (1984) Carbon dioxide laser and electrosurgical wound study with an animal model: a comparison of tissue damage and healing patterns in peritoneal tissue *Am J Obstet Gynecol* **148** 327-34

Bhowmick P, Coad J E, Bhowmick S, Pryor J L, Larson T, de la Rosette J and Bischofs J C (2004) In vitro assessment of the efficacy of thermal therapy in human benign prostatic hyperplasia. *Int J Hyperthermia* **4** 421-39

Bischof J C and He X (2005) Thermal stability of proteins *Ann N Y Acad Sci* **1066** 12-33

Bohm B, Milsom J W, Kitago K, Brand M and Fazio V W (1994a) Laparoscopic oncologic total abdominal colectomy with intraperitoneal stapled anastomosis in a canine model *J Laparoendosc Surg* **4** 23-30

Bohm B, Milsom J W, Kitago K, Brand M and Fazio V W (1994b) Monopolar electrosurgery and Nd:YAG Contact Laser in laparoscopic intestinal surgery *Surg Endosc* **8** 677-81

Bohm B, Milsom J W, Kitago K, Brand M, Stolfi V M and Fazio V W (1995) Use of laparoscopic techniques in oncologic right colectomy in a canine model *Ann Surg Oncol* **2** 6-13

Borenstein N, et al. (2004) Minimally invasive patent ductus arteriosus occlusion in 5 dogs *Vet Surg* **33** 309-13

Brdecka D, Rawlings C, Howerth E, Cornell K and Stiffler K (2007) A histopathological comparison of two techniques for soft palate resection in normal dogs *J Am Anim Hosp Assoc* **43** 39-44

Brissot H N, Dupre G P, Bouvy B M and Paquet L (2003) Thoracoscopic treatment of bullous emphysema in 3 dogs *Vet Surg* **32** 524-9

Brown D H (2000) The versatile contact Nd:YAG laser in head and neck surgery: an in vivo and clinical analysis *Laryngoscope* **110** 854-67

Burkhard F C, Kessler T M, Fleischmann A, Thalmann G N, Schumacher M and Studer U E (2006) Nerve sparing open radical retropubic prostatectomy--does it have an impact on urinary continence? *J Urol* **176** 189-95

Bussey J G, Luks F, Carr S R, Plevyak M and Tracy T F, Jr. (2004) Minimal-access fetal surgery for twin-to-twin transfusion syndrome *Surg Endosc* **18** 83-6

Cambio A J and Evans C P (2006) Minimising postoperative incontinence following radical prostatectomy: considerations and evidence *Eur Urol* **50** 903-13; discussion 13

Catalona W J, Carvalhal G F, Mager D E and Smith D S (1999) Potency, continence and complication rates in 1,870 consecutive radical retropubic prostatectomies *J Urol* **162** 433-8

Cespedes R D and Swanson D A (1998) Complications of Radical Prostatectomy *Surgery of the Prostate* ed M I Resnick and I M Thompson (New York: Churchill Livingstone Inc.) pp 181-95

Cheong W F (1995) Summary of Optical Properties *Optical-Thermal Response of Laser-Irradiated Tissue* ed A J Welch and M J C van Gemert (New York: Plenum Press) pp 275-303

Chinali G, Ferulano G P, Vanni L, Fresini A, Califano G and Bocchini V (1983) Liver regeneration after atypical hepatectomy in the rat. A comparison of CO2 laser with scalpel and electrical diathermy *Eur Surg Res* **15** 284-8

Cornell K K, et al. (2000) Clinical and pathologic aspects of spontaneous canine prostate carcinoma: a retrospective analysis of 76 cases *Prostate* **45** 173-83

Cromeens D M, Johnson D E, Stephens L C and Gray K N (1996) Visual laser ablation of the canine prostate with a diffusing fiber and an 805-nanometer diode laser *Lasers Surg Med* **19** 135-42

Cromeens D M, Price R E and Johnson D E (1994) Pathologic changes following transurethral canine prostatectomy with a cylindrically diffusing fiber *Lasers Surg Med* **14** 306-13

Diller K R and Pearce J A (1999) Issues in modeling thermal alterations in tissues *Ann N Y Acad Sci* **888** 153-64

Dupre G P, Corlouer J P and Bouvy B (2001) Thoracoscopic pericardectomy performed without pulmonary exclusion in 9 dogs *Vet Surg* **30** 21-7

Einstein A (1917) Quantentheorie der Strahlung *Physikalische Zeitschrift* **18** 121-8

Emam T A and Cuschieri A (2003) How safe is high-power ultrasonic dissection? *Ann Surg* **237** 186-91

Erian J, El-Toukhy T, Chandakas S, Hill N C and Theodoridis T (2005) Laparoscopic laser sterilisation: an alternative option *J Obstet Gynaecol* **25** 681-4

Evangelou G N, Stathakos H P, Baltayiannis N E and Gonianakis G I (1996) Argon coagulation in laparoscopic cholecystectomy *Surg Endosc* **10** 414-7

Fan T M and Lorimier L (2007) Tumors of the Male Reproductive System *Whithrow and Macewen's Small Animal Clinical Oncology* ed S J Withrow and D M Vail (St. Louis: Saunders) pp 637-48

Fankhauser F and Kwasniewska S (2002) Applications of the neodymium:YAG laser in plastic surgery of the face and lacrimal surgery. Wound repair. A review *Ophthalmologica* **216** 381-98

Freeman L J (ed) (1999) *Veterinary Endosurgery* (St. Louis: Mosby, Inc.)

Gaker D L and Steel B L (2004) Radical prostatectomy with preservation of urinary continence: pathology and long-term results *J Urol* **172** 2549-52

Gill I S and Ukimura O (2007) Thermal energy-free laparoscopic nerve-sparing radical prostatectomy: one-year potency outcomes *Urology* **70** 309-14

Goff J S (1986) Bipolar electrocoagulation versus Nd-YAG laser photocoagulation for upper gastrointestinal bleeding lesions *Dig Dis Sci* **31** 906-10

Goldsmid S E and Bellenger C R (1991) Urinary incontinence after prostatectomy in dogs *Vet Surg* **20** 253-6

Gurdal M, Tekin A, Yucebas E, Kirecci S and Sengor F (2003) Contact neodymium: YAG laser ablation of recurrent urethral strictures using a side-firing fiber *J Endourol* **17** 791-4

Hardie E M, Barsanti J A and Rawlings C A (1984) Complications of Prostatic Surgery *J Am Anim Hosp Assoc* **20** 50-6

He X, Wolkers W F, Crowe J H, Swanlund D J and Bischof J C (2004) In situ thermal denaturation of proteins in dunning AT-1 prostate cancer cells: implication for hyperthermic cell injury *Ann Biomed Eng* **32** 1384-98

Hecher K, Lewi L, Gratacos E, Huber A, Ville Y and Deprest J (2006) Twin reversed arterial perfusion: fetoscopic laser coagulation of placental anastomoses or the umbilical cord *Ultrasound Obstet Gynecol* **28** 688-91

Heisterkamp J, van Hillegersberg R and Ijzermans J N (1999) Interstitial laser coagulation for hepatic tumours *Br J Surg* **86** 293-304

Henriques F C (1947) Studies of thermal injury V: The predictability and significance of thermally induced rate processes leading to irreversible epidermal injury. *Arch Pathol* **43** 489-502

Hewitt S A, Brisson B A, Sinclair M D, Foster R A and Swayne S L (2004) Evaluation of laparoscopic-assisted placement of jejunostomy feeding tubes in dogs *J Am Vet Med Assoc* **225** 65-71

Hillegersberg R (1993). Laser Treatment for Liver Metastases - Thermal and Photodynamic Therapy. Rotterdam, the Netherlands, Erasmus university.

Hui W M, Ng M M, Lok A S, Lai C L, Lau Y N and Lam S K (1991) A randomized comparative study of laser photocoagulation, heater probe, and bipolar electrocoagulation in the treatment of actively bleeding ulcers *Gastrointest Endosc* **37** 299-304

Hunter J G (1992) Laser use in laparoscopic surgery *Surg Clin North Am* **72** 655-64

Jacques S L (1992) Laser-tissue interactions. Photochemical, photothermal, and photomechanical *Surg Clin North Am* **72** 531-58

Janda P, Sroka R, Baumgartner R, Grevers G and Leunig A (2001) Laser treatment of hyperplastic inferior nasal turbinates: a review *Lasers Surg Med* **28** 404-13

Janda P, Sroka R, Mundweil B, Betz C S, Baumgartner R and Leunig A (2003) Comparison of thermal tissue effects induced by contact application of fiber guided laser systems *Lasers Surg Med* **33** 93-101

Jiang S C and Zhang X X (2005) Dynamic modeling of photothermal interactions for laser-induced interstitial thermotherapy: parameter sensitivity analysis *Lasers Med Sci* **20** 122-31

Joffe S N (1989) Liver Resection *Lasers in General Surgery* ed S N Joffe (Baltimore: Wiliams & Wilkinson) pp 82-95

Judy M M, Matthews J L, Aronoff B L and Hults D F (1993) Soft tissue studies with 805 nm diode laser radiation: thermal effects with contact tips and comparison with effects of 1064 nm Nd:YAG laser radiation *Lasers Surg Med* **13** 528-36

Kabalin J N (1998) Laser prostatectomy: Free Beam *Surgery of the Prostate* ed M I Reshnick and I M Thompson (New York: Churchill Livingstone Inc.) pp 267-82

Kabalin J N, Gong M, Issa M M and Sellers R (1995) Insight into mechanism of neodymium: yttrium-aluminum-garnet laser prostatectomy utilizing the high-power contact-free beam technique *Urology* **45** 421-6

Karaman Y, Bingol B and Gunenc Z (2007) Prevention of complications in laparoscopic hysterectomy: experience with 1120 cases performed by a single surgeon *J Minim Invasive Gynecol* **14** 78-84

Kaseki H, Araki T and Valle R F (2001) Laser Hysteroscopic Myomectomy Guided by Laparoscopically Assisted Intra-Abdominal Sonohysterography (LHMY-GLAIS): A Preliminary Report *Journal of Gynecologic Surgery* **17** 79-86

Kessler T M, Burkhard F C and Studer U E (2005) Clinical indications and outcomes with nerve-sparing cystectomy in patients with bladder cancer *Urol Clin North Am* **32** 165-75

Kessler T M, Burkhard F C and Studer U E (2007) Nerve-sparing open radical retropubic prostatectomy *Eur Urol* **51** 90-7

Kinoshita T, Kanehira E, Omura K, Kawakami K and Watanabe Y (1999) Experimental study on heat production by a 23.5-kHz ultrasonically activated device for endoscopic surgery *Surg Endosc* **13** 621-5

Kostewicz W and Hara M (1996) [Laser laparoscopic cholecystectomy] [abstract] *Pol Tyg Lek* **51** 198-9

Kristensen J and Kjer J J (2007) Laparoscopic laser resection of rectovaginal pouch and rectovaginal septum endometriosis: the impact on pelvic pain and quality of life *Acta Obstet Gynecol Scand* **86** 1467-71

Kuntzman R S, Malek R S, Barrett D M and Bostwick D G (1996) Potassium-titanyl-phosphate laser vaporization of the prostate: a comparative functional and pathologic study in canines *Urology* **48** 575-83

Kuntzman R S, Malek R S, Barrett D M and Bostwick D G (1997) High-power (60-watt) potassium-titanyl-phosphate laser vaporization prostatectomy in living canines and in human and canine cadavers *Urology* **49** 703-8

Lane G E and Lathrop J C (1993) Comparison of results of KTP/532 laser versus monopolar electrosurgical dissection in laparoscopic cholecystectomy *J Laparoendosc Surg* **3** 209-14

Lansdowne J L, Monnet E, Twedt D C and Dernell W S (2005) Thoracoscopic lung lobectomy for treatment of lung tumors in dogs *Vet Surg* **34** 530-5

Lantis J C, II, Durville F M, Connolly R and Schwaitzberg S D (1998) Comparison of coagulation modalities in surgery *J Laparoendosc Adv Surg Tech A* **8** 381-94

Laranne J, Lagerstedt A, Pukander J and Rantala I (1997a) Wound healing and soft tissue effects of CO2, contact Nd: YAG and combined CO2-Nd: YAG laser beams on rabbit trachea *Acta Otolaryngol* **117** 909-17

Laranne J, Lagerstedt A, Pukander J, Rantala I, Hanamure Y and Ohyama M (1997b) Immediate histological changes in soft palate after uvulopalatopharyngoplasty with CO2, contact Nd:YAG or combined CO2 and Nd:YAG laser beams *Acta Otolaryngol Suppl* **529** 206-9

Lippert B M, Teymoortash A, Folz B J and Werner J A (2003) Coagulation and temperature distribution in Nd: YAG interstitial laser thermotherapy: an in vitro animal study *Lasers Med Sci* **18** 19-24

Litwin G D and Kirpitchev A G (1991) Lasers in surgical hepatology *J Clin Laser Med Surg* **9** 201-4

Lucroy M D and Bartels K E (2003) Surgical Lasers *Slatter: Textbook of Small Animal Surgery, 3rd ed.* ed (USA: Elsevier Science) pp 227-35

Mahoney E J and Shapshay S M (2005) Nd-YAG laser photocoagulation for epistaxis associated with hereditary hemorrhagic telangiectasia *Laryngoscope* **115** 373-5

Mair E A, Battiata A and Casler J D (2003) Endoscopic laser-assisted excision of juvenile nasopharyngeal angiofibromas *Arch Otolaryngol Head Neck Surg* **129** 454-9

Majoros A, Bach D, Keszthelyi A, Hamvas A and Romics I (2006) Urinary incontinence and voiding dysfunction after radical retropubic prostatectomy (prospective urodynamic study) *Neurourol Urodyn* **25** 2-7

Mason G R (1989) Hepatic resection technique *Am J Surg* **157** 343-5

McQueen C T and Cullen R D (2003) Endoscopic ablation of distal tracheal lesions using Nd:YAG contact laser *Int J Pediatr Otorhinolaryngol* **67** 181-3

Mecke H, Schunke M, Schnaidt S, Freys I and Semm K (1991) Width of thermal damage after using the YAG contact laser for cutting biological tissue: animal experimental investigation *Res Exp Med (Berl)* **191** 37-45

Miller N A, Van Lue S J and Rawlings C A (2004) Use of laparoscopic-assisted cryptorchidectomy in dogs and cats *J Am Vet Med Assoc* **224** 875-8, 65

Monnet E and Twedt D C (2003) Laparoscopy *Vet Clin North Am Small Anim Pract* **33** 1147-63

Moritz A R and Henriques F C (1947) Studies of thermal injury II: The relative importance of time and surface temperature in the causation of cutaneous burns *Am J Pathol* **23** 695-720

Motamedi M, Torres J H, Orihuela E, Pow-Sang M, Cowan D F and Warren M M (1995) Laser photocoagulation of prostate: influence of dosimetry *Lasers Surg Med* **17** 49-58

Murphy S M, Rodriguez J D and McAnulty J F (2007) Minimally invasive cholecystostomy in the dog: evaluation of placement techniques and use in extrahepatic biliary obstruction *Vet Surg* **36** 675-83

Nau W H, Roselli R J and Milam D F (1999) Measurement of thermal effects on the optical properties of prostate tissue at wavelengths of 1,064 and 633 nm *Lasers Surg Med* **24** 38-47

Nelson C P, Montie J E, McGuire E J, Wedemeyer G and Wei J T (2003) Intraoperative nerve stimulation with measurement of urethral sphincter pressure changes during radical retropubic prostatectomy: a feasibility study *J Urol* **169** 2225-8

Nikfarjam M and Christophi C (2003) Interstitial laser thermotherapy for liver tumours *Br J Surg* **90** 1033-47

Nikfarjam M, Malcontenti-Wilson C and Christophi C (2005) Comparison of 980- and 1064-nm wavelengths for interstitial laser thermotherapy of the liver *Photomed Laser Surg* **23** 284-8

Odell R C (1995) Electrosurgery in Laparoscopy *Principles of Laparoscopic Surgery: Basic and Advanced Techniques* ed M E Arregui (New York: Springer-Verlag) pp 732-9

Ogan K, Wilhelm D, Lindberg G, Lotan Y, Napper C, Hoopman J, Pearle M S and Cadeddu J A (2002) Laparoscopic partial nephrectomy with a diode laser: porcine results *J Endourol* **16** 749-53

Ong A M, Su L M, Varkarakis I, Inagaki T, Link R E, Bhayani S B, Patriciu A, Crain B and Walsh P C (2004) Nerve sparing radical prostatectomy: effects of hemostatic energy sources on the recovery of cavernous nerve function in a canine model *J Urol* **172** 1318-22

Ono Y, Hattori R, Gotoh M, Yoshino Y, Yoshikawa Y and Kamihira O (2005) Laparoscopic radical nephrectomy for renal cell carcinoma: the standard of care already? *Curr Opin Urol* **15** 75-8

Oraevsky A A, Jacques S L and Tittel F K (1997) Measurement of tissue optical properties by time-resolved detection of laser-induced transient stress *Applied Optics* **36** 402-15

Orihuela E, Motamedi M, Cammack T, Torres J H, Pow-Sang M, Lahaye M, Cowan D F and Warren M M (1995) Comparison of thermocoagulation effects of low power, slow heating versus high power, rapid heating Nd: YAG laser regimens in a canine prostate model *J Urol* **153** 196-200

Oswal V and Remacle M (2002). Lasers in Otorhinolaryngology and Head and Neck Surgery. The Hague, Kugler Publications.

Owaki T, Nakano S, Arimura K and Aikou T (2002) The ultrasonic coagulating and cutting system injures nerve function *Endoscopy* **34** 575-9

Parker J D, Sinaii N, Segars J H, Godoy H, Winkel C and Stratton P (2005) Adhesion formation after laparoscopic excision of endometriosis and lysis of adhesions *Fertil Steril* **84** 1457-61

Pearce J and Thomsen S (1995) Rate process analysis of thermal damage *Optical-Thermal Response of Laser-Irradiated Tissue* ed A J Welch and M J C van Gemert (New York: Plenum) pp 562-606

Peavy G M (2002) Lasers and laser-tissue interaction *Vet Clin North Am Small Anim Pract* **32** 517-34, v-vi

Pedrotti F L and Pedrotti L S (1996). Introduction to optics, 2nd ed. Englewood Cliffs, New Jersey, Prentice Hall Inc.

Perissat J (1995) The Development of Laparoscopi Cholecystectomy abd its Impact *principles of Laparoscopic Surgery: Basic and Advanced Techniques* ed M E Arregui (New York: Springer-Verlag) pp 110-2

Perlmutter A P and Muschter R (1998) Interstitial laser prostatectomy *Mayo Clin Proc* **73** 903-7

Perry D A, Goodis H E and White J M (1997) In vitro study of the effects of Nd:YAG laser probe parameters on bovine oral soft tissue excision *Lasers Surg Med* **20** 39-46

Philipp C M, Rohde E and Berlien H P (1995) Nd:YAG laser procedures in tumor treatment *Semin Surg Oncol* **11** 290-8

Phillips D R (1994) A comparison of endometrial ablation using the Nd:YAG laser or electrosurgical techniques *J Am Assoc Gynecol Laparosc* **1** 235-9

Pierorazio P M, Spencer B A, McCann T R, McKiernan J M and Benson M C (2007) Preoperative risk stratification predicts likelihood of concurrent PSA-free survival,

continence, and potency (the trifecta analysis) after radical retropubic prostatectomy *Urology* **70** 717-22

Pierre S A and Albala D M (2007) The future of lasers in urology *World J Urol* **25** 275-83

Pietrow P K and Smith J A, Jr. (2001) Laser treatment for invasive and noninvasive carcinoma of the bladder *J Endourol* **15** 415-8; discussion 25-6

Price T T, Sharma A and Montgomery P Q (2007) How we do it: vocal cord Nd-YAG laser surgery, under local anaesthetic, using a flexible trans-nasal laryngo-oesophagoscope *Lasers Med Sci* **22** 127-30

Radlinsky M G, Mason D E, Biller D S and Olsen D (2002) Thoracoscopic visualization and ligation of the thoracic duct in dogs *Vet Surg* **31** 138-46

Rawlings C A, Foutz T L, Mahaffey M B, Howerth E W, Bement S and Canalis C (2001) A rapid and strong laparoscopic-assisted gastropexy in dogs *Am J Vet Res* **62** 871-5

Rawlings C A, Mahaffey M B, Barsanti J A, Quandt J E, Oliver J E, Jr., Crowell W A, Downs M O, Stampley A R and Allen S W (1997) Use of partial prostatectomy for treatment of prostatic abscesses and cysts in dogs *J Am Vet Med Assoc* **211** 868-71

Rem A I, Oosterhuis J A, Journee-de Korver J G, van den Berg T J T P and Keunen J E E (2001) Temperature Dependence of Thermal Damage to the Sclera: Exploring the Heat Tolerance of the Sclera for Transscleral Thermotherapy. *Exp Eye Res* **72** 153-62

Ritz J P, Roggan A, Germer C T, Isbert C, Muller G and Buhr H J (2001) Continuous changes in the optical properties of liver tissue during laser-induced interstitial thermotherapy *Lasers Surg Med* **28** 307-12

Schmittenbecher P P (1990) The neodymium YAG laser in surgery of parenchymatous organs in childhood *Prog Pediatr Surg* **25** 23-31

Schneider P D (1992) Liver Resection and Laser Hyperthermia *The Surgical Clinics of North America* **72** 623-39

Schroder T, Brackett K and Joffe S N (1987a) An experimental study of the effects of electrocautery and various lasers on gastrointestinal tissue *Surgery* **101** 691-7

Schroder T, Brackett K and Joffe S N (1987b) Proximal pancreatectomy: a comparison of electrocautery and contact and noncontact Nd:YAG laser techniques in the dog *Am J Surg* **154** 493-8

Schroder T, Hasselgren P O, Brackett K and Joffe S N (1987c) Techniques of liver resection. Comparison of suction knife, ultrasonic dissector, and contact neodymium-YAG laser *Arch Surg* **122** 1166-71

Schroder T and Ramo O J (1989) Lasers in pancreatic surgery *Lasers in General Surgery* ed S Joffe (Baltimore: Williams & Wilkins) pp 96-9

Schroder T, Ramo O J and Joffe S N (1988) Laser pancreatectomy. A comparison between dog and pig *Res Exp Med (Berl)* **188** 227-33

Schurr M O, Wehrmann M, Kunert W, Melzer A, Lirici M M, Trapp R, Kanehira E and Buess G (1994) Histologic effects of different technologies for dissection in endoscopic surgery: Nd:YAG laser, high frequency and water-jet *Endosc Surg Allied Technol* **2** 195-201

Shapshay S M (1987) Laser applications in the trachea and bronchi: a comparative study of the soft tissue effects using contact and noncontact delivery systems *Laryngoscope* **97** 1-26

Sinha U K and Gallagher L A (2003) Effects of steel scalpel, ultrasonic scalpel, CO2 laser, and monopolar and bipolar electrosurgery on wound healing in guinea pig oral mucosa *Laryngoscope* **113** 228-36

Skinner M G, Everts S, Reid A D, Vitkin I A, Lilge L and Sherar M D (2000) Changes in optical properties of ex vivo rat prostate due to heating *Phys Med Biol* **45** 1375-86

Slack A, Child T, Lindsey I, Kennedy S, Cunningham C, Mortensen N, Koninckx P and McVeigh E (2007) Urological and colorectal complications following surgery for rectovaginal endometriosis *Bjog* **114** 1278-82

Stratton P, Winkel C A, Sinaii N, Merino M J, Zimmer C and Nieman L K (2002) Location, color, size, depth, and volume may predict endometriosis in lesions resected at surgery *Fertil Steril* **78** 743-9

Sturesson C, Liu D L, Stenram U and Andersson-Engels S (1997) Hepatic inflow occlusion increases the efficacy of interstitial laser-induced thermotherapy in rat *J Surg Res* **71** 67-72

Sultan R A and Boulnois J L (1989) Abdominal and Anorectal Surgery *Lasers in General Surgery* ed S N Joffe (Baltimore: Wiliams& Wilkins) pp 100-24

Takkar D and Sinha A (2002) Lasers in Gynecology *Medical Applications of Lasers* ed D R Vij and K Mahesh (Norwell: Kluwer Academic Publishers) pp 309-25

Tan A H and Gilling P J (2003) Free-beam and contact laser soft-tissue ablation in urology *J Endourol* **17** 587-93

Tan A H and Gilling P J (2005) Lasers in the treatment of benign prostatic hyperplasia: an update *Curr Opin Urol* **15** 55-8

Taylor D L, Schafer S A, Nordquist R, Payton M E, Dickey D T and Bartels K E (1997) Comparison of a high power diode laser with the Nd:YAG laser using in situ wound strength analysis of healing cutaneous incisions *Lasers Surg Med* **21** 248-54

Teichmann H O, Herrmann T R and Bach T (2007) Technical aspects of lasers in urology *World J Urol* **25** 221-5

Thomsen S (1991) Pathologic analysis of photothermal and photomechanical effects of laser-tissue interactions *Photochem Photobiol* **53** 825-35

Thomsen S, Pearce J A and Cheong W F (1989) Changes in birefringence as markers of thermal damage in tissues *IEEE Trans Biomed Eng* **36** 1174-9

Tulikangas P K, Smith T, Falcone T, Boparai N and Walters M D (2001) Gross and histologic characteristics of laparoscopic injuries with four different energy sources *Fertil Steril* **75** 806-10

Van Goethem B E, Rosenveldt K W and Kirpensteijn J (2003) Monopolar versus bipolar electrocoagulation in canine laparoscopic ovariectomy: a nonrandomized, prospective, clinical trial *Vet Surg* **32** 464-70

Vannozzi I, Benetti C and Rota A (2002) Laparoscopic cryptorchidectomy in a cat *J Feline Med Surg* **4** 201-3

Vashi A R and Oesterling J E (1998) Anatomic Radical Retropubic Postatectomy: Indications and technique: Nerve-Sparing Method *Surgery of the Prostate* ed M I Reshnick and I M Thompson (New York: Churchill Livingstone Inc.) pp 85-108

Veenendaal L M, de Jager A, Stapper G, Borel Rinkes I H and van Hillegersberg R (2006) Multiple fiber laser-induced thermotherapy for ablation of large intrahepatic tumors *Photomed Laser Surg* **24** 3-9

Ventrucci M, Di Simone M P, Giulietti P and De Luca G (2001) Efficacy and safety of Nd:YAG laser for the treatment of bleeding from radiation proctocolitis *Dig Liver Dis* **33** 230-3

Verdaasdonk R M, Borst C and van Gemert M J (1990) Explosive onset of continuous wave laser tissue ablation *Phys Med Biol* **35** 1129-44

Verdaasdonk R M, Jansen E D, Holstege F C and Borst C (1991) Mechanism of CW Nd:YAG laser recanalization with modified fiber tips: influence of temperature and axial force on tissue penetration in vitro *Lasers Surg Med* **11** 204-12

Weber H, Enders S and Hessel S (1991) Thermal effects and histologic changes from Nd:YAG laser irradiation on normal and diseased aortic tissue using a novel angioplasty catheter with a mobile optical fiber: an in vitro assessment *Angiology* **42** 597-606

Wright C H G, Barrett S F and Welch A J (2002) Laser-Tissue Interaction *Medical Applications of Lasers* ed D R Vij and K Mahesh (Norwell: Kluwer Academic Publishers) pp 21-58

Wyman A, Sweetland H M and Rogers K (1991) Parameters for and safety of contact Nd:YAG laser irradiation of early gastric cancer: an in vitro study *Gastrointest Endosc* **37** 170-4

Xu L X, Zhu L and Holmes K R (1998) Blood perfusion measurements in the canine prostate during transurethral hyperthermia *Ann N Y Acad Sci* **858** 21-9

2

Chapter 2

Dynamic color schlieren imaging of Nd:YAG laser-induced temperature distribution in a tissue model: a pilot study

S.A. van Nimwegen[1], A.I. Rem[2], J. Kirpensteijn[1]

[1]Department of Clinical Sciences of Companion Animals, Faculty of Veterinary Medicine, Utrecht University, Utrecht, The Netherlands;
[2]Department of Clinical Physics, University Medical Center, Utrecht, The Netherlands.

Abstract

The investigation of spatial temperature distribution in tissue is complicated. Schlieren imaging is a relatively straightforward technique to visualize inhomogeneities in transparent media, such as those caused by temperature gradients. A transparent polyacrylamide gel may serve as a model for laser tissue interaction. Spatial distribution of Nd:YAG laser-induced temperature distribution was investigated in a polyacrylamide gel using a dynamic color schlieren technique, comparing contact and free beam laser exposure. The use of a polyacrylamide gel as a model for canine prostate tissue was investigated.

Introduction

There are many ways in which laser tissue interaction can be investigated. Temperature and damage distributions in tissues can be measured or modeled in order to improve therapeutic strategies and develop new applications. Many advances were made in the modeling of tissue damage as a function of temperature and temperature history. However, the modeling of laser-induced temperature distribution can be rather complex, being dependent on many factors such as the method of laser application, the laser wavelength and the tissue characteristics. Gel models have been used to investigate temperature distribution in vitro and to validate theoretical models (van Swol *et al* 1994, Olsrud *et al* 1999). Real-time monitoring of laser-induced temperature distribution in a tissue or phantom has several restrictions. Temperature can be measured using invasive probes that give temperature information of certain points in space with which the overall temperature distribution can be estimated, but these probes (thermocouples, infrared sensors, thermistors) are often influenced directly by laser irradiation. New, non-invasive techniques to monitor temperature, such as MRI, are promising but complex and require considerable investment and dedicated equipment. A relatively old, but not outdated optical technique to visualize temperature gradients in transparent media (Hooke 1665) is the schlieren technique (Rienitz 1997), which visualizes changes in refractive index, such as induced by temperature gradients. The color or rainbow schlieren technique (Howes 1984) makes use of a spatial filter (rainbow filter) through which the degree of deflection of light, caused by the refractive index gradient in the transparent medium, is visualized by a change in color. Color schlieren visualization for dynamic modeling of temperature gradients in biological tissues has been used for years and is still under investigation (Verdaasdonk *et al* 1999, Verdaasdonk *et al* 2006). A big advantage of the technique is that it is relatively simple and economical, and it produces real-time images of refractive index gradients. A disadvantage

is that the technique is mainly valid as a qualitative means to visualize temperature distribution. It is tempting to interpret the colored lines in color schlieren images as isotherms. Attempts have been made to quantify the images, using ray-trace simulations (Verdaasdonk *et al* 1999). The images can be quantified mathematically if they represent basic planar (unidirectional), cylindrical or radial temperature gradients, although the latter two are relatively complex. However, the outer lateral shape of the schlieren images is probably a good estimation of isothermal temperature distribution, and could possibly be used to describe laser-induced temperature distribution in tissues.

In the present pilot study, schlieren images were recorded that were made of non-contact Nd:YAG laser irradiation in a polyacrylamide gel that served as a tissue phantom. Because the transparent gel is by definition non-light-scattering, light attenuation is dependent on absorption (*Chapter 1, Section 2.2*). Copper sulfate ($CuSO_4$) acts as an absorber for near infrared light (Figure 1). Several gels with different $CuSO_4$ concentrations were used to visualize laser-induced spatial temperature distributions. An attempt was made to quantify the resulting schlieren images, and to relate these results to the theoretical optical penetration depth of 1064 nm laser irradiation in canine prostate tissue that was calculated in *Chapter 1 (Section 2.2)*. Furthermore, the difference of contact mode versus non-contact (free beam) mode laser irradiation was investigated. It was expected that an increased temperature spread would occur underneath the gel surface in non-contact laser exposure compared to a more limited superficial heating during contact mode exposure, as described in *Chapter 1 (Section 3.2)*.
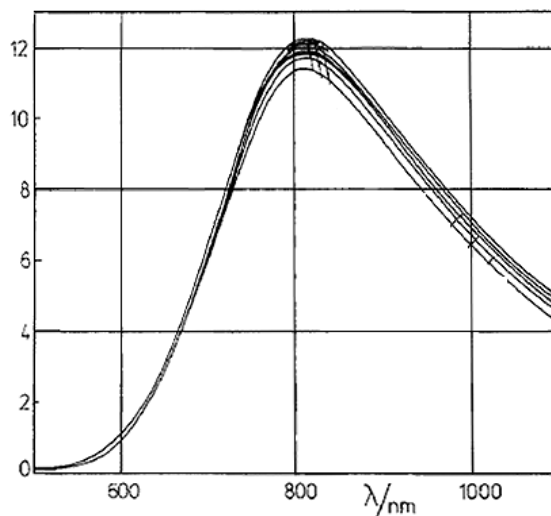

Figure 1: Absorption spectrum for several concentrations of a $CuSO_4$ aqueous solution (0.003-1.08 M) (Libus *et al* 1980).

Materials and methods

Color schlieren technique

The setup for color schlieren imaging is displayed in Figure 2. A point source of white light is positioned in the focal plane of lens 1 (collimating lens), creating a parallel light field between lens 1 and 2. The polyacrylamide gel, approximately 20 x 70 x 5 mm in dimensions, is placed perpendicular in this parallel light field (object plane, Figure 2). The laser fiber is positioned above the gel, at a variable distance. A rainbow filter is placed in the focal plane of lens 2 (de-collimating lens). In thermo-neutral state, most of the light is blocked by the center of the filter. By blocking non-deflected light at the center of the color filter, contrast of the image of deflected light will be enhanced. The refracted and diffracted light generates a baseline bluish image in the camera, which is positioned in the image plane of lens 2. Surrounding the non-transparent center of the rainbow filter are semi-transparent concentric rings of various colors (in the order: blue – green – yellow – orange – red) divided by black rings (Figure 6).
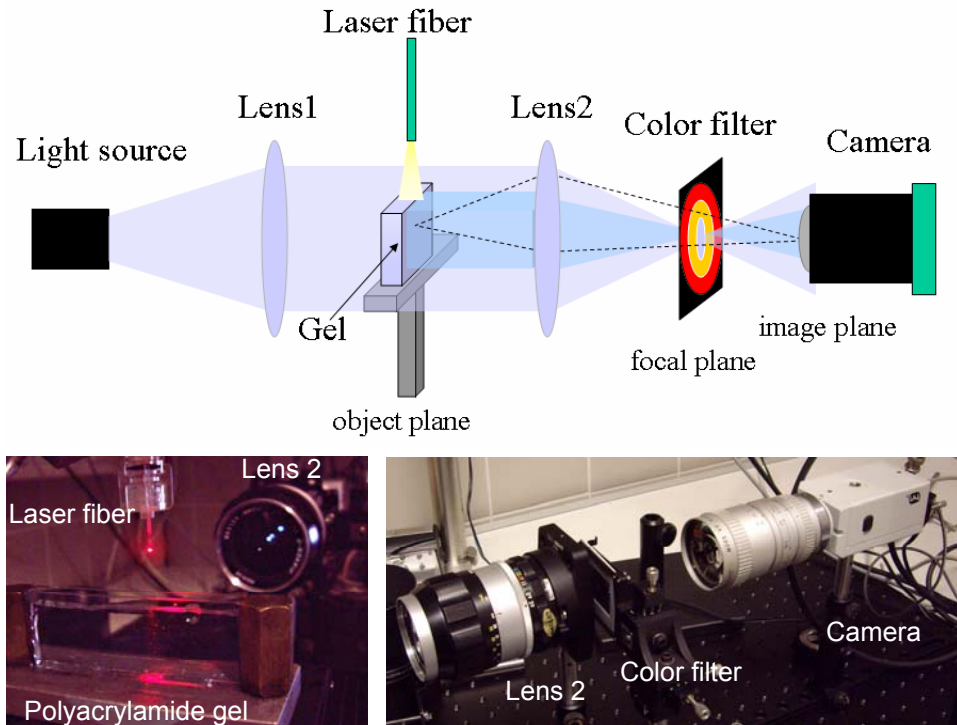

Figure 2: Color schlieren setup. Lens 1 collimates the light of a point light source. The polyacrylamide gel is positioned in the collimated light field. Lens 2 projects the image of the gel in the camera. The center of the color filter is positioned in the focal point of lens 2.

When the gel is irradiated with a Nd:YAG laser beam, a certain volume is heated, creating a temperature gradient in the gel and thus a gradient of refractive index. The parallel light rays passing the gel will be deflected by the refractive index gradient and will pass the color filter more or less off-centered through the colored rings, creating a colored image in the camera. The angle of deflection of the rays leaving the gel thus determines the color in the image. The color at distance d from the center of the filter is determined by the deflection angle θ and focal distance f of lens 2 according to:

$$d = f \tan \theta \tag{1}$$

When the temperature gradient is high, the deflection angle is high and the color in the image will be towards red (outwards on the rainbow filter). This way, the temperature gradients in the gel are visualized as colors in the image. Steep gradients are recognizable from the short distance between subsequent color lines in the schlieren image.

The gel model

Schlieren imaging requires that the medium of investigation is transparent. A polyacrylamide gel was used for this purpose. The high water content (80-90%) makes the thermal conduction properties comparable to tissue, being dominated by water. The 1064 nm Nd:YAG laser wavelength is not well absorbed by water and requires an absorber added to the gel to mimic laser absorption of tissue. $CuSO_4$ was added for this purpose. Scattering can not be created in the gel, because adding a substance or particles to increase scattering will greatly decrease transparency, making the gel useless for schlieren imaging. The process of thermal coagulation does not occur in the gel. Gel composition changes due to dehydration, and above $100^{\circ}C$ water evaporates and the polymer structure will eventually decompose and turn brown (Verdaasdonk *et al* 2006). Carbonization, vaporization and the 'popcorn effect' occur in the polyacrylamide gel and are comparable to these effects in tissue.

Desired $CuSO_4$ gel concentrations were obtained by storing the polyacrylamide gel, which initially contains no $CuSO_4$, in an aqueous solution of $CuSO_4$ for several days.

The fluence rate in canine prostate tissue was calculated in *Chapter 1* (*Section 2.2, Figure 5*), using experimentally determined optical properties (Nau *et al* 1999), resulting in an optical penetration depth of δ=2.63 mm. Scattering causes an increase and lateral spread of fluence rate inside tissue. This effect can be mimicked in the gel model by using a broader laser beam (or spot size) and higher absorption compared to tissue (Verdaasdonk *et al* 2006).

Experiment

Four types of schlieren gels were used: one plain and three with increasing concentrations of CuSO$_4$ (5, 7 and 9 mg/ml). The gels were placed in a transparent (glass) container and were irradiated, using a Nd:YAG laser (TT YAG-80; Trumpf Medizine Systeme, Umkirch, Germany) at various power settings and various fiber distances (Figure 2). To image contact-mode effects, the gel (9 mg/ml CuSO$_4$) was locally carbonized using the laser fiber in contact (high power density) with the gel. Subsequently, schlieren recordings were made of temperature distributions after 2 s of 15 W laser irradiation at the carbonized area with the fiber tip at 5 mm distance. The carbonized surface area will absorb the laser energy similar to contact mode exposure. These recordings were compared to recordings of temperature distributions after 2 s laser irradiation using the same power, gel, and fiber distance above a plain (not carbonized) gel surface. The plain surface will not carbonize during 2 s of this relatively high power density, demonstrating non-contact laser exposure. The diverging half-angle of the optical fiber (600µm diameter bare fiber) was 9.4 ± 0.9^o (NA=0.16 ± 0.02), measured using thermal print paper at 3 cm distance from the fiber tip. Power output of the fiber was 87 ± 0.5% of power setting. Results are given as means ± s. Differences in results between gels were tested for significance using Students t-test. Significance was assumed for $p<0.05$. Mentioned powers are compliant to power settings in *Chapter 3*.

A. fiber distance: 6 mm
spot size: 2.0 mm
no absorber
20 W, 20 s

B. fiber distance: 7 mm
spot size: 2.3 mm
5 mg/ml CuSO$_4$
10 W, 20 s

C. fiber distance: 14 mm
spot size: 4.6 mm
5 mg/ml CuSO$_4$
15 W, 20 s
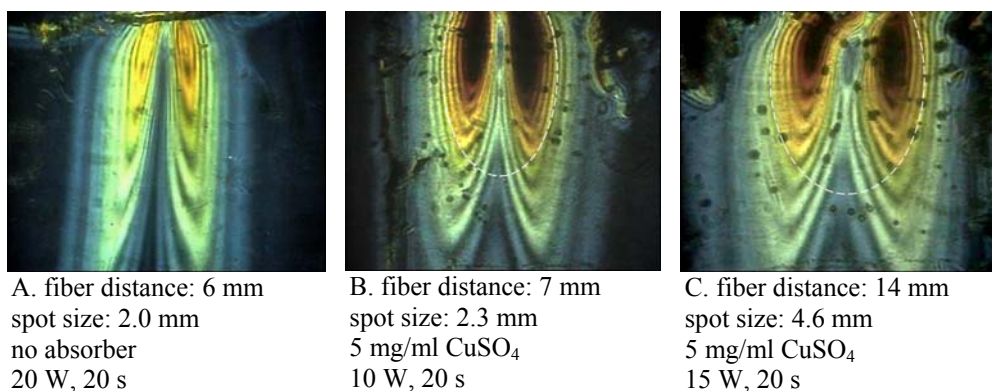
Figure 3: examples of schlieren images after 20s non-contact Nd:YAG laser irradiation, showing qualitative effects of absorber and spot size. The images were made during pilot recordings using a plain gel (A) and a gel containing approximately 5 mg/ml CuSO$_4$ (B, C). Dimensions of the images are approximately 9x12mm (HxW). The white dashed line is an indication of the actual shape of isothermal temperature distribution. The white line was drawn along the first yellow schlieren line to denote the difference in shape due to change in spot size. The central axial portion of the elliptical shape was estimated.

Results

After applying several powers at various fiber distances from the gel surface, a power of 15 W and a fiber distance of 12-14 mm above the surface were chosen to obtain video recordings for each concentration $CuSO_4$. Using these settings, measurements in the 9 mg/ml gel were possible without popcorn effect, which often appeared with higher laser beam power densities.

The seemingly low temperature zone in the midline of the images is an artifact of the technique that was used. Typical differences in schlieren images due to the use of an absorber are displayed in Figure 3. Also, an indication of the actual isothermal shape of the laser-induced temperature distribution is given (white dashed line), disregarding the artificial 'dip' in the mid region. When no absorber is used, the resulting temperature distribution resembles a cylinder, with only a very small vertical (axial) temperature decrease in depth of the gel. There is a steep temperature decrease sideways (lateral), depicted by the short distance between subsequent schlieren lines. Adding copper sulfate as an absorber of Nd:YAG wavelength, changes the temperature distribution to a more ellipsoid shape. Propagation of laser irradiation in the gel is diminished by enhanced absorption. Figure 3 also displays the effect of changing the spot size: the width of the temperature distribution changes.

Representative schlieren images after 20 s non-contact laser exposure of gels containing 0, 5, 7 and 9 mg/ml $CuSO_4$ are displayed in Figure 4. A higher power (20 W) was used for the gel with no absorber added, because the low absorbance of 15 W at 14 mm fiber distance did not result in a representative image. The effect of decreasing fiber distance (and thus increasing power density of the beam) is clearly visible in Figure 3A, where the same power was used with a fiber distance of 6 mm.

To quantify the differences between the schlieren results of different concentrations of $CuSO_4$, the schlieren-line density (a measure of temperature gradient) between 3 and 6 mm depth, the total amount of schlieren lines in the image and the width of the 4th schlieren line (the light-green line, ahead of the green line, Figure 4) were compared for 5, 7 and 9 mg/ml $CuSO_4$ gel concentrations (Table 1). Furthermore, the mean vertical distance between subsequent schlieren lines (Inter-Line Distance, ILD) was measured at 3 mm (ILD3) and at 6 mm depth (ILD6) after 20 s laser exposure as a measure of temperature gradient at these two distinct depths, and to determine the ratio (ILD6/ILD3).

No CuSO₄ added
20W non contact, 20s
dimensions: mm

5 mg/ml CuSO₄
15W non-contact, 20s
dimensions: mm

7 mg/ml CuSO₄
15W non-contact, 20s
dimensions: mm

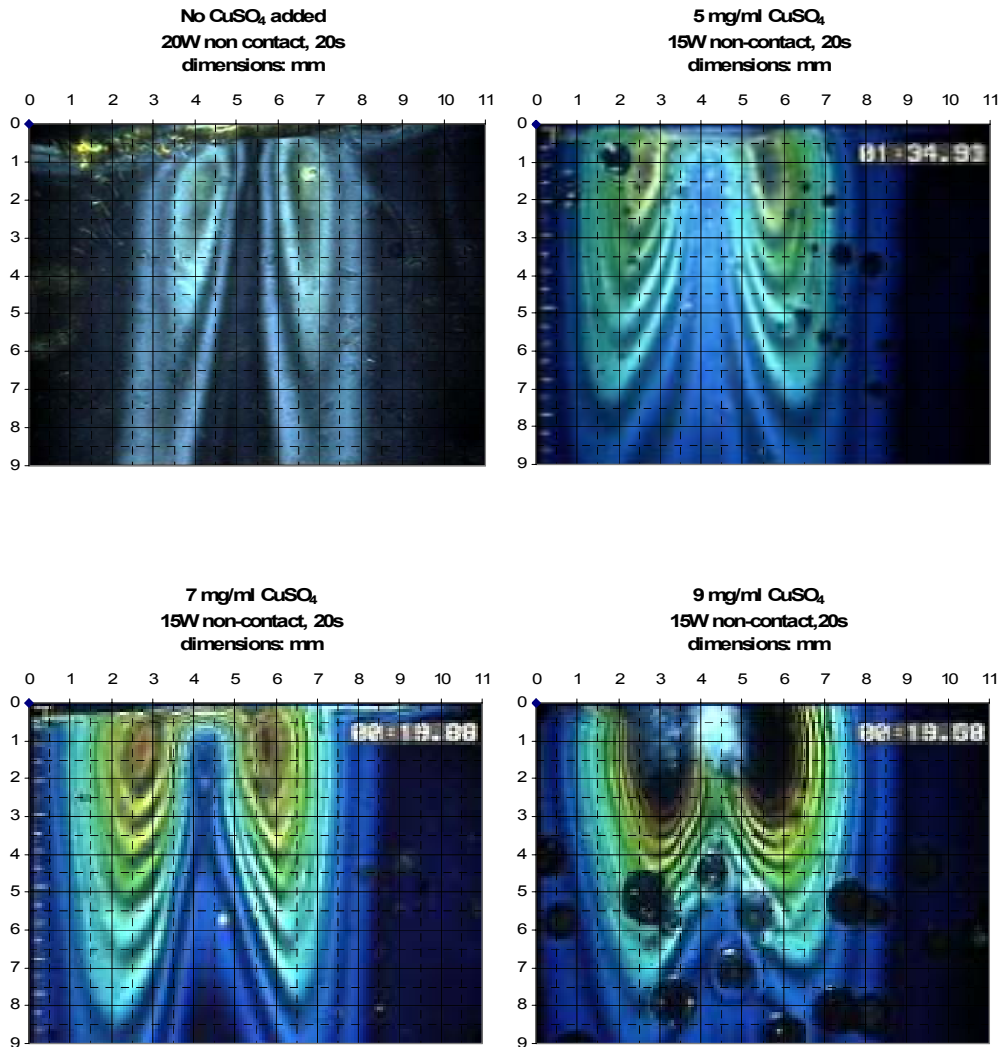**9 mg/ml CuSO₄**
15W non-contact,20s
dimensions: mm

Figure 4: Schlieren image after 20 s non-contact laser irradiation at 15 W and fiber distance above the surface of 12-14 mm for 0, 5, 7 and 9 mg/ml CuSO₄ concentration. Dimensions: 9 x 11 mm. The round spots in the 7 and 9 mg/ml CuSO₄ gels are artifacts caused by small air bubbles at the gel-glass interface.

Concentration CuSO$_4$ gel	5 mg/ml, n=4	7 mg/ml, n=5	9 mg/ml, n=8	p-value
Nr of lines 3-6 mm depth	2.7 ± 0.2	3.6 ± 0.1	5.1 ± 0.3	<0.001
Total number of lines	5.4 ± 0.5	6.9 ± 0.4	8.8 ± 0.3*	<0.001
Width of 4th line [mm]	4.8 ± 0.4	5.5 ± 0.2	6.1 ± 0.2	0.002
ILD3 [mm]	1.43 ± 0.10	0.92 ± 0.08	0.49 ± 0.07	<0.001
ILD6 [mm]	2.18 ± 0.13	1.66 ± 0.15	1.09 ± 0.18	<0.001
Ratio (ILD6/ILD3)	1.53 ± 0.08	1.82 ± 0.24	2.27 ± 0.36	0.033

Table 1: Differences between temperature distributions in 5, 7 and 9 mg/ml CuSO$_4$ gel concentrations after 20 s laser exposure. Number of lines between 3-6 mm depth in the gel. Total number of lines created in the schlieren image. Width of the temperature distribution, measured at the 4th schlieren line (light green line, ahead of the green line, Figure 3 and 4). Mean Inter-Line Distance at 3 (ILD3) and 6 mm depth (ILD6). *Maximum number of lines is 9 with the used color filter. Differences between groups (CuSO$_4$ concentrations) were significant (p-value given for 7 mg/ml versus 9 mg/ml CuSO$_4$).

Temperature distributions after 2 s of laser exposure of a carbonized surface compared to a transparent surface are displayed in Figure 5. Distributions of schlieren lines are typically in the order of 1 mm or less below the carbonized surface. During laser exposure, vaporization occurred, denoted by the slowly increasing crater in the gel (Figure 6). Non-contact temperature spread inside the gel is obviously increased compared to the carbonized (contact mode-like) surface.
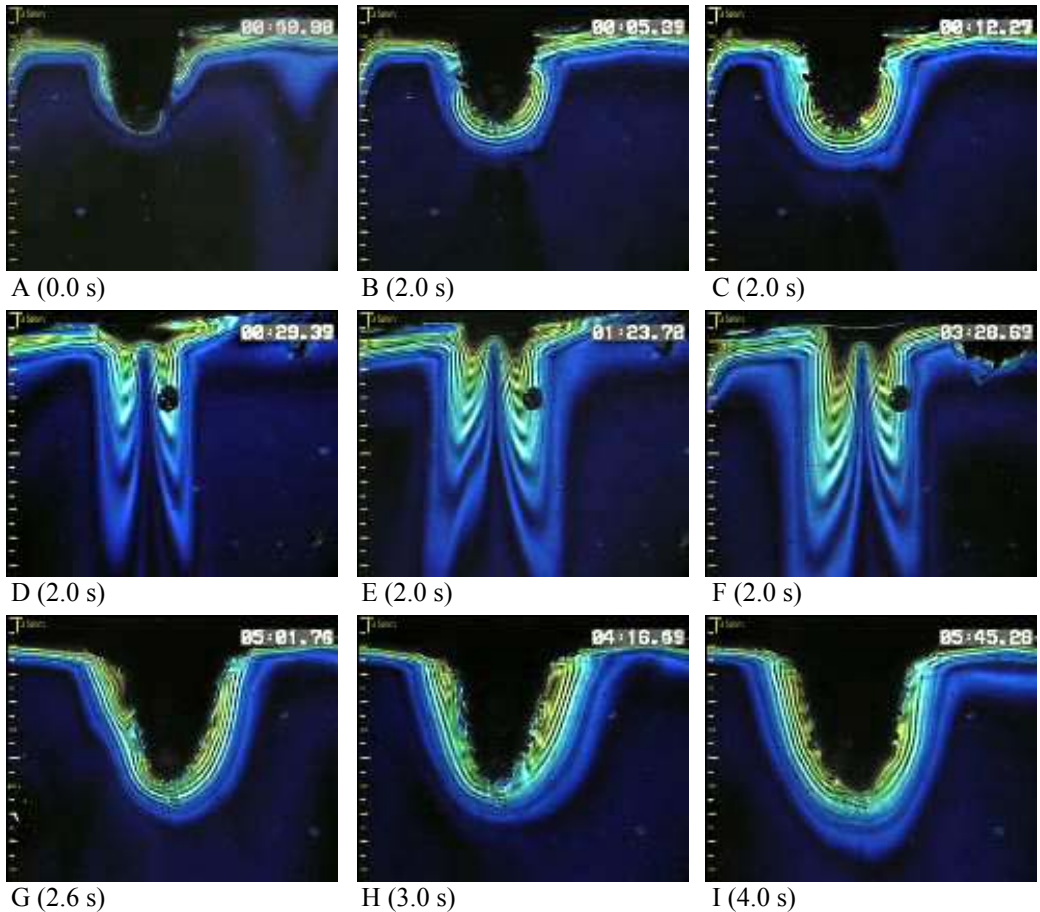
Figure 5: Schlieren images directly after 2 s 15 W laser exposure of a carbonized (crater) surface (B, C), and transparent surface (D, E, F) of the gel (9 mg/ml CuSO₄). A: image before laser exposure. B and D are images after one 2 s exposure in a cool gel. C, E and F are from subsequent exposure with 5-8 s cooling time in between. G, H and I show schlieren images after increasing exposure times. Fiber distance above the surface (excluding crater) was 5 mm. Individual exposure times are given in parentheses. 0.5 mm scale included on left side of images.

J (0.0 s)   K (0.8 s)   L (1.2 s)

M (1.8 s)   N (2.0 s)   O (1.6 s)

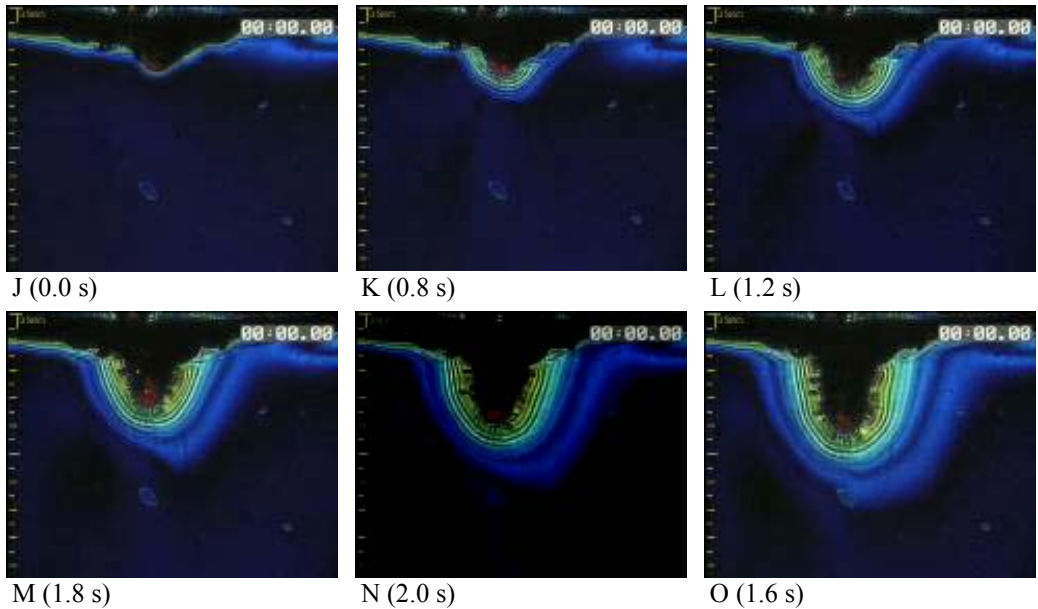**Figure 6**: Formation of a vaporization crater through subsequent laser exposures. J-O depict subsequent exposures of 0.8-2.0 s each with 1.0-1.5 s cooling time in between, showing the creation of a vaporization crater. 0.5 mm scale included on left side of images.

Discussion

Short duration (up to 20 s) non-contact and contact mode laser exposure was investigated using color schlieren imaging in a transparent polyacrylamide gel. The effect of variation in $CuSO_4$ concentration on laser-induced temperature distribution in the gel was investigated.

The color schlieren image of Nd:YAG irradiation

An important pitfall of the schlieren technique is that it images a 3D process in 2D, but not like a 2D picture of a 3D object. Ideally, the Nd:YAG temperature distribution in the gel is in the form of a 3D ellipsoid, mimicking the distribution in tissue (Figure 3). However, the resulting schlieren images show a steep depression of color lines in the midline portion of the image, where temperatures are actually highest. This is a consequence of the symmetrical cylinder shape of the temperature distribution. The effect of the cylinder-shaped temperature distribution can be appreciated from the schlieren image in Figure 3, where no absorber was added to the gel. The outer shape of the cylindrical temperature distribution generates relatively straight parallel colored schlieren lines delineating a

relatively steep temperature gradient outward. Because the laser beam irradiance is distributed in a Gaussian curve, a perpendicular cross section of the temperature distribution in the gel obeys a Gaussian shape. Inwards the cylinder, in contrast to the increasing temperature, the color lines give an impression of a "decrease" in temperature. This is caused by the 3D symmetry of the temperature distribution in depth of the gel. The path and final deflection angle of a light ray is determined by the summation of changes in refractive index encountered on its way through the 3D temperature field (Figure 7). As a simplified example: light rays traveling through the gel in the central axis of the cylindrical temperature distribution (i.e. perpendicular to the temperature gradient) will not be deflected, while light rays traveling more off-centered will be deflected with increase of deflection angle with distance from the center. This continues up to a certain point where the situation reverses and (total) deflection angle decreases further outwards the cylinder (Figure 7).

The temperature decrease of the ellipsoid distribution is visible in vertical direction, except in the mid portion of the image. Lateral displacement of the image is negligible because the maximum angle of deflection in the schlieren setup is relatively small ($\theta < 2^{o}$, f=135 mm, d_{max}<5 mm, Equation 1) (Howes 1984, Greenberg *et al* 1995). Thus, the schlieren image of the outer shape of an axially symmetrical (cylindrical) temperature distribution is an acceptable representation of the actual image of temperature distribution in the gel. Furthermore, the outer lines represent isothermal temperature ('iso-refractive-index') areas probably up to their 'deepest' point in the image, where the lines curve towards the axis of symmetry, forming the image artifact (see example ellipsoid shape in Figure 3). Therefore, the assumption was made that the outer shape of the temperature distribution can represent an acceptable "2D" image of the temperature (-gradient) distribution, and can therefore be used as an approximating 2D model of the laser-induced temperature field.

The schlieren lines are determined by the focal distance of lens 2, the dimensions of the rainbow filter and the relative change in refractive index (the temperature gradient) in a 3D temperature distribution. An exact interpretation of the color versus temperature in the gel can be obtained for basic geometries by ray-tracing (Verdaasdonk *et al* 1999) calculations, but is complicated to apply in real time recordings. Another way to determine color-temperature relations is by measuring temperature inside the gel, which however, was not part of this study.
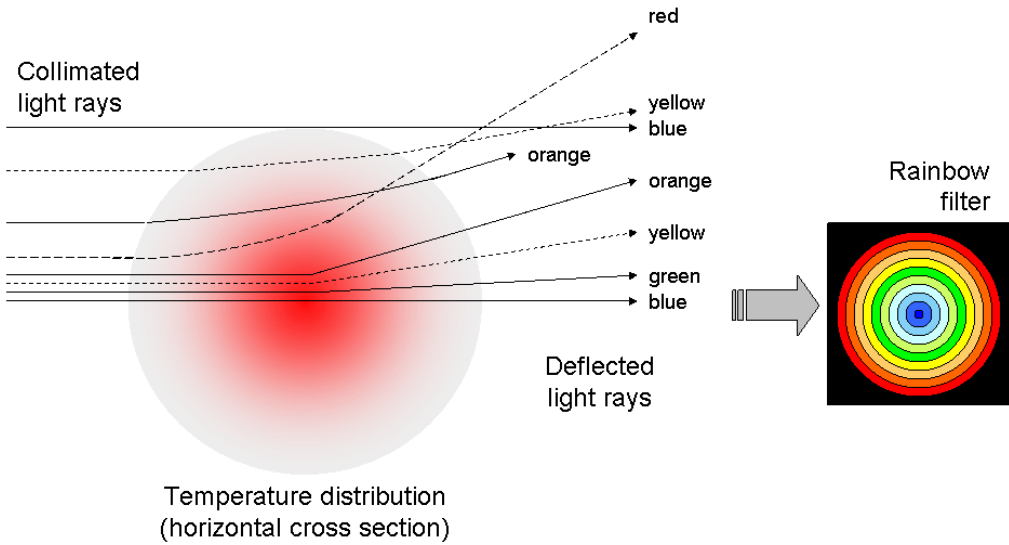
Figure 7: Simplified example of the deflection and accompanying schlieren color of light rays traveling through a cylinder-shaped temperature distribution. Horizontal cross section of the schlieren gel with cylindrical (laser-induced) temperature distribution. In reality, the schlieren image is composed of light rays deflected < 2°.

Effect of CuSO$_4$ concentration on laser-induced temperature distributions

Increasing concentrations of CuSO$_4$ in the polyacrylamide gel result in increased heating more superficially in the gel, denoted by more schlieren lines of 'higher color' (towards red) and a steeper temperature decay inwards the gel (increased temperature gradient), which causes a higher density of schlieren lines per unit length. Furthermore, the shape of the temperature distribution changes from a cylinder towards an ellipsoid (Figure 4, Table 1).

By measuring the ILD at 3 and 6 mm depth, some degree of quantification of the schlieren images is possible. The theoretical laser-induced fluence rate *Φ(z)* inside canine prostate tissue is calculated in *Chapter 1 (Figure 5 in Section 2.2)*, using experimentally-derived optical parameters (Nau *et al* 1999) and

$$\phi(z) = (1 - R)E_0 be^{-z/\delta} \tag{2}$$

in which *δ* is the optical penetration depth and *E$_0$* the irradiance of the incident laser beam (Jacques 1992) (*Chapter 1, Section 2*). If heat conduction is disregarded, *Φ(z)* determines, and is linearly related to, temperature *T(z)*, ($\phi(z) \propto T(z)$); and *Φ'(z)* is linearly related to

the temperature gradient *T'(z)*, ($\phi'(z) \propto T'(z)$) and thus to the refractive index gradient. Therefore:

$$\frac{ILDz_2}{ILDz_1} \approx \frac{\phi'(z_2)}{\phi'(z_1)} = e^{\frac{z_2 - z_1}{\delta_{gel}}} \qquad \text{and} \qquad \delta_{gel} \approx \frac{z_2 - z_1}{\ln\left(\dfrac{ILDz_2}{ILDz_1}\right)} \qquad (3)$$

in which z_i represents the depth in the gel, $\Phi(z_i)$ the fluence rate and δ_{gel} the optical penetration depth of laser irradiation in the gel (or $1/\mu_{eff}$, see *Chapter 1, Section 2*). If the temperature distribution in the gel resembles that in (theoretical) prostate tissue, than: $\delta_{gel} = \delta_{tissue}$. Since heat conduction is disregarded, Equation 3 only gives an estimation of δ_{gel} which is most accurate during short exposure times. Using the results from Table 1, for the 9 mg/ml $CuSO_4$ gel, Equation 3 gives: $\delta_{gel} = 3.8 \pm 0.9$ mm. For canine prostate tissue, it was calculated that $\delta = 2.63$ mm (Nau *et al* 1999). Published experimental values of δ vary, depending on the methods used, ranging from 2.65 to 8.0 mm (*Chapter 1, Section 2.2, Table 2*). However, because of the scattering nature of canine prostate tissue (Anvari *et al* 1994), which is advocated by the very low value of $g = 0.45$, as measured by Nau et al. (Nau *et al* 1999), the optical penetration depth in prostate tissue is more likely to be in the range of 3-5.5 mm than 5.5-8 mm. Therefore, it is concluded that a polyacrylamide gel containing 9 mg/ml $CuSO_4$, and $\delta_{gel} = 3.8 \pm 0.9$ mm, gives an acceptable estimation of laser-induced temperature distribution in prostate tissue.

An uncertainty that might affect Equation 3 is that of the proportionality of the color in the rainbow filter (i.e. *d* in Equation 1) to tan*θ,* the angle of deflection. In the rainbow filter used in the present study, the colors are distributed at equal subsequent inter-color distances. By using ILD as a measure of temperature gradient and relating $ILDz_2$ to $ILDz_1$, it is assumed that ILD is linearly related to temperature gradient, independent of *d* (i.e. color), and thus that tan*θ* is linearly related to the temperature gradient in the gel, which can be assumed for a planar (unidirectional) temperature gradient (Verdaasdonk *et al* 2006). The laser-induced temperature gradient in a polyacrylamide gel approaches a unidirectional gradient with increasing radius, or distance from the axis, of a cylindrical distribution, and with increasing depth when absorption ($CuSO_4$ concentration) increases (see below).

In the present study, the vertical (axial) temperature gradient was observed and measured using the 'deepest' point of the schlieren lines, where they curve towards the central axis of the image. It was assumed that these points are not part of an imaging artifact but represent the actual temperature gradient in depth. One observation supporting this assumption is that with higher concentrations of $CuSO_4$ the shape of the temperature distribution becomes more ellipsoid-like. In theory, if the concentration of $CuSO_4$ increases, the optical

penetration depth decreases and the temperature distribution will eventually start to resemble that of a planar geometry, depending on conduction only, and loose its imaging artifact in the central area such as observed in the contact mode experiments (Figure 5 and 6).

Some variation in schlieren images was observed during experimentation which was probably due to an inhomogeneous distribution of $CuSO_4$ to some extent. If a more homogenous $CuSO_4$ distribution in the polyacrylamide gel can be achieved by altering the preparation method remains to be investigated.

Contact mode versus non-contact mode laser exposure

A carbonized surface acted as a contact mode situation and strongly blocked laser irradiation compared to a transparent gel surface (Figure 5). The difference in temperature distribution after 2 s laser exposure, using the same power setting, is substantial. It was also observed that laser energy caused vaporization of the gel and that the vaporization crater extended with every subsequent laser exposure, while the temperature-gradient distribution underneath the surface was relatively constant (Figure 6). A considerable amount of laser energy is used for vaporization of gel substance, resulting in relatively shallow temperature increase underneath the surface. This temperature distribution shows a relatively steep decay inside the gel (i.e. a considerable temperature gradient, located superficially at the surface). Furthermore, laser irradiation does not enter the gel, which is depicted by the absence of a cylindrical temperature distribution with its inherent imaging artifact (i.e. two 'lobes' of a cylindrical distribution, which are visible in the non-contact images).

Further research, including temperature measurements in the gel, is required to refine the model and resolve uncertainties such as that of the relation between line color and temperature gradient. Eventually, the model will have to be validated to real tissue, obtaining additional information about beam-diameter corrections to mimic the effect of scattering in tissue. However, when using a polyacrylamide gel with a laser attenuation coefficient (μ_{eff}), heat conduction, and a specific heat capacity similar to tissue, heating of a certain volume V over over a certain temperature interval ΔT at laser power P during time interval Δt, will be similar to tissue if the beam diameter is altered correctly. Since the 'popcorn effect' (i.e. a sub-surface temperature $>100^{o}C$ creating exploding vapor bubbles) also occurs in the gel, choosing a power- and fiber distance setting just below the threshold for creating popcorn in the gel (as was done in the present study) will give a prediction of temperature distribution in tissue (with comparable start temperature T_0), using the same power setting and altered (smaller) beam diameter under the same circumstances concerning the onset of the popcorn effect (i.e. heating over a comparable temperature (ΔT) and time (Δt) interval).

Since the absorption of laser light by $CuSO_4$ is dependent on wavelength (Figure 1), the gel has to be calibrated for the type of laser used. Absorption will be higher for a diode laser (802-980 nm wavelength) compared to Nd:YAG laser (1065 nm) in the same gel.

When the gel model is calibrated for a tissue (i.e. determining of correct absorbance and beam diameter), it describes laser-induced temperature progression (for short exposure times) independent of absolute temperature (i.e. start temperature of the gel is irrelevant as long as T<100°C).

Conclusion

The use of dynamic color schlieren imaging as a means to describe laser-tissue interaction for the near infrared Nd:YAG laser was investigated. The schlieren technique visualizes temperature distribution of non-contact and contact Nd:YAG laser irradiation. Except from being of great value for the qualitative analysis of laser-tissue interaction, a polyacrylamide gel with an absorption coefficient similar to the effective attenuation coefficient of tissue can be used to describe an approximate 2D image of laser-induced temperature gradient distribution.

References

Anvari B, Rastegar S and Motamedi M (1994) Modeling of intraluminal heating of biological tissue: implications for treatment of benign prostatic hyperplasia *IEEE Trans Biomed Eng* **41** 854-64

Greenberg P S, Klimek R B and Buchele D R (1995) Quantitative schlieren deflectrometry *Applied Optics* **34** 3810-22

Hooke R (1665) Of a New Property in the Air *Micrographia* ed (London: Observation LVIII) pp 217-9

Howes W L (1984) Rainbow schlieren and its applications *applied optics* **23** 2449-60

Jacques S L (1992) Laser-tissue interactions. Photochemical, photothermal, and photomechanical *Surg Clin North Am* **72** 531-58

Libus W, Sadowska T and Libus Z (1980) Correlation Between Thermodynamic Properties and Coordination States of Aqueous Bivalent Transition Metal Sulfates *Journal of Solution Chemistry* **9** 341-54

Nau W H, Roselli R J and Milam D F (1999) Measurement of thermal effects on the optical properties of prostate tissue at wavelengths of 1,064 and 633 nm *Lasers Surg Med* **24** 38-47

Olsrud J, Wirestam R, Persson B R and Tranberg K G (1999) Simplified treatment planning for interstitial laser thermotherapy by disregarding light transport: a numerical study *Lasers Surg Med* **25** 304-14

Rienitz J (1997) Optical inhomogeneities: schlieren and shadowgraph methods in the seventeenth and eighteenth centuries *Endeavour* **21** 77-81

van Swol C F, Verdaasdonk R M, Mooibroek J and Boon T A (1994) Optimization of laser prostatectomy *Prog Clin Biol Res* **386** 511-9

Verdaasdonk R M, Lodder R, van Swol C F P and Grimbergen M C M (1999) Thermal imaging of laser-tissue interaction using color Schlieren techniques quantified by ray-trace simulation *proc SPIE* **3601** 156-65

Verdaasdonk R M, van Swol C F, Grimbergen M C and Rem A I (2006) Imaging techniques for research and education of thermal and mechanical interactions of lasers with biological and model tissues *J Biomed Opt* **11** 041110

3

Chapter 3

Nd:YAG surgical laser effects in canine prostate tissue: Temperature and damage distribution.

**S A van Nimwegen[1], H F L'Eplattenier[1],
A I Rem[2], J J van der Lugt[3] and J Kirpensteijn[1]**

[1]Department of Clinical Sciences of Companion Animals, Faculty of Veterinary Medicine, Utrecht University, Utrecht, The Netherlands;
[2]Department of Clinical Physics, University Medical Center, Utrecht, The Netherlands;
[3]Department of Pathobiology, Faculty of Veterinary Medicine, Utrecht University, Utrecht, The Netherlands.

Abstract

An *in vitro* model was used to predict short-term, laser-induced, thermal damage in canine prostate tissue. Canine prostate tissue samples were equipped with thermocouple probes to measure tissue temperature at 3, 6, 9 and 12 mm depth. The tissue surface was irradiated with Nd:YAG laser in contact or non-contact mode for up to 20 s, using powers from 5 to 20 W. Prediction of thermal damage using Arrhenius theory was discussed and compared to the *in vitro* damage threshold, determined by histological evaluation. Threshold temperature for acute thermal tissue damage was 69 ± 6 ^{o}C (means $\pm$ sd), irrespective of exposure time. Contact mode laser application caused vaporization of tissue, leaving a crater underneath the fiber-tip. Mean extend of tissue damage underneath the vaporization crater floor was 0.9 ± 0.6 mm after 5, 10 or 20 s of contact mode laser irradiation at 10 W, whereas 20 W non-contact exposure up to 20 s causes up to 4.7 ± 0.2 mm coagulation necrosis. It was concluded that short-term acute thermal tissue damage can be comprehensively described by a single threshold temperature.

1. Introduction

Prostate surgery has several indications in dogs, such as the treatment of prostatic cysts or abscesses, and studies are being performed concerning the surgical treatment of prostate carcinoma (L'Eplattenier *et al* 2006). Radical (total) prostatectomy is often not an option in dogs because of the high incidence of urine incontinence after surgery, probably because of damage of the nerves and vessels located in the capsule of the canine prostate (Gordon 1960, Basinger *et al* 1987, Hardie *et al* 1990). A subcapsular debulking prostatectomy has been performed in dogs, preserving urinary continence by sparing the prostatic urethra and the prostate capsule (Robertson and Bojrab 1984, Rawlings *et al* 1994).

The extent of tissue damage in laser procedures is mainly dependent on the power density (W/cm^2) of the laser beam at the tissue surface and the irradiation time. Differences in tissue interaction due to changes in power density may be utilized in contact versus non-contact mode usage of a fiber-guided Nd:YAG laser (Shapshay 1987, Janda *et al* 2003). In contact mode, the high energy density at the fiber tip causes rapid carbonization of tissue. Carbonized tissue strongly absorbs laser irradiation leading to rapid heating and subsequent vaporization of tissue which enables tissue resection. Further heat distribution in the underlying tissue is mainly dependent on conduction and diffusion of the heat produced at the carbonized site. During laser resection of tissue the produced heat causes coagulation at

the cut-surface so bleeding is reduced to a minimum. The non-contact mode, or free beam, technique applies lower energy density to avoid such superficial alterations of tissue, and permits deeper light-penetration and subsequent larger coagulated volumes (Motamedi *et al* 1995, Orihuela *et al* 1995, Lippert *et al* 2003). Apart from tumor coagulation and interstitial thermotherapy, the free beam is appreciated for its ability to conduct hemostasis (Ventrucci *et al* 2001, Mahoney and Shapshay 2005).

There is a need for knowledge about the extent of thermal damage caused by laser resection of prostate tissue and free beam hemostasis, for the laser to be used in prostate surgery in a safe and effective way. Most studies on Nd:YAG laser surgery on the dog prostate are based on transurethral laser applications for the treatment of benign prostatic hyperplasia (BPH) in men, in which the prostatic urethra is often destroyed and prolonged catheterization is required for re-epithelization. Transurethral 40-60W Nd:YAG contact mode vaporization of prostate tissue, using a moving side-firing contact probe, caused a relatively small coagulation zone of up to 2 mm underneath the carbonized surface (Muschter and Perlmutter 1994). Contact mode laser incision effects (bare fiber or contact probe) have been evaluated for several tissues *in vivo* (Shapshay 1987, Mecke *et al* 1991, Laranne *et al* 1997) and *in vitro* (Weber *et al* 1991, Perry *et al* 1997, Janda *et al* 2003), but not for prostate tissue. Results of these studies show minimal thermal tissue effects in depth, probably due to power-loss caused by carbonization and vaporization at the surface (Verdaasdonk *et al* 1990).

Aims of the present study were to set up an *in vitro* model for laser induced thermal tissue damage and to determine safe surgical margins prior to a clinical study investigating subcapsular laser prostatectomy, which is presented in *Chapter 4* (L'Eplattenier *et al* 2006). The effects of bare-end fiber contact and non-contact laser application on canine prostate tissue were investigated during exposure times of up to 20 s, in contrast to several studies describing other techniques (i.e. transurethral side-firing probes) using longer irradiation times (minutes to hours).

2. Materials and methods

Temperature distribution was measured during contact and non-contact mode laser application on *ex vivo* canine prostate tissue samples. The expected onset of thermal damage for *in vivo* tissue was estimated using the combination of measured temperature distribution in time and Arrhenius parameters, commonly used for damage prediction in prostate tissue. In addition, a threshold temperature for acute thermal damage in canine prostate tissue was determined through histological examination of *ex vivo* laser-induced thermal damage.

2.1   Tissue samples

Prostate tissue (< 12 hours post mortem) was collected from dogs without prostatic disease and was either stored at 5ºC to be used for the experiment on the same day or stored at -20ºC to be used on a later time. Sample sizes were approximately 3 - 5 cm³. Only fresh samples (<8 hours post mortem, not previously frozen) were used for histological evaluation.

2.2   Temperature distribution in prostate tissue samples

A 1064 nm Nd:YAG laser (Medilas 40 N, MBB-Medizintechnik GmbH, München, Germany) was used to irradiate prostate tissue samples. Laser energy was applied through an optical fiber (600 μm diameter; Ultraline, Heraeus LaserSonics, Milpitas, CA). Four K-type thermocouple probes (0.26 mm diameter, response time < 20 ms) were inserted in the tissue samples through 18 G hypodermic needles fixed in a spacing device. The thermocouple probes were placed at 3, 6, 9 and 12 mm below the tissue surface (Figure 1). For non-contact mode, the laser fiber was positioned 6 mm above the tissue-surface area under which the thermocouple array was placed. This distance was chosen so that the highest power used (20 W) did not cause charring of the tissue surface. If charring nevertheless did occur, the measurements were discarded. For contact mode, the fiber tip was positioned against the tissue surface.
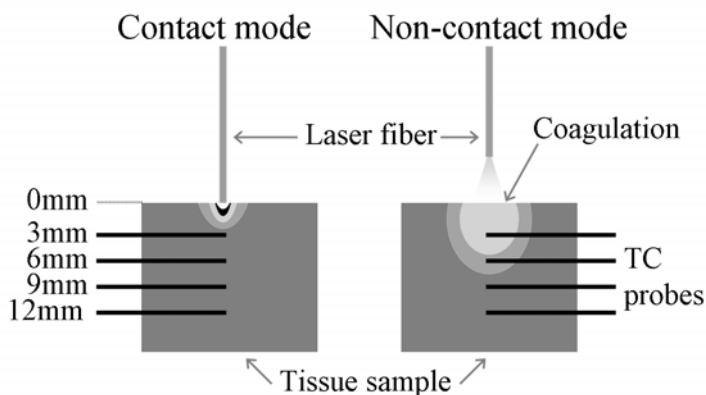

Fig 1: Experimental setup for temperature measurements during contact and non-contact mode laser irradiation of *ex vivo* prostate tissue. Also displayed are indications of theoretical difference in coagulation and thermal damage distribution. TC: thermocouple.

Thermocouple probes were connected to a thermocouple-amplifier and temperature recordings were made through an AD-converter (Labjack U12, Pimzos Pinckard, The

Netherlands) on a computer, resulting in temperature-time curves for each thermocouple probe. Probes and amplifier were calibrated using a precision Hg-thermometer (0.5°C/div) and hot water bath.

Apart from the surrounding tissue, the thermocouple probes are also heated directly by laser irradiation. This phenomenon is visible as a sudden change in measured temperature value when the laser is turned on or off, respectively (Figure 2). This measurement artifact was corrected for, using the fact that the response time for laser-induced temperature change is much faster for the small thermocouple probes compared to tissue (Verdaasdonk *et al* 1991). All temperature recordings were corrected for this thermocouple artifact by separating the thermocouple response from the tissue response via a non-linear curve-fit of the tissue-cooling curve after the laser is turned off. The *measured* tissue cooling curve is assumed to be an exponential function: $T_m(t)=A+Be^{-Ct}+De^{-Et}$ (A-E: constant parameters), in which Be^{-Ct} represents the gradual tissue cooling component and De^{-Et} represents the rapid thermocouple cooling component (following laser switch-off) of the curve. The *calculated* (corrected) tissue temperature after laser switch-off is: $T_c(t)=A+Be^{-Ct}$ (Figure 2).

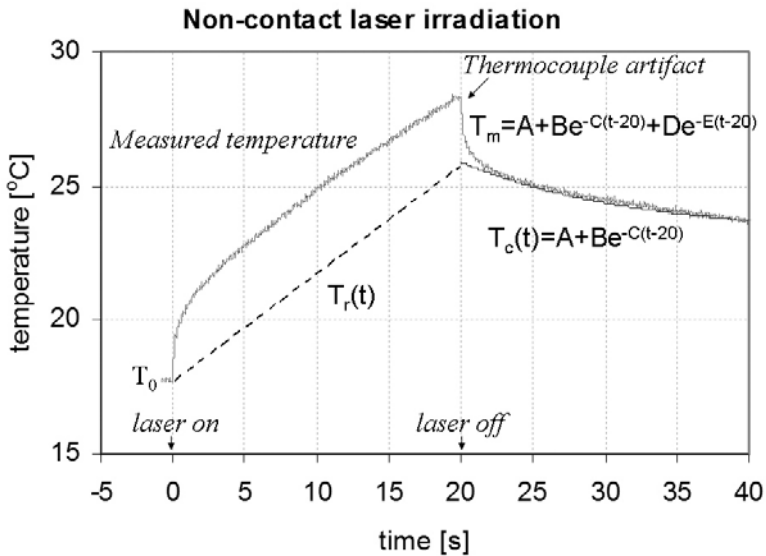**Figure 2**: Example of a temperature recording at 6 mm tissue depth during 20 s non-contact mode laser irradiation, showing the measured temperature in time, the thermocouple artifact, the corrected cooling curve (t>20 s) and the calculated tissue temperature during laser exposure (dashed line). T_m: measured temperature. T_c: calculated temperature (t>20 s). T_r: reconstructed temperature during laser exposure.

It is assumed that at constant laser power, tissue temperature rises linear with time during short (up to 30 s) irradiation intervals, because the thermal relaxation time of tissue is much longer than the irradiation time (Manns *et al* 1998). Therefore, tissue heating during the irradiation period ($T_r(t)$) can be easily reconstructed using the corrected temperature at laser switch-off after a known irradiation interval (Figure 2). Mean temperature of the tissue samples at start was: T_0=27 ± 2 ^{o}C. In non-contact mode experiments, temperature increase was recorded for 20 s of laser irradiation at 5, 10, 15 and 20 W laser settings. In the contact mode experiment, temperature increase was recorded for 5, 10 and 20 s of 10 W contact mode laser application. The measured temperature increase was adjusted to body temperature (T_0+T_{adjust}=38°C at t=0 s) to simulate *in vivo* situations.

The abovementioned laser powers were power settings of the laser device (Medilas 40N). The output-power of the laser fiber was measured using a standard power meter. The measured transmission of the laser fiber was 87 ± 0.5 %. Thus, the actual power output of the laser fiber with the applied settings of 5, 10, 15 and 20 W was 4.3, 8.8, 13.0 and 17.5 W respectively. The measured divergence half-angle of the laser beam, its transverse intensity typically being distributed in a Gaussian shape, was 9.4 ± 0.9^o (NA=0.16 ± 0.02), measured using thermal print paper at 3 cm distance from the fiber tip. When applicable, the experimental data are displayed as the actual power-output of the fiber.

2.3 Prediction of thermal damage

The most extensively used empirical model to describe time-dependent, temperature-induced tissue damage is derived from the temperature dependence of molecular reaction rates described by the Arrhenius parameters. This temperature relation for reaction speed was used by Henriques (1947) to formulate the Arrhenius damage integral, in which tissue damage is modeled as a first order rate process. The integral describes the relation between accumulated tissue damage and both temperature and time:

$$\Omega = A_f \int_0^{\tau} e^{-E_a/RT(t)} dt \qquad (1)$$

Ω represents the logarithm of the ratio of the original concentration of native state tissue constituent to the remaining concentration after a time τ. For instance, Ω=1 means that 63% of the tissue molecules are damaged, which is assumed to produce coagulation necrosis. A_f is the frequency factor; a measure of the molecular collision-rate (s^{-1}). E_a is the activation energy barrier (J mol^{-1}) for molecules to denature. R is the universal gas constant (8.31 J mol^{-1} K^{-1}) and T(t) the tissue temperature in time.

Arrhenius parameters for skin injury are frequently used in prostate tissue heating models (Prapavat *et al* 1996, Bolmsjo *et al* 1998, Huidobro *et al* 2004). A_f=3.1*10^{98}s^{-1} and

$\Delta E_a = 6.28 * 10^5$ J mol^{-1}, describing necrosis threshold temperature for pig skin (Henriques 1947), are most widely used.

2.4   *Histological evaluation of ex vivo laser induced thermal damage*

Acute temperature induced irreversible tissue damage (i.e. coagulation necrosis) is macroscopically visible as whitening of the tissue. Microscopic investigation shows that the border of this bleached zone coincides with the border of coagulation necrosis (Pearce and Thomsen 1995). With short exposure times, and thus fast heating rates, this border represents the transition zone of necrosis to viable tissue (Janda *et al* 2002). To investigate laser-induced tissue damage in our experiments, fresh prostate tissue samples (< 8 hours post mortem) were heated to 38°C in Ringer's lactate and irradiated at several power and time settings. These fresh tissue samples were sectioned at the irradiated spot and the extent of coagulation (bleached zone) was measured macroscopically, using a caliper. Samples were also stored in 4% buffered formaldehyde to be embedded in paraffin, sliced and stained with hematoxylin and eosin (HE) for microscopic evaluation.

2.5   *Statistics*

Statistically derived experimental results are given as means ± sd. Curve-fits of the experimental results were made using the mean values. Differences in results between depths were tested for significance using Students t-test and were considered significant when p<0.05 (two-tailed).

3   Results

3.1   *Tissue samples*

A paired samples t-test (fresh versus frozen-thawed, p=0.35) was used on the non-contact results (see Figure 3) of all depths per laser power (16 groups with equal distributions of fresh versus frozen-thawed samples). No significant differences were found between results obtained from frozen-thawed tissue and results obtained from fresh tissue at the various depths and power settings. Therefore, all samples in this study are considered to have comparable optical and thermal properties and were treated as one group.

3.2   *Temperature distribution in prostate tissue samples*

Temperature rise after *20 s non-contact mode* laser exposure varied linear with applied laser power at every depth (R^2≥0.97; Figure 3). Temperatures differed significantly between

depths (t-test; p<0.0005). Temperature below the tissue surface decreased with tissue depth in an exponential fashion. The reconstructed temperature increase in time at 3, 6, 9 and 12 mm depth is displayed in Figure 5.

During *10 W contact mode* laser exposure, tissue temperature increased linearly with time at 6, 9 and 12 mm tissue depth ($R^2 > 0.99$; Figure 4). This linearity was less evident at 3 mm tissue depth, where $R^2 = 0.93$. Measured temperatures significantly differed between depths (p<0.005). Tissue temperature decreased with distance from the surface in an exponential fashion.
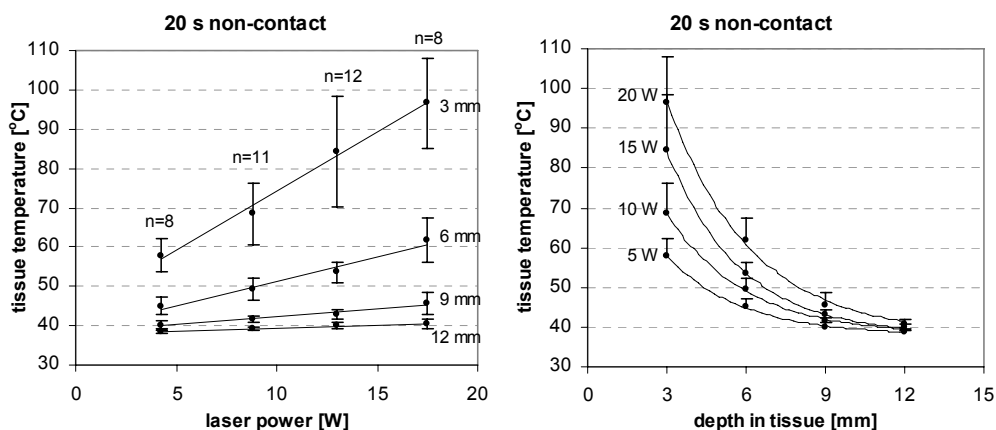

Figure 3: Mean measured temperatures ± sd after 20 s non-contact laser irradiation, adjusted to body temperature (38°C). Linearity of temperature increase with laser power is evident (linear fits, $R^2 \geq 0.97$). Temperature decrease with depth of the tissue was fitted by an exponential equation ($T(x)=38+Ae^{B(x-C)}$, $R^2 > 0.99$, where 'x' represents the distance from the tissue surface and $T_0=38$°C. In the temperature versus depth figure, only +sd values are shown to improve readability of the figure, avoiding overlapping error bars.

During contact mode laser irradiation of prostate tissue samples, carbonization and subsequent vaporization of the tissue occurred directly under the fiber-tip. This resulted in the formation of a narrow (1-2 mm in diameter) char-coated crater. The depth of this crater varied linearly ($R^2 = 0.98$) with laser exposure time and was 1.29 ± 0.67, 2.28 ± 0.62 and 3.48 ± 0.56 mm for 5, 10 and 20 s of laser irradiation, respectively.
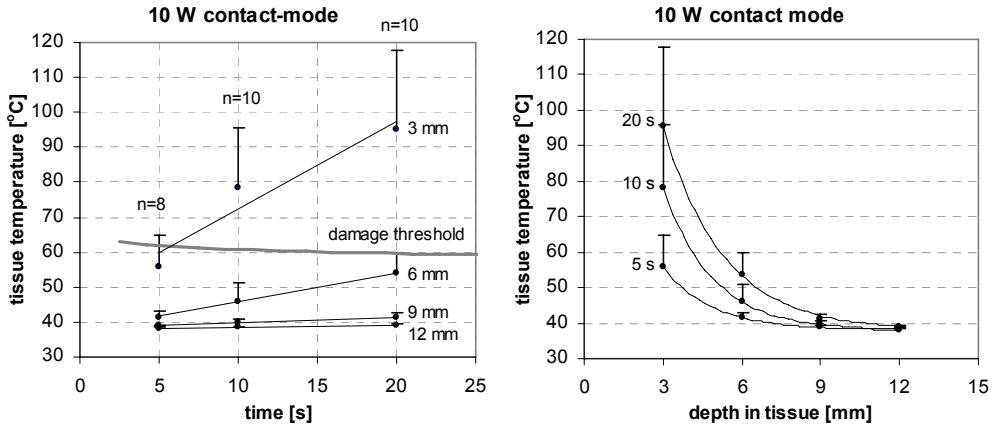
Figure 4: Measured tissue temperatures (means ± sd) after 5, 10 and 20 s of 10 W (8.8 W actual fiber output power) contact mode laser application at prostate tissue samples. Results were adjusted to body temperature. The calculated Arrhenius damage threshold (Henriques 1947) is displayed in grey. Linear fits are displayed for temperature versus time. Exponential fits trough the mean values are displayed for temperature versus tissue depth ($T(x)=38+Ae^{B(x-C)}$, $R^2>0.99$). Only +sd values are shown to improve readability of the figure.
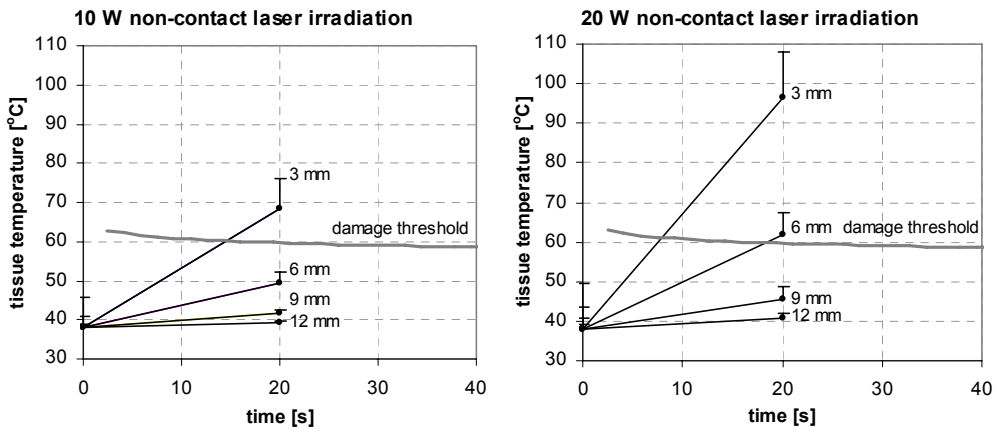

Figure 5: Reconstructed temperature increase during 20 s non-contact laser irradiation at 10 and 20 W, showing the temperature increase at 3, 6, 9 and 12 mm tissue-depth respectively. The grey line represents the Arrhenius irreversible damage limit for linear temperature increase in time, using A_f and E_a as determined by Henriques (1947).

3.3 Theoretical prediction of tissue damage threshold limits

Theoretical thermal damage limits were constructed by combining the Arrhenius damage integral (Eq. 1) with the tissue temperature distribution in time. An Arrhenius damage threshold graph was constructed by solving the Arrhenius equation (Eq. 1) numerically for $\Omega=1$ and *linear* temperature increase in time: $T(t)=38+s*t$ ('s' is the slope, varying from 0.2 to 10 ^{o}C s^{-1}; Figure 6). The resulting damage-threshold graph is displayed (grey line) in Figure 4 (contact mode) and Figure 5 (non-contact mode), demonstrating the onset of thermal damage in the measured temperature versus time distributions, according to the applied rate parameters (Henriques 1947).
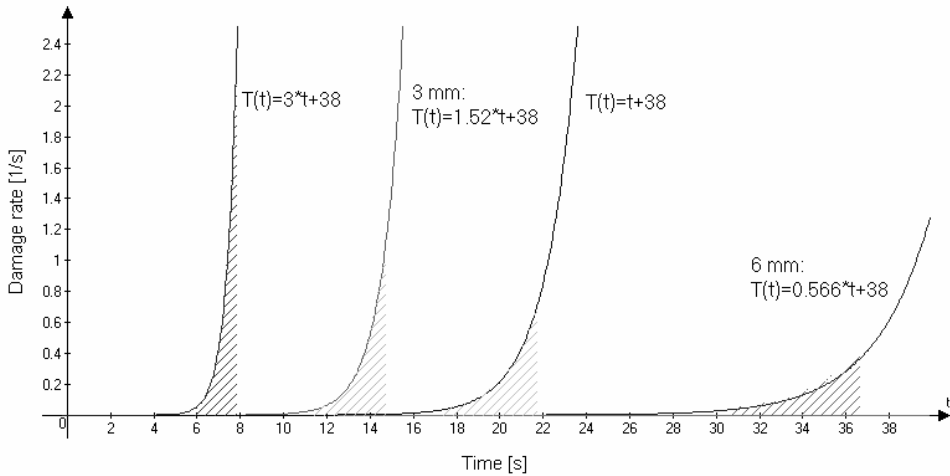

Figure 6: Example of plots of $y=Ae^{-E/RT(t)}$, for different heating regimes (T(t)) and numerical calculation of $\Omega = 1$ (area under curve = 1) to determine τ (point of 63 % protein denaturation or irreversible tissue damage). The 3 mm and 6 mm graphs denote the temperature increase and accompanying damage threshold time (τ) at 3 mm and 6 mm tissue depth during 10 W non-contact laser exposure.

3.4 Histological evaluation and damage threshold

Depth and width of thermal coagulation necrosis was measured macroscopically after 20 s of non-contact laser exposure at 5, 10, 15 and 20 W. The results are displayed in Figure 7, together with the theoretically predicted damage depth. For the 15 W setting, measurements were taken after 5, 10, 15 and 20 s, as to examine damage progression in time (Figure 8). Lesion volume was estimated by assuming a half ellipsoid: volume=$\pi/6*$(depth)(width)^{2}. Histological analysis of HE stained sections showed a damage area, comparable in size to the bleached area on macroscopic examination (Figure 9). A threshold temperature value for acute laser-induced thermal damage can be retrieved via several ways using the

histological results (Table 1). It has to be noted that damage boundaries of 5 W exposures and of 5 s exposures were not as sharp as for the other exposure regimes. Coagulation-damage extent underneath the contact mode crater was < 1 mm. Using the threshold (T=69 $\pm$ 6°C) for acute tissue damage as determined using the non-contact histology results (Table 1), the damage extent underneath the vaporizarion crater was calculated (Table 2).
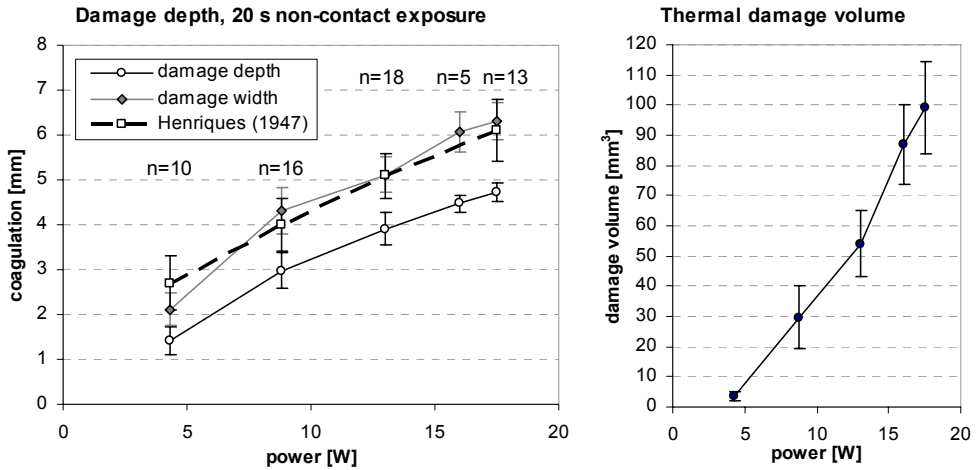
Figure 7: Macroscopically measured damage depth and width after 20 s non-contact laser exposure, means $\pm$ sd. The predicted damage depth according to Arrhenius calculation is also displayed. Damage volume was calculated assuming a half ellipsoid shape.
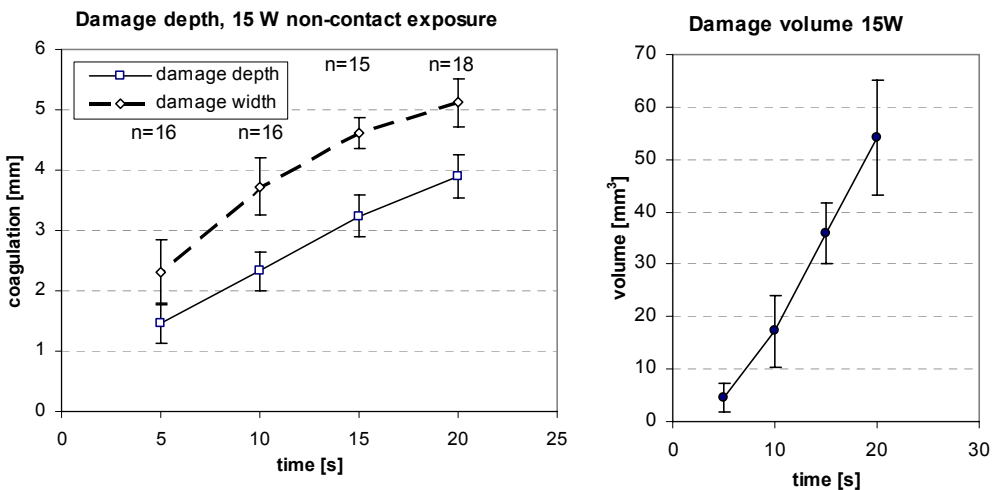
Figure 8: Macroscopically measured damage depth and width in time of 15W non-contact laser exposure, means $\pm$ sd. Damage volume was calculated assuming a half ellipsoid shape.
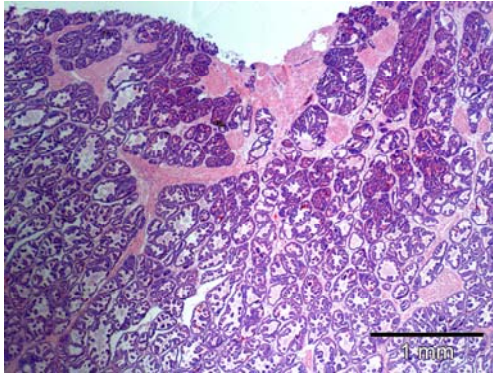
A. Thermal lesion, 15 W, 20s
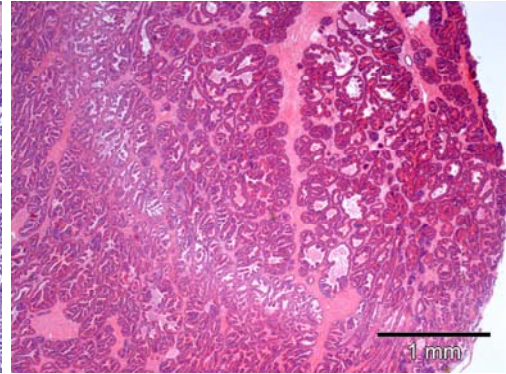
D. Thermal lesion, 20 W, 20s

B. Normal tissue
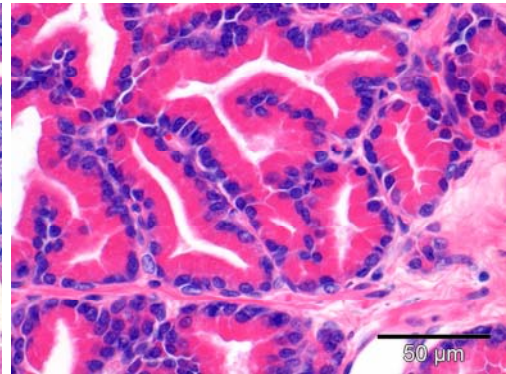
E. Normal tissue
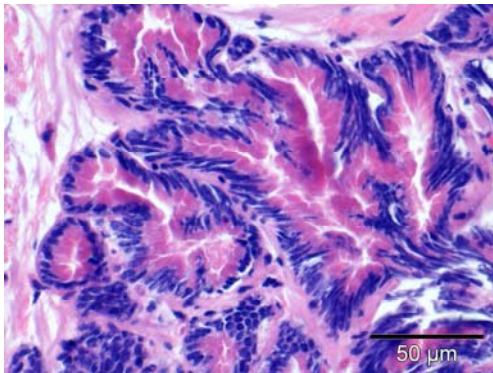
C. Thermal damage
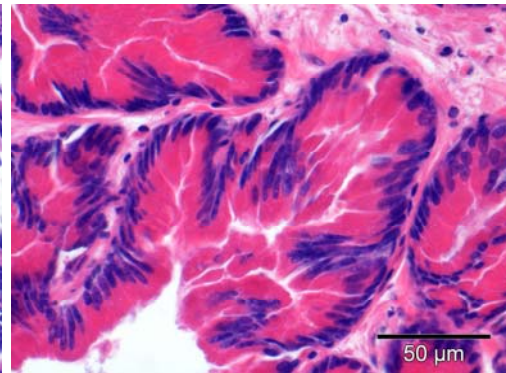
F. Thermal damage

Figure 9: Pathological changes in laser irradiated prostate tissue samples. See caption on next page.
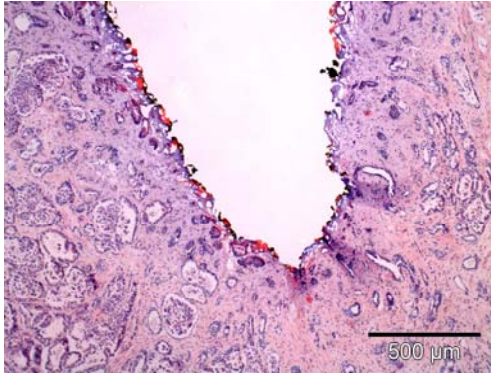
G. Vaporization crater after 5 s contact mode exposure

I. Macroscopic images of cross sections of 20s, 15 W and 20 W non-contact exposure, mm-scale included

H. Magnification of crater edge near crater floor

Figure 9, continued: Pathological changes in laser irradiated prostate tissue samples. Macroscopically, thermal necrosis was distinctly visible as whitening of tissue (I). Microscopic examination was performed on HE stained sections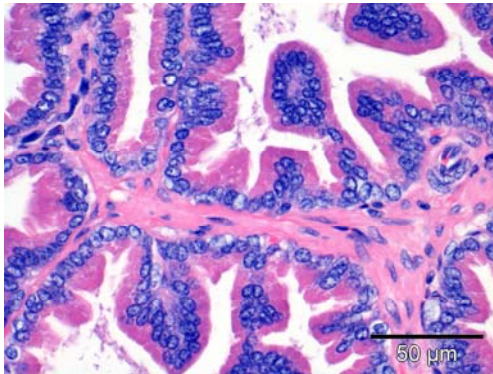 of thermal lesions. A, B, C: 20 s, 15 W non-contact exposure. D, E, F: 20 s, 20 W non-contact exposure. G, H: contact mode laser exposure. Using low magnification, HE stained sections of non-contact lesions showed increased dye uptake of an area, comparable to the macroscopic lesions (A, D). Tissue damage after 20 W laser exposure sometimes showed a slightly pale stained zone at the periphery of the lesion (D). At high magnification, thermal tissue damage was marked by increased dye uptake (eosinophilic cytoplasm and darker stained nuclei), less granulated cytoplasm, loss of nuclear detail and conformational changes of the nuclei and cells, the nuclei many times having a stretched appearance (C and F versus B and E). Contact mode laser exposure caused vaporization of tissue (G) and showed additional superficial vacuole formation, caramelization (brown-red) and carbonization (black) (H). The transition of carbonization and thermal damage to normal tissue under the vaporization-crater surface was generally <1 mm (G). Loss of birefringence was noticeable, but was not a convincing marker of thermal damage due to the limited amount of birefringence in native prostate tissue.

Point of measure	Damage [mm]	$T_{threshold}$ [^{o}C]	Mean $T_{threshold}$ [^{o}C]	Mean $T_{threshold}$ [^{o}C]*
10W, 20s	2.97 ± 0.39	69 ± 8		
15W, 13.6 ± 1.6s	3.0 ± 0.36	70 ± 10		69 ± 6
15W, 20s	3.91 ± 0.36	71 ± 8	70 ± 4	
20W, 20s	$4.72 \pm 0,20$	72 ± 9		

Table 1: Acute tissue damage threshold temperature, derived through measured damage depths and temperature distributions, means ± sd. *Apart from an overall mean threshold temperature, a mean value is also derived from only the 10W-20s and 15W-13.6s results, excluding the highest exposures, for reasons discussed in the text.

Contact mode 10 W	Mean crater depth [mm]	Damage depth from crater floor [mm]
5 s	1.29 ± 0.67	0.71 ± 0.97
10 s	2.28 ± 0.62	1.22 ± 1.06
20 s	3.48 ± 0.56	0.92 ± 0.98
Mean damage depth from crater floor: 0.93 ± 0.58 mm		

Table 2: Damage depth underneath the crater floor after 5, 10 and 20 s contact mode laser exposure at 10W (sd in crater depth is included in the calculations for damage depth).

4   Discussion

Temperature increase was measured in prostate tissue samples during contact and non-contact mode laser application. The onset of thermal damage was predicted using an Arrhenius equation, which serves as a model for *in vivo* laser induced tissue damage. Histological examination of laser irradiated tissue was used to determine the threshold temperature for acute thermal damage in *ex vivo* prostate tissue. Effects after short duration laser exposure were considered, as they reflect the situation seen during resection surgery. The cooling effect of blood flow on heat distribution is considered to increase with increasing laser exposure time (Hillegersberg 1993, Anvari *et al* 1994, Sturesson *et al* 1997). It is not always observed with short duration laser exposure (Fried *et al* 2000) and is assumed to be negligible up to 20 s of irradiation duration (see also *Chapter 1, Section 4.2*).

In general, thermal tissue damage is dependent on both temperature and the duration of increased temperature. Several studies mention damage threshold temperatures ranging from 43°C (with treatment-times up to 180 minutes (Nissenkorn and Meshorer 1993)) up to 60°C (treatment times less than 1 minute). Threshold temperatures in the range of 60-70°C are mentioned for *acute* (instantaneous) tissue damage in several tissues throughout the literature (Jacques and Prahl 1987, Thomsen *et al* 1989, Rem *et al* 2001). Nau *et al* (1999) recorded a rapid change in scattering coefficient with onset of coagulation between 60 and 65°C in canine prostate tissue. However, these tissue samples had a temperature history of subsequent exposures to increasing temperatures. Graham *et al* (1999) suggested a coagulation threshold of around 60°C for several tissues, including human prostate, using MRI techniques. However, prostate tissue showed a greater variability in results and showed prolonged MRI changes at higher temperatures compared to other tissues, leaving a definitive result unclear.

Solving the Arrhenius equation for linearly increasing temperature in time, using the rate parameters derived by Henriques (1947), returns a relatively constant damage threshold value of 60 $\pm$ 1°C for up to 30 s exposure (Figure 4 and 5). This value differs from the threshold temperature derived through histological examination (T=69 $\pm$ 6°C), which indicates that the used Arrhenius parameters are not suitable to predict acute thermal damage in prostate tissue. The Arrhenius calculation for linear temperature increase does however support the assumption that with short term exposure, tissue damage can be described by a single threshold temperature value, as proposed by others (Whelan and Wyman 1999). Using the 60 $\pm$ 1°C threshold value, calculated using the Arrhenius equation, the predicted damage depth was derived from the measured temperature distributions to be compared to the macroscopically measured damage depth in Figure 7.

Although the Arrhenius damage integral greatly simplifies the process of thermal tissue damage by assuming a single first order rate process, it has been successfully used to describe the threshold of tissue damage as a function of temperature and exposure time (Pearce and Thomsen 1995). Experimental data of the Arrhenius rate parameters (E_a and A_f) have been determined for several tissues (Bischof and He 2005), including prostate (*Chapter 1, Figure 8*). However, there are currently no Arrhenius rate parameters that describe short-term thermal damage in prostate tissue. Arrhenius parameters were determined *in vitro* for human BPH tissue (Bhowmick *et al* 2004). The Arrhenius model was fitted to data concerning a 90% drop in viability of BPH stromal tissue, implicating a threshold of 1 minute at 70°C. Skinner *et al* (2000) fitted the rate of change of optical parameters (scattering and absorption) of rat prostate at several temperatures to an Arrhenius equation. The resulting damage-time relation would imply coagulation damage at 80°C after 100 s, or at 60°C after 10 minutes. However, a mean calibration time (duration

for tissue samples to acquire static temperature) of 90 s was disregarded in their methodology, which could have affected their results. Experiments, using *in vitro* rat prostate cancer cells (Dunning AT-1), gave varying results for E_a and A_f, strongly depending on methods used and on temperature range (He *et al* 2004). Most probably, different cell-proteins show conformational changes at different rates and at different temperatures and this can not be described by a single first order rate process. It seems that apart from tissue specificity, Arrhenius rate parameter values strongly depend on methodology of investigation and temperature range (Bischof and He 2005). Therefore, it seems reasonable to conclude that Arrhenius parameters can not be extrapolated outside the temperature and exposure range in which they were experimentally determined. This means that the abovementioned prostate data are not useful for a model of acute thermal damage in the present study, since short duration exposures (up to 20s) were not considered in these studies. The very limited amount of published data concerning Arrhenius relations in short exposure thermal damage is not surprising, since several experimental limitations exist using the common method of relating damage to exposure time at static temperatures, most importantly achieving an instantaneous elevated static tissue temperature, and determining the correct end-point at high temperature (Diller and Pearce 1999).

The linear reconstruction of temperature-time curves is based on a study by Manns *et al* (1998). However, at 3 mm depth with 15 W and 20 W laser powers, the recorded temperature-graphs occasionally were more concave-shaped. This is probably due to superficial tissue alterations (change in optical and thermal properties) induced with these power densities at the surface (Nau *et al* 1999, Skinner *et al* 2000, Ritz *et al* 2001). Increased scattering (and to a lesser extent decreased conduction) of coagulated tissue will change temperature distribution: superficial temperatures would increase faster, while deeper in the tissue temperatures would increase slower compared to the non-coagulated state. However, temperature increase at 6, 9 and 12 mm does not seem to be affected much by superficial alterations, showing linear increase, suggesting that the effect on temperature distribution at these depths is minimal for short laser exposure.

The Arrhenius-predicted damage graph in Figure 7, although using an incorrect threshold value ($60 \pm 1^{o}C$, derived from Arrhenius skin parameters (Henriques 1947)), is expected to be parallel to the measured damage graph. The decreasing trend in damage depth with increasing laser power of the measured damage compared to the predicted damage, might be caused by a slight overestimation of the temperature used for the prediction. This overestimation could have been introduced by adjusting the temperatures to $38^{o}C$ at t=0 s, disregarding some of the changes in optical-thermal properties that would occur at these higher temperatures (as discussed in the previous paragraph). The effect is small and not apparent up to 10 W. However, it is probably the cause of the increasing trend in

determined threshold temperature with increasing laser power and exposure time in Table 1. Therefore, the threshold temperature for acute tissue damage in the present study derived through histological examination of 10W laser exposure and 15W damage progression up to 3 mm is considered most reliable (T=$69 \pm 6^{\circ}$C, Table 1).

Thermal tissue damage was inflicted and evaluated in *ex vivo* specimens. Our histological results comply with common observations in temperature-induced tissue damage (Pearce and Thomsen 1995). The possibility that true damage extend does not match our observations can not be ruled out, since the most reliable method for tissue damage evaluation would be to wait 3 days using living tissue (Pearce and Thomsen 1995). However, several studies indicate that our method of damage evaluation is valid for short exposure experiments. In rapid heating regimes in rabbit myocardium (up to 20 s exposure (Pearce and Thomsen 1995)) and in contact mode experiments (Janda *et al* 2002) the transition of coagulated to normal tissue was abrupt and visible macroscopically. Lethal injury that is not directly visible, or not visible *in vitro*, may occur at temperature-time regimes that do not induce coagulation but destroy enough intracellular mechanisms to kill the cells. Generally, to induce a substantial zone of non-coagulative cell death, prolonged exposure times (minutes-hours) are required, which were not used in the present experiment. Several *in vivo* transurethral canine vaporization and coagulation laser prostatectomy studies, with exposure times of *up to 10 minutes*, typically created coagulation-necrosis surrounded by a distinct rim of hemorrhage representing the transition to normal tissue (Muschter and Perlmutter 1994, Perlmutter and Muschter 1994, Motamedi *et al* 1995, Peters *et al* 2000). In time, the coagulation-necrosis zone sloughs off and a cavity remains (Gill *et al* 1994), dimensions of which do many times not exceed dimensions of direct postoperative coagulation-necrosis zone (Cromeens *et al* 1994, Cromeens *et al* 1996, Kuntzman *et al* 1996, Kuntzman *et al* 1997). Information about postoperative expansion of visible lesions in time varies, however, and is likely to be dependent on temperature history of the tissue. One study of *20 minute* exposure laser prostatectomy, using a cylindrically diffusing fiber tip, reported a broad transition zone: a non-coagulative degenerative zone of 4 - 5 mm surrounded the coagulation-necrosis zone in the acute phase, which developed coagulation necrosis en sloughing after one week. On the other hand, acute damage (1 mm, hyperemic zone included) surrounding contact mode incisions in rabbit liver *in vivo* did not extend in time (Judy *et al* 1993), supporting the assumption that *short-term* acute thermal tissue damage extent can be measured using the initial visible tissue changes.

The narrow margin from coagulation necrosis to viable tissue in short exposure regimens can be explained using the Arrhenius damage integral. Due to its exponential nature, temperature-dependent irreversible tissue damage occurs within a relatively narrow

temperature range (*Chapter 1, Figure 7*) (Pearce and Thomsen 1995), which is crossed in a relatively short time interval in rapid tissue heating procedures (Figure 6). In slow-heating procedures, creating a rather gradual temperature gradient in depth of the tissue, the temperature range to overcome coagulation threshold is spread over a larger time interval and a larger area of the tissue and the transition zone becomes broader and less well defined on histology. Furthermore, a substantial zone of non-coagulative cell death and of sub-lethal cell injury can occur due to prolonged supra-physiological temperatures.

The less distinctly visible damage boundaries at lowest power and at shortest exposure time are probably caused by the fact that Nd:YAG laser-induced tissue damage does not start at the tissue surface to travel inwards the tissue, showing a clear "damage-front" at all times. In stead, the 1064 nm irradiation propagates inside the tissue and spreads over a certain volume through scattering before being absorbed and heating takes place. Heating is not equally distributed over this volume and coagulation starts in a certain area in which the damage threshold is initially crossed (area of highest temperature). Initial damage threshold is probably distributed over a gradual transition, with accompanying vague margins.

It was expected that in contact mode, temperature and damage distributions underneath the surface are reduced in depth compared to non-contact mode, as described in *Chapters 1 and 2*. A more pronounced decrease of temperature in depth of the tissue with contact mode, caused by absorption of laser energy by the carbonized tissue surface, compared to non-contact mode was not directly evident in the study reported here, because of the expanding vaporization crater underneath the laser fiber (which was fixed in position). Temperature distributions measured during these contact mode experiments are not readily valid to reflect contact mode temperature distributions during surgery because movement of the fiber tip prevents crater formation in depth of the tissue. Therefore, shorter laser times (5 and 10 s) represent a more realistic contact mode laser model. However, damage progression underneath the contact/vaporization mode laser resection surface (bottom of the crater), as determined using a damage threshold of T=69 $\pm$ 6°C was 0.9 $\pm$ 0.6 mm in the experiments reported here (Table 2). This was consistent with histological findings (Figure 9). As an additional example, the *Appendix of Chapter 4* shows a HE stained sections of prostate tissue from *in vivo* subcapsular laser prostatectomy on a normal dog (L'Eplattenier *et al* 2006). At the edges, a zone of coagulation necrosis and moderate interstitial haemorrhage is noticeable of typically <1 mm, occasionally extending up to 1-2 mm, probably because of prolonged or non-contact exposure.

5 Conclusions

It is concluded that thermal damage is governed by a constant threshold temperature during short exposure (<<1 min). Under this assumption, threshold temperature is not coupled to duration in short term heating. An acute damage threshold temperature was determined *in vitro* for canine prostate tissue (69 ± 6 ^{o}C). The extent of tissue damage during contact mode surgery will generally be 0.9 ± 0.6 mm or less underneath the surface (Table 2). The free beam/non-contact technique can produce deeper thermal coagulation, at a rate described in Figures 7 and 8.

References

Anvari B, Rastegar S and Motamedi M (1994) Modeling of intraluminal heating of biological tissue: implications for treatment of benign prostatic hyperplasia *IEEE Trans Biomed Eng* **41** 854-64

Basinger R R, Rawlings C A, Barsanti J A, Oliver J E, Jr. and Crowell W A (1987) Urodynamic alterations after prostatectomy in dogs without clinical prostatic disease *Vet Surg* **16** 405-10

Bhowmick P, Coad J E, Bhowmick S, Pryor J L, Larson T, de la Rosette J and Bischofs J C (2004) In vitro assessment of the efficacy of thermal therapy in human benign prostatic hyperplasia. *Int J Hyperthermia* **4** 421-39

Bischof J C and He X (2005) Thermal stability of proteins *Ann N Y Acad Sci* **1066** 12-33

Bolmsjo M, Sturesson C, Wagrell L, Andersson-Engels S and Mattiasson A (1998) Optimizing transurethral microwave thermotherapy: a model for studying power, blood flow, temperature variations and tissue destruction *Br J Urol* **81** 811-6

Cromeens D M, Johnson D E, Stephens L C and Gray K N (1996) Visual laser ablation of the canine prostate with a diffusing fiber and an 805-nanometer diode laser *Lasers Surg Med* **19** 135-42

Cromeens D M, Price R E and Johnson D E (1994) Pathologic changes following transurethral canine prostatectomy with a cylindrically diffusing fiber *Lasers Surg Med* **14** 306-13

Diller K R and Pearce J A (1999) Issues in modeling thermal alterations in tissues *Ann N Y Acad Sci* **888** 153-64

Fried N M, Lardo A C, Berger R D, Calkins H and Halperin H R (2000) Linear lesions in myocardium created by Nd:YAG laser using diffusing optical fibers: in vitro and in vivo results *Lasers Surg Med* **27** 295-304

Gill H S, Kabalin J N and Mikus P W (1994) Characterization of tissue effects produced by the Prolase II lateral-firing neodymium:YAG laser fiber in the canine prostate *Lasers Surg Med* **15** 185-90

Gordon N (1960) Surgical anatomy of the bladder, prostate gland, and urethra in the male dog *J Am Vet Med Assoc* **136** 215-21

Graham S J, Stanisz G J, Kecojevic A, Bronskill M J and Henkelman R M (1999) Analysis of changes in MR properties of tissues after heat treatment *Magn Reson Med* **42** 1061-71

Hardie E M, Stone E A, Spaulding K A and Cullen J M (1990) Subtotal canine prostatectomy with the neodymium: yttrium-aluminum-garnet laser *Vet Surg* **19** 348-55

He X, Wolkers W F, Crowe J H, Swanlund D J and Bischof J C (2004) In situ thermal denaturation of proteins in dunning AT-1 prostate cancer cells: implication for hyperthermic cell injury *Ann Biomed Eng* **32** 1384-98

Henriques F C (1947) Studies of thermal injury V: The predictability and significance of thermally induced rate processes leading to irreversible epidermal injury. *Arch Pathol* **43** 489-502

Hillegersberg R (1993). Laser Treatment for Liver Metastases - Thermal and Photodynamic Therapy. Rotterdam, the Netherlands, Erasmus university.

Huidobro C, Bolmsjo M, Larson T, de la Rosette J, Wagrell L, Schelin S, Gorecki T and Mattiasson A (2004) Evaluation of microwave thermotherapy with histopathology, magnetic resonance imaging and temperature mapping *J Urol* **171** 672-8

Jacques S L and Prahl S A (1987) Modeling optical and thermal distributions in tissue during laser irradiation. *Lasers Surg Med* **6** 494-503

Janda P, Sroka R, Betz C S, Baumgartner R and Leunig A (2002) Comparison of laser induced effects on hyperplastic inferior nasal turbinates by means of scanning electron microscopy *Lasers Surg Med* **30** 31-9

Janda P, Sroka R, Mundweil B, Betz C S, Baumgartner R and Leunig A (2003) Comparison of thermal tissue effects induced by contact application of fiber guided laser systems *Lasers Surg Med* **33** 93-101

Judy M M, Matthews J L, Aronoff B L and Hults D F (1993) Soft tissue studies with 805 nm diode laser radiation: thermal effects with contact tips and comparison with effects of 1064 nm Nd:YAG laser radiation *Lasers Surg Med* **13** 528-36

Kuntzman R S, Malek R S, Barrett D M and Bostwick D G (1996) Potassium-titanyl-phosphate laser vaporization of the prostate: a comparative functional and pathologic study in canines *Urology* **48** 575-83

Kuntzman R S, Malek R S, Barrett D M and Bostwick D G (1997) High-power (60-watt) potassium-titanyl-phosphate laser vaporization prostatectomy in living canines and in human and canine cadavers *Urology* **49** 703-8

L'Eplattenier H F, van Nimwegen S A, van Sluijs F J and Kirpensteijn J (2006) Partial prostatectomy using Nd:YAG laser for management of canine prostate carcinoma *Vet Surg* **35** 406-11

Laranne J, Lagerstedt A, Pukander J and Rantala I (1997) Wound healing and soft tissue effects of CO2, contact Nd: YAG and combined CO2-Nd: YAG laser beams on rabbit trachea *Acta Otolaryngol* **117** 909-17

Lippert B M, Teymoortash A, Folz B J and Werner J A (2003) Coagulation and temperature distribution in Nd: YAG interstitial laser thermotherapy: an in vitro animal study *Lasers Med Sci* **18** 19-24

Mahoney E J and Shapshay S M (2005) Nd-YAG laser photocoagulation for epistaxis associated with hereditary hemorrhagic telangiectasia *Laryngoscope* **115** 373-5

Manns F, Milne P J, Gonzalez-Cirre X, Denham D B, Parel J M and Robinson D S (1998) In situ temperature measurements with thermocouple probes during laser interstitial thermotherapy (LITT): quantification and correction of a measurement artifact *Lasers Surg Med* **23** 94-103

Mecke H, Schunke M, Schnaidt S, Freys I and Semm K (1991) Width of thermal damage after using the YAG contact laser for cutting biological tissue: animal experimental investigation *Res Exp Med (Berl)* **191** 37-45

Motamedi M, Torres J H, Orihuela E, Pow-Sang M, Cowan D F and Warren M M (1995) Laser photocoagulation of prostate: influence of dosimetry *Lasers Surg Med* **17** 49-58

Muschter R and Perlmutter A P (1994) The optimization of laser prostatectomy. Part II: Other lasing techniques *Urology* **44** 856-61

Nau W H, Roselli R J and Milam D F (1999) Measurement of thermal effects on the optical properties of prostate tissue at wavelengths of 1,064 and 633 nm *Lasers Surg Med* **24** 38-47

Nissenkorn I and Meshorer A (1993) Temperature measurements and histology of the canine prostate during transurethral hyperthermia *J Urol* **149** *1613-1616*

Orihuela E, Motamedi M, Cammack T, Torres J H, Pow-Sang M, Lahaye M, Cowan D F and Warren M M (1995) Comparison of thermocoagulation effects of low power, slow heating versus high power, rapid heating Nd: YAG laser regimens in a canine prostate model *J Urol* **153** 196-200

Pearce J and Thomsen S (1995) Rate process analysis of thermal damage *Optical-Thermal Response of Laser-Irradiated Tissue* ed A J Welch and M J C van Gemert (New York: Plenum) pp 562-606

Perlmutter A P and Muschter R (1994) The optimization of laser prostatectomy. Part I: Free beam side fire coagulation *Urology* **44** 847-55

Perry D A, Goodis H E and White J M (1997) In vitro study of the effects of Nd:YAG laser probe parameters on bovine oral soft tissue excision *Lasers Surg Med* **20** 39-46

Peters R D, Chan E, Trachtenberg J, Jothy S, Kapusta L, Kucharczyk W and Henkelman R M (2000) Magnetic resonance thermometry for predicting thermal damage: an application of interstitial laser coagulation in an in vivo canine prostate model *Magn Reson Med* **44** 873-83

Prapavat V, Roggan A, Walter J, Beuthan J, Klingbeil U and Muller G (1996) In vitro studies and computer simulations to assess the use of a diode laser (850 nm) for laser-induced thermotherapy (LITT) *Lasers Surg Med* **18** 22-33

Rawlings C A, Crowell W A, Barsanti J A and Oliver J E, Jr. (1994) Intracapsular subtotal prostatectomy in normal dogs: use of an ultrasonic surgical aspirator *Vet Surg* **23** 182-9

Rem A I, Oosterhuis J A, Journee-de Korver J G, van den Berg T J T P and Keunen J E E (2001) Temperature Dependence of Thermal Damage to the Sclera: Exploring the Heat Tolerance of the Sclera for Transscleral Thermotherapy. *Exp Eye Res* **72** 153-62

Ritz J P, Roggan A, Germer C T, Isbert C, Muller G and Buhr H J (2001) Continuous changes in the optical properties of liver tissue during laser-induced interstitial thermotherapy *Lasers Surg Med* **28** 307-12

Robertson J J and Bojrab M J (1984) Subtotal Intracapsular Prostatectomy - Results in Normal Dogs. *Vet Surg* **13** 6-10

Shapshay S M (1987) Laser applications in the trachea and bronchi: a comparative study of the soft tissue effects using contact and noncontact delivery systems *Laryngoscope* **97** 1-26

Skinner M G, Everts S, Reid A D, Vitkin I A, Lilge L and Sherar M D (2000) Changes in optical properties of ex vivo rat prostate due to heating *Phys Med Biol* **45** 1375-86

Sturesson C, Liu D L, Stenram U and Andersson-Engels S (1997) Hepatic inflow occlusion increases the efficacy of interstitial laser-induced thermotherapy in rat *J Surg Res* **71** 67-72

Thomsen S, Pearce J A and Cheong W F (1989) Changes in birefringence as markers of thermal damage in tissues *IEEE Trans Biomed Eng* **36** 1174-9

Ventrucci M, Di Simone M P, Giulietti P and De Luca G (2001) Efficacy and safety of Nd:YAG laser for the treatment of bleeding from radiation proctocolitis *Dig Liver Dis* **33** 230-3

Verdaasdonk R M, Borst C and van Gemert M J (1990) Explosive onset of continuous wave laser tissue ablation *Phys Med Biol* **35** 1129-44

Verdaasdonk R M, Holstege F C, Jansen E D and Borst C (1991) Temperature along the surface of modified fiber tips for Nd:YAG laser angioplasty *Lasers Surg Med* **11** 213-22

Weber H, Enders S and Hessel S (1991) Thermal effects and histologic changes from Nd:YAG laser irradiation on normal and diseased aortic tissue using a novel angioplasty catheter with a mobile optical fiber: an in vitro assessment *Angiology* **42** 597-606

Whelan W M and Wyman D R (1999) Dynamic modeling of interstitial laser photocoagulation: implications for lesion formation in liver in vivo *Lasers Surg Med* **24** 202-8

Initial validation of the color schlieren prostate model using the measured damage propagation in canine prostate tissue

S.A. van Nimwegen[1], A.I. Rem[2], J. Kirpensteijn[1]

[1]Department of Clinical Sciences of Companion Animals, Faculty of Veterinary Medicine, Utrecht University, Utrecht, The Netherlands;
[2]Department of Clinical Physics, University Medical Center, Utrecht, The Netherlands.

Introduction

Color schlieren recordings were made of non-contact laser exposure in a polyacrylamide gel in *Chapter 2*. It was assumed that the schlieren lines of the outer (lateral) shape of the temperature distribution represent isothermal regions. Since acute damage onset in *ex vivo* canine prostate tissue, as determined in *Chapter 3*, is determined by a constant threshold temperature of $69 \pm 6^{\circ}$C, damage progression inside the tissue represents progression of an isotherm during laser exposure. It was concluded in *Chapter 2* that the polyacrylamide gel, containing 9 mg/ml $CuSO_4$, is an acceptable model for canine prostate tissue. Therefore, it was hypothesized that the measured damage progression in time in tissue will be in pace with progression in time of schlieren lines in the schlieren recordings of comparable settings (similar power, broader beam size to overcome differences in scattering of the gel compared to tissue).

In an attempt to further test the accuracy of the schlieren gel as a model for canine prostate tissue, tissue-damage progression (*Chapter 3*) was compared to the schlieren recordings (*Chapter 2*).

Methods

In *Chapter 2*, schlieren recordings were made of 20 s of 15 W laser exposures at a fiber distance of 12-14 mm from the gel surface, which was near popcorn threshold. Similar

circumstances were encountered in the canine prostate tissue experiments in *Chapter 3*, using 15 W laser power with a fiber distance of 6 mm. To test accuracy of the gel, damage progression margins were incorporated in the schlieren recordings of 7 and 9 mg/ml $CuSO_4$, to see if movement of the damage boundary during laser exposure is in pace with schlieren lines. Observations in these experiments were quantified by determining the speed of progression of schlieren lines relative to the damage boundary from 10 s to 15 s and from 15 s to 20 s at the level of the damage boundary. This was done by measuring the difference in position ('d1' in Figure 1, B) at 15 s, of the measured damage depth (dashed red line) and the (deepest point of the) schlieren line that was nearest to the damage depth at 10 s. The same was done at 20 s, for the nearest schlieren line at 15 s ('d2' in Figure 1, C). In other words: the deviation of schlieren lines compared to the damage boundary was measured twice during a time interval of 5 s at the level of the damage boundary. Furthermore, the width and depth of the schlieren line that best fitted the damage depth and width in time was measured for the gel that best fitted the tissue damage results. Differences in results were tested using Students t-test. Results are given as means ± sd.

Results

Representative schlieren images of 15 W non-contact Nd:YAG laser exposure for 7 and 9 mg/ml concentrations of $CuSO_4$ are displayed in Figure 1. The measured damage depth and width at 15 W non-contact Nd:YAG exposure of canine prostate tissue are included in the images (dashed red lines). The actual shape of the damage area in prostate tissue was estimated by an ellipsoid shape (dashed white lines), assuming the area of highest temperature (center of the ellipse) to be at around 1.0-1.5 mm underneath the tissue surface. The results of the relative-speed measurements of the schlieren lines compared to the damage depth are given in Table 1. The schlieren line nearest to the damage depth was the 6th (yellow) line in the 9 mg/ml gel. The width and depth of the 6th schlieren line was measured to be compared to the tissue damage depth at 15 s and 20 s (Table 2).

Polyacrylamide gel	7 mg/ml $CuSO_4$, n=5	9 mg/ml $CuSO_4$	n	p-value
Relative schlieren speed 10-15 s [mm/s]	0.18 ± 0.026	0.066 ± 0.037	9	<0.001
Relative schlieren speed 15-20 s [mm/s]	0.11 ± 0.023	0.033 ± 0.021	9	<0.001
Nearest schlieren line in depth, t=15 s		5.8 ± 0.6	8	
Nearest schlieren line in depth, t=20 s		6.2 ± 0.6	8	

Table 1: Results of relative-speed measurements of schlieren lines compared to damage depth at the exposure intervals of 10-15 s and 15-20 s, during 15 W non-contact Nd:YAG laser irradiation.

Point of measure	6th schlieren line	n	Tissue damage	n
Width [mm], t=15 s	4.5 ± 0.2	6	4.6 ± 0.3	14
Width [mm], t=20 s	5.1 ± 0.4	8	5.1 ± 0.4	15
Depth [mm], t=15 s	3.1 ± 0.5	8	3.2 ± 0.4	18
Depth [mm], t=20 s	3.9 ± 0.5	7	3.9 ± 0.4	18

Table 2: The width and depth of the 6th schlieren line was measured in the 9 mg/ml $CuSO_4$ gel at t=15 s and t=20 s of 15 W non-contact laser exposure. The width and depth of the tissue damage is also diplayed, as measured in *Chapter 3, Figure 8*.
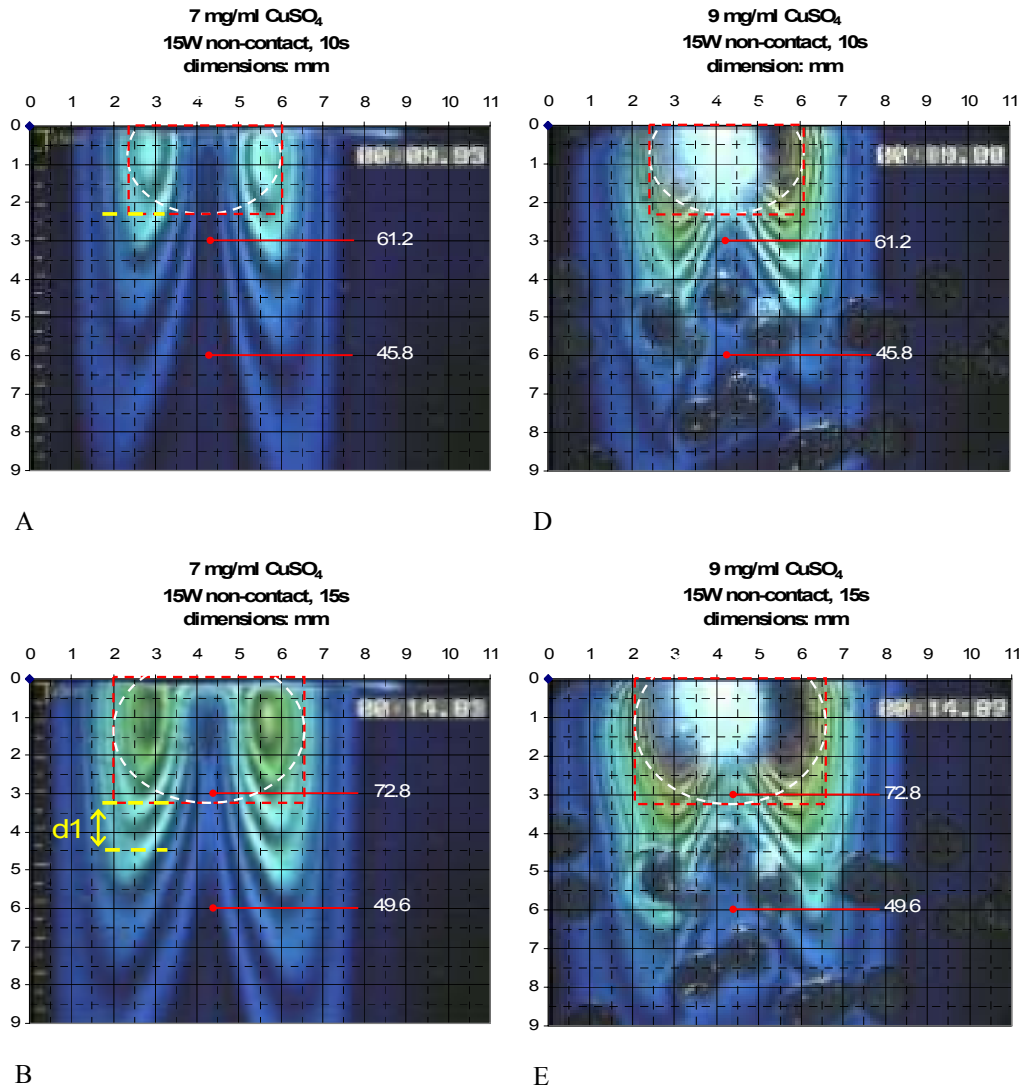
Figure 1: Examples of schlieren images. See next page for caption.

7 mg/ml CuSO₄
15W non-contact, 20s
dimensions: mm

9 mg/ml CuSO4
15W non-contact, 20s
dimensions: mm

C

F
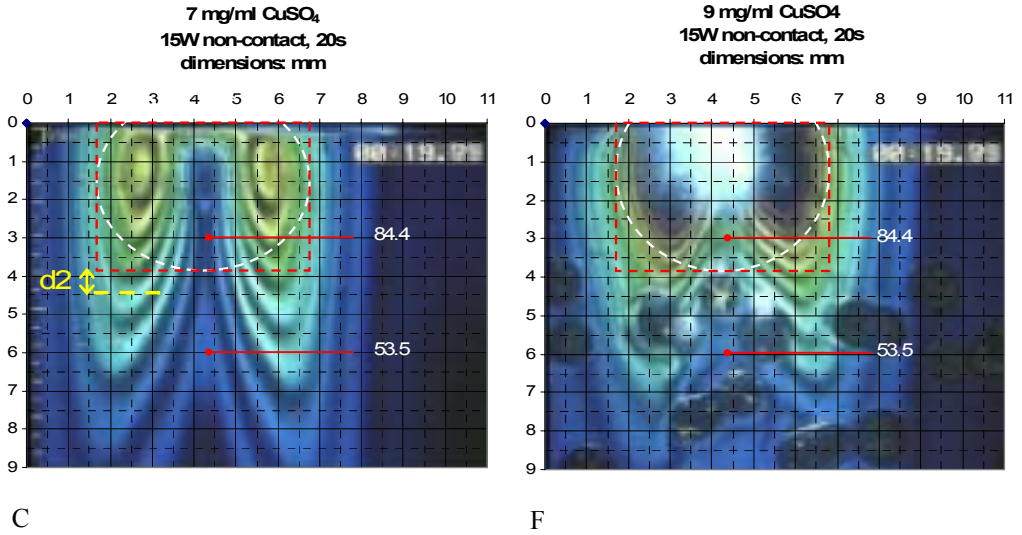
Figure 1, continued: Examples of schlieren images of 15 W laser exposure at t=10, 15 and 20 s. The fiber distance was 12-14 mm, using two gel concentrations of $CuSO_4$ (A, B, C: 7 mg/ml; D, E, F: 9 mg/ml). The damage margins, as measured in Chapter 3 during 20 s of 15 W laser exposure at a fiber distance of 6 mm, are incorporated in the images. The dashed red lines represent the measured depth and width of the thermal tissue damage. The dashed white ellipsoid lines are arbitrary, denoting the approximate damage margin. Measured *tissue* temperatures at 3 and 6 mm depth are also displayed. The cloudy white spot and the air bubbles in D, E and F are artifacts.

Discussion

The speed of the schlieren lines in the 9 mg/ml $CuSO_4$ concentration approaches that of the measured damage progression (Figure 1, Table 1). The difference in speed of the schlieren lines compared to the damage progression was reduced by a factor of 2.7-3.3 for the 9 mg/ml $CuSO_4$ polyacrylamide gel compared to the 7 mg/ml concentration. In the 9 mg/ml gel, the range of the speed-lag of the damage front compared to the schlieren lines was 0.0 to 0.06 mm/s in the 15-20 s interval. The depth and width of the tissue-damage extent coincided with the 6th (yellow) schlieren line. Therefore, the depth and width of the 6th schlieren line was measured and is displayed in Table 2. The measured width of the tissue damage after 15 s and 20 s of 15 W laser exposure was 4.6 ± 0.3 mm and 5.1 ± 0.4 mm respectively (*Chapter 3, Figure 8*) and is comparable with the measured width of the 6th schlieren line of 4.5 ± 0.2

mm and 5.1 ± 0.4 mm respectively (Table 2). The measured tissue damage depth after 15 s and 20 s laser exposure was 3.2 ± 0.4 mm and 3.9 ± 0.4 mm respectively (*Chapter 3, Figure 8*) and is comparable with the measured depth of the 6th schlieren line of 3.1 ± 0.5 mm and 3.9 ± 0.5 mm respectively (Table 2).

It has to be mentioned that the depth of the schlieren lines was measured at their deepest point (where they bend towards the central axis; d1 and d2 in Figure 1), which is however not the deepest point of the actual isotherm, which is not visible because of the imaging artifact in the central axial region. The damage depth in the *tissue* was measured at the deepest point of the damage distribution, in the central axial area. This means that the correct pace of schlieren lines at the measured ('bending') point may in reality show a slight deviation compared to the measured damage depth, since they are not measured at the same location.

It is concluded from the findings in the present study, that the polyacrylamide schlieren gel, containing 9 mg/ml $CuSO_4$, can be used to model the shape of Nd:YAG laser-induced temperature distribution for canine prostate tissue for up to 20 s exposure. However, further investigation, including temperature measurements in the gel, is required to calibrate the schlieren model if it were to be used to predict laser tissue interaction in a quantitative way.

4

Chapter 4

Partial Prostatectomy Using Nd:YAG Laser for

Management of Canine Prostate Carcinoma

Henry F. L'Eplattenier, DrMedVet, Diplomate ECVS
Sebastiaan A. van Nimwegen, DVM
Frederik J. van Sluijs, DVM, PhD, Diplomate ECVS
Jolle Kirpensteijn, DVM, PhD, Diplomate ACVS & ECVS

Department of Clinical Sciences of Companion Animals,
University of Utrecht, The Netherlands.

Abstract

Objective—To report a technique for partial prostatectomy by laser dissection and to evaluate outcome and complications in dogs with prostate carcinoma (PCA).

Study Design—Experimental and clinical case series.

Animals—Four normal dogs and 8 dogs with PCA.

Methods—Subcapsular partial prostatectomy, sparing the urethra and the dorsal aspect of the prostatic capsule, using Nd:YAG laser dissection to remove the prostatic parenchyma and control hemorrhage was performed in 4 normal dogs and subsequently in 8 dogs with histologically confirmed PCA. Additional treatment of PCA dogs included local application of interleukin-2 and systemic administration of meloxicam. Prostate size, complications, and survival time were recorded. Laser-associated thermal damage to surrounding tissue was evaluated by histology.

Results—In normal dogs, no damage to the dorsal prostatic capsule or urethra was detected. In PCA dogs, median survival was 103 days (range, 5–239 days). Three dogs died from complications within 16 days, whereas 5 (median survival, 183 days; range, 91–239 days) had improvement or resolution of clinical signs. Urinary incontinence did not occur.

Conclusion—Laser assisted subcapsular partial prostatectomy can be performed in dogs with PCA without development of postoperative incontinence.

Clinical Relevance—Subcapsular partial prostatectomy is a potential palliative treatment for PCA in dogs and may lead to the resolution of clinical signs for several months.

Introduction

Canine prostate carcinoma (PCA) is uncommon with an estimated prevalence of 0.2–0.6% (Bell *et al* 1991). True prevalence is unknown as population-based data is not available (Cooley and Waters 2001). Canine PCA has an invasive growth pattern and commonly metastasizes to the sublumbar lymph nodes; occasionally, metastases to the lungs and lumbar vertebrae are observed (Waters *et al* 1998). Castration has no effect on disease progression, nor does it prevent occurrence of PCA; in fact, it appears that castrated males are at an increased risk of developing PCA compared with intact males (Teske *et al* 2002). Clinically, canine PCA therefore resembles late stage, hormone-independent human PCA and the dog is an appropriate model for understanding the pathogenesis of PCA in humans. Unlike humans, total prostatectomy is not an option for treatment of PCA in dogs because of a high incidence of postoperative incontinence (Goldsmid and Bellenger 1991). The

cause of incontinence in dogs after total prostatectomy is uncertain. Total prostatectomy in dogs with prostatic disease is more likely to cause incontinence than prostatectomy in dogs with a normal prostate (Basinger *et al* 1987, Basinger *et al* 1989), suggesting that primary prostatic disease rather than surgical technique may be responsible for this complication. For these reasons, therapeutic modalities for PCA in dogs need to optimize removal of neoplastic tissue without compromising urethral sphincter function, which is controlled by the hypogastric nerve lying dorsolateral to the prostate and bladder neck (Evans and Christensen 1993). Ideally, the technique for removal of prostatic tissue should permit careful dissection of prostatic parenchyma and optimal control of hemorrhage to maintain good visibility and a high level of precision for maximal removal of neoplastic tissue, but preserving the neurovascular structures on the dorsolateral aspect of the prostate. We hypothesized that these principles could be respected by use of Neodymium:Yttrium Aluminum Garnet (Nd:YAG) laser to perform subcapsular partial prostatectomy to substantially reduce prostatic volume, alleviate clinical signs of PCA and maintain urinary continence.

Because removal of neoplastic tissue would be incomplete, adjuvant therapy is required to ensure that remaining neoplastic tissue and metastases are prevented from proliferating. Interleukin-2 (IL-2), a cytokine with a wide range of immunologic effects including the activation of cytotoxic T lymphocytes, natural killer cells and lymphokine-activated killer cells (Eklund and Kuzel 2004, Jacobs *et al* 2005), has been used systemically and intralesionally for treatment of various neoplasia in cows, horses, and humans, and reportedly induces regression of metastatic tumors in humans (Eklund and Kuzel 2004, Jacobs *et al* 2005, Satoh *et al* 2005). IL-2 has been administered intralesionally in doses ranging from 200,000 IU/tumor (Den Otter *et al* 1995) to 6 million IU (Satoh *et al* 2005). In addition, prostate cancer cells like other cancer cell types express cyclooxygenase-2 (COX-2), whereas normal prostatic cells do not. Although the exact significance of COX-2 for carcinogenesis is not entirely understood (Hussain *et al* 2003), studies using cell cultures and in vivo mouse models show that inhibition of COX-2 could be beneficial in management of patients with PCA (Liu *et al* 2000, Kamijo *et al* 2001). Meloxicam is a non-steroidal anti-inflammatory drug with high specificity for COX-2 inhibition (Riendeau *et al* 1997) and is registered for long-term treatment of dogs.

Thus, we report use of a Nd:YAG laser-assisted technique for partial prostatectomy in 4 normal dogs, and then outcome in 8 dogs with histologically confirmed PCA also treated with intralesional IL-2 and systemic meloxicam.

Materials and Methods

Dogs

The technique was first tested in 4 non-survival, healthy, intact, adult male Beagles (weight, 14.5–21.5 kg; age, 5–7 years), then used in 8 patients with a suspicion of PCA, based on cytological examination of an ultrasound-guided fine needle aspirate of the prostate.

Anesthesia

Dogs were premedicated with medetomidine (20 µg/kg intravenously [IV] initially then 10 µg/kg hourly), and anesthesia was induced with propofol (1–2 mg/kg IV to effect) and maintained with isoflurane (<1% end-tidal concentration in 50% air and 50% O_2). Lactated Ringers solution (5 mL/kg/h) was administered throughout anesthesia. A combination of buprenorphine (20 µg/kg subcutaneously 4 times daily until hospital discharge) and meloxicam (0.2 mg/kg before surgery, then 0.1 mg/kg orally once daily) was administered for analgesia.

Surgical Procedure

We performed subcapsular partial prostatectomy, sparing the urethra and the dorsal aspect of the prostatic capsule including the neurovascular structures essential to the normal function of the urethral sphincter. A urethral catheter was inserted to allow localization of the urethra during surgery. The prostate was approached by caudal median celiotomy, the bladder was retracted cranially, and periprostatic fat tissue was dissected from the prostate to allow observation of the ventral portion of the prostatic capsule. An Nd:YAG surgical laser (Medilas 40N, MBB-Medizintechnik GmbH, München, Germany) with a 600 µm optical fiber (Ultraline, Heraeus LaserSonics, Milpitas, CA) was used at 10 W (continuous wave) to incise the ventral part of the prostatic capsule along the midline. Prostatic tissue was bluntly separated from the capsule, then parenchymal segments were removed using laser dissection to control hemorrhage. Prostatic tissue samples were submitted for microscopic examination to confirm a diagnosis of PCA. The urethra remained intact and prostatic tissue was removed on each side of the urethra as far dorsally as possible. Finally the edges of the capsule were trimmed and the capsule was sutured ventrally over the urethra without leaving dead space, using a continuous pattern of 3-0 polyglecaprone 25, then the celiotomy was closed in layers.

Postoperative Evaluation

Prostate size was measured pre- and post-operatively by ultrasonography and prostate volume calculated (Kamolpatana *et al* 2000). Prostate volume was divided by body weight to obtain prostatic index to compare prostate volume in dogs of differing body size. Experimental dogs were euthanatized immediately postoperatively and the prostate was submitted for histologic examination to determine laser thermal damage to the dorsal part of the prostatic capsule and urethra. Prostatic tissue was fixed in formalin, embedded in paraffin, sectioned, and stained with hematoxylin–eosin.

Postoperative Treatment

After surgery in dogs with PCA, IL-2 (4.5 million IU in 1 mL 0.9% NaCl) was injected into the remaining prostatic tissue and meloxicam (0.1 mg/kg orally once daily) was administered. Dogs were examined 1 month postoperatively, then every other month. On each follow-up visit, chest radiographs were taken and abdominal ultrasonography performed.

Statistical Analysis

Survival times were reported as median and range. Prostate dimensions were as mean±SD. Where appropriate, a t-test for paired samples was performed to compare preoperative and postoperative means. Pearson's correlation was used to test the correlation between prostate index and survival. Significance was $P<.05$ (2-tailed).

Results

In normal and PCA dogs, use of the Nd:YAG laser provided excellent control of hemorrhage during prostatic tissue dissection. Occasional hemorrhage from larger vessels running beneath the prostatic capsule was controlled by laser or electrocautery. In normal dogs, prostatic volume was reduced by 50.5±15.0% ($P=.013$) and 2 mm of periurethral tissue remained. There was no visible damage to the dorsal prostatic capsule or urethra on histologic examination.

Dogs with PCA

Clinical signs associated with PCA were present for 1–4 months except for 1 dog that had urethral blood loss for >36 months (Table 1). Median survival time was 103 days (range, 5–239 days (Fig 1).

There was a weak positive, but non-significant correlation ($R^2=0.32$, $P=.56$) between prostatic index and survival time (Fig 2). One dog was omitted from this analysis because

the prostate contained large fluid filled cysts and the measured volume of the prostate did not accurately reflect the volume of neoplastic tissue. Five dogs recovered well from surgery and clinical signs improved or resolved; median survival time was 183 days (range, 91–239 days). None of the dogs developed urinary incontinence.
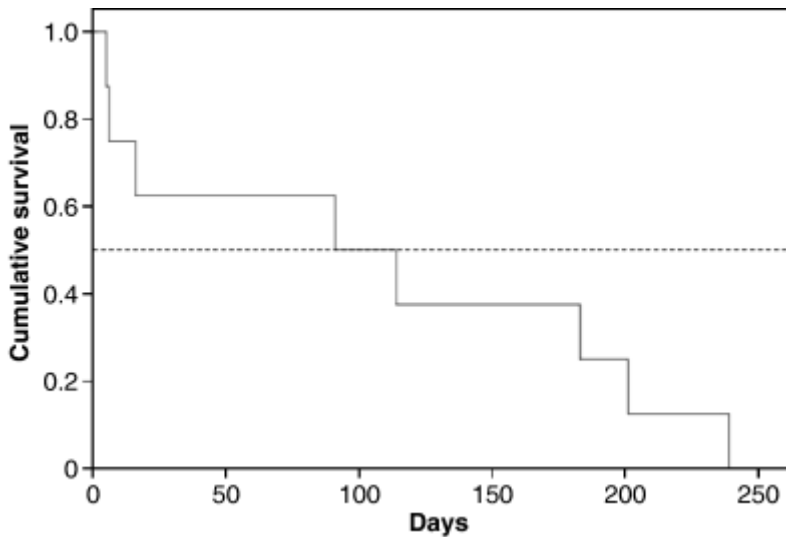

Fig 1: Kaplan–Meier cumulative survival curve for 8 dogs with prostate carcinoma (PCA) treated by partial prostatectomy facilitated by use of Nd:YAG laser dissection.
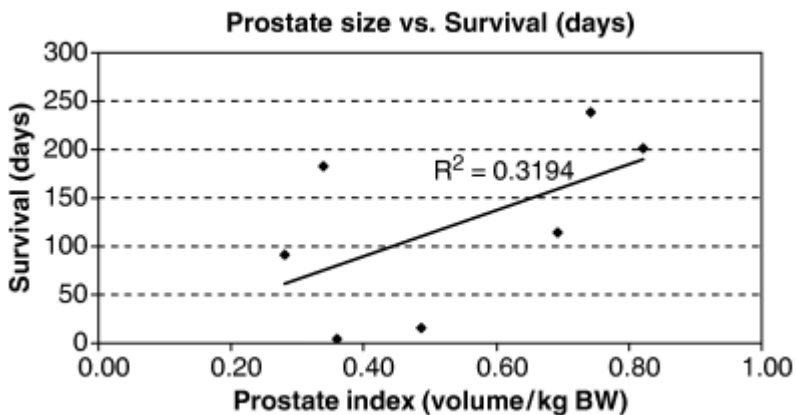

Fig 2: Linear regression curve showing survival as a function of prostatic index (prostate volume [mL] divided by body weight [kg]).

All dogs were eventually euthanatized because of recurrence of clinical signs like dyschezia and dysuria. In 1 dog, these signs were related to urinary tract infection that resolved with antibiotic administration. Clinical signs in all dogs recurred even though the prostate was not clinically substantially enlarged compared with its immediate postoperative size. Necropsy examination of the prostate invariably revealed an aggressive histologic pattern with invasion of tumor cells into blood vessels and the prostatic capsule.

Three dogs developed postoperative complications and died or were euthanatized within 16 days of surgery. In 1 dog, severe dysuria present before surgery did not resolve and the dog was unable to urinate postoperatively, despite administration of a sympathicolytic drug (prazosin, 0.033 mg/kg orally every 8 hours) and meloxicam. Another dog was euthanatized because of bilateral ureteral obstruction from tumor ingrowth into the trigone region of the bladder. Both dogs were admitted preoperatively with severe stranguria requiring daily catheterization. The 3rd dog, a Bouvier des Flandres mixed breed that had clinical signs of prostatic disease for 36 months before admission had 2 very large prostatic cysts that were drained and omentalized before subcapsular prostatectomy. Preoperatively, there was moderate hypoalbuminemia, slight thrombocytopenia, and slightly increased activated partial thromboplastin time (APTT). Intraoperatively, the dog had an increased bleeding tendency suggestive of a clotting disorder. Immediately postoperatively, the dog had signs of oliguria requiring aggressive fluid therapy including plasma transfusion. On the day after surgery the dog developed severe hind limb edema.

Ultrasonographic examination of the caudal abdomen revealed a dorsally enlarged prostate, possibly from a hematoma, however no evidence of abnormal circulation to the hind limbs was detected. It was not clear whether the edema was caused by hypoalbuminemia, if changes in the prostate region caused disturbance of lymphatic drainage from the hind limbs, or whether it was a reaction to the plasma transfusion. Despite continued fluid therapy, blood transfusion, and medical management the dog did not recover appropriately. The owners insisted on taking the dog home and it died 6 days after surgery.

Two of the 8 dogs had metastases to the sublumbar lymph nodes at the time of surgery. A 3rd dog developed visible pulmonary metastases during follow-up (2 metastases were visible on thoracic radiographs 1 month postoperatively and remained visible during subsequent rechecks).

Breed	Age (Years)	Clinical Signs	Prostate Index[*]	Survival (Days)
Bearded collie†	11	Tenesmus, hemorrhagic urethral discharge	0.34	183
Labrador retriever	10	Purulent urethral discharge	0.82	201
Heidewachtel	10	Tenesmus, stranguria	0.69	114
Hovawart	10	Pollakiuria, hemorrhagic urethral discharge	0.28	91
Bouvier des Flandres Crossbreed**	14	Tenesmus, hematuria, hemorrhagic urethral discharge	—	6
Bearded collie	11	Tenesmus, dysuria, pollakiuria	0.74	239
Golden retriever	11	Severe stranguria‡	0.49	16
Labrador retriever†	9	Tenesmus, severe stranguria‡	0.36	5

[*]Volume of prostate (mL) divided by body weight (kg).

†Patients diagnosed with metastases to the local lymph nodes.

‡Severe stranguria was defined as stranguria requiring daily catheterization.

**Prostate contained large cysts, therefore prostate size was not considered a relevant indicator of the volume of neoplastic tissue.

Table 1: Signalment, Clinical Signs and Survival of 8 Castrated Male Dogs with Prostate Carcinoma Treated by Partial Prostatectomy Facilitated by Nd:YAG Laser Dissection.

Discussion

In normal dogs, the technique we report was effective in removing prostate parenchyma and controlling hemorrhage and resulted in a significant reduction in prostate volume. Ideally, these dogs should have been followed postoperatively to check for incontinence and other complications; however, that experimental design was considered ethically unacceptable in the Netherlands. The absence of histologic evidence of thermal damage to important regional anatomic structures suggests that Nd:YAG laser may safely be used to dissect prostatic tissue within millimeters of either the urethra or the dorsal prostatic capsule with its associated neurovascular structures. This assumption was confirmed by the outcome of the procedure in dogs with PCA where none developed urinary incontinence.

Various partial prostatectomy techniques have been described using either electrocoagulation (Harari and Dupuis 1995), ultrasonic aspiration (Rawlings *et al* 1994, Rawlings *et al* 1997), or Nd:YAG laser excision (Hardie *et al* 1990) in normal dogs or dogs with benign prostatic disease. Subcapsular dissection as we describe was similar to previously reported techniques using electrocoagulation (Harari and Dupuis 1995) and ultrasonic aspiration (Rawlings *et al* 1994, Rawlings *et al* 1997). The absence of postoperative incontinence in our dogs corresponds to similar results reported for other dissection techniques. Another study reported partial prostatectomy using a Nd:YAG laser (Hardie *et al* 1990) not for subcapsular dissection of prostate tissue but resection of prostatic capsule and parenchyma on each side of the urethra, including the dorsolateral aspect of the capsule. With that technique no incontinence occurred in normal dogs but the postoperative incidence in dogs with prostatic disease was similar to the incidence after total prostatectomy. Our results corroborate our hypothesis that partial prostatectomy maintaining the dorsolateral aspect of the prostatic capsule intact is seemingly necessary to avoid postoperative incontinence.

Canine PCA is an invasive tumor and complete removal of the prostate to obtain sufficient tumor margins leads to intractable and thus, unacceptable urinary incontinence. Marginal, partial prostatectomy without additional radiotherapy is, by definition, a palliative procedure. In most of our dogs clinical signs improved substantially or resolved completely. Dogs survived up to 240 days after surgery before clinical signs recurred and the dogs were euthanatized. Interestingly, clinical signs recurred in the absence of substantial prostatic enlargement. The invasive nature of PCA seen at necropsy indicated that recurrence of signs was probably because of tumor progression into the lumen of the urethra or the wall of the rectum.

Published information on outcome after diagnosis of PCA in dogs is very sparse. In 1 report describing clinical aspects of PCA in dogs without surgical treatment, 58 of 72 dogs were euthanatized at diagnosis and mean survival time for those surviving >1 week was 30 days. Reports of surgical treatment of PCA in dogs is limited to a few cases. Surgical placement of a retained urethral catheter in 3 dogs with PCA and stranguria enabled the dogs to survive 3–5 months after surgery (Mann *et al* 1992). In another report, 3 male dogs with prostatic neoplasia were treated by transurethral resection using an electrocautery loop (combined with intraoperative radiation therapy in 2 dogs) (Liptak *et al* 2004). Survival times were 32, 74, and 264 days; however, 2 dogs were diagnosed with prostatic transitional cell carcinoma and 1 with undifferentiated carcinoma, therefore it is uncertain whether these results are comparable with our patients. Treatment of PCA by transurethral photodynamic therapy allowed 1 dog to survive nearly 9 months after treatment (Lucroy *et al* 2003). Survival times of the dogs in our study therefore compare favorably with

previously published results of surgical treatment of PCA in dogs. It is possible that other forms of adjuvant treatment directed toward local control of remaining neoplastic tissue could allow prolonged survival times after laser surgery in dogs with PCA.

Severe complications developed in 3 dogs. Because of the high level of emotional distress of owners it was not possible to collect necropsy information. In 2 dogs, complications were associated with persistence of dysuria and stranguria. Because these 2 dogs had severe stranguria before surgery, we believe these complications likely resulted from tumor ingrowth into the urethra, rather than from a direct effect of the surgical procedure on the proximal urethra. In the 3rd dog, the complications were systemic (hypoalbuminemia, shock, hind limb edema) and not specifically related to the prostate. These complications probably resulted from the clotting disorder diagnosed preoperatively, however a treatment-related effect cannot entirely be excluded. Severe stranguria preoperatively (i.e., stranguria requiring catheterization) may be a negative prognostic factor for survival after treatment, as evident in these dogs. Duration of clinical signs before diagnosis, tumor size at admission, and metastases to the sublumbar lymph nodes did not significantly correlate with survival time.

We lack a control group. Inclusion of a control group (dogs that did not have surgery) however, was considered a bias because these dogs often have the worst clinical signs. Additionally, owner motivation of a dog that has had surgery cannot be compared with that of an owner of an unoperated dog. Owner motivation to pursue treatment is an aspect of prime importance influencing the choice of time for euthanasia and therefore survival time after beginning treatment. Based on our experiences with these PCA dogs, we believe that partial prostatectomy facilitated by Nd:YAG laser dissection and accompanied by adjuvant treatment can be considered as a palliative treatment that can provide resolution of clinical signs for at least several months postoperatively.

Acknowledgements

References

Basinger R R, Rawlings C A and Barsanti J A (1989) Urodynamic Alterations Associated with Clinical Prostatic Diseases and Prostatic Surgery *J Am Anim Hosp Assoc* **25** 385-92

Basinger R R, Rawlings C A, Barsanti J A, Oliver J E, Jr. and Crowell W A (1987) Urodynamic alterations after prostatectomy in dogs without clinical prostatic disease *Vet Surg* **16** 405-10

Bell F W, Klausner J S, Hayden D W, Feeney D A and Johnston S D (1991) Clinical and pathologic features of prostatic adenocarcinoma in sexually intact and castrated dogs: 31 cases (1970-1987) *J Am Vet Med Assoc* **199** 1623-30

Cooley D M and Waters D J (2001) Tumors of the male reproductive system *Small Animal Clinical Oncology* (ed.3) ed S J Withrow and E G MacEwen (Philadelphia: Saunders) pp 478-89

Den Otter W, et al. (1995) Therapy of bovine ocular squamous-cell carcinoma with local doses of interleukin-2: 67% complete regressions after 20 months of follow-up *Cancer Immunol Immunother* **41** 10-4

Eklund J W and Kuzel T M (2004) A review of recent findings involving interleukin-2-based cancer therapy *Curr Opin Oncol* **16** 542-6

Evans H E and Christensen G C (1993) The urogenital system *Miller's Anatomy of the Dog* (ed.3) ed H E Evans (Philadelphia: Saunders) pp 494-558

Goldsmid S E and Bellenger C R (1991) Urinary incontinence after prostatectomy in dogs *Vet Surg* **20** 253-6

Harari J and Dupuis J (1995) Surgical treatments for prostatic diseases in dogs *Semin Vet Med Surg (Small Anim)* **10** 43-7

Hardie E M, Stone E A, Spaulding K A and Cullen J M (1990) Subtotal canine prostatectomy with the neodymium: yttrium-aluminum-garnet laser *Vet Surg* **19** 348-55

Hussain T, Gupta S and Mukhtar H (2003) Cyclooxygenase-2 and prostate carcinogenesis *Cancer Lett* **191** 125-35

Jacobs J J, Sparendam D and Den Otter W (2005) Local interleukin 2 therapy is most effective against cancer when injected intratumourally *Cancer Immunol Immunother* **54** 647-54

Kamijo T, Sato T, Nagatomi Y and Kitamura T (2001) Induction of apoptosis by cyclooxygenase-2 inhibitors in prostate cancer cell lines *Int J Urol* **8** S35-9

Kamolpatana K, Johnston G R and Johnston S D (2000) Determination of canine prostatic volume using transabdominal ultrasonography *Vet Radiol Ultrasound* **41** 73-7

Liptak J M, et al. (2004) Transurethral resection in the management of urethral and prostatic neoplasia in 6 dogs *Vet Surg* **33** 505-16

Liu X H, Kirschenbaum A, Yao S, Lee R, Holland J F and Levine A C (2000) Inhibition of cyclooxygenase-2 suppresses angiogenesis and the growth of prostate cancer in vivo *J Urol* **164** 820-5

Lucroy M D, Bowles M H, Higbee R G, Blaik M A, Ritchey J W and Ridgway T D (2003) Photodynamic therapy for prostatic carcinoma in a dog *J Vet Intern Med* **17** 235-7

Mann F A, Barrett R J and Henderson R A (1992) Use of a retained urethral catheter in three dogs with prostatic neoplasia *Vet Surg* **21** 342-7

Rawlings C A, Crowell W A, Barsanti J A and Oliver J E, Jr. (1994) Intracapsular subtotal prostatectomy in normal dogs: use of an ultrasonic surgical aspirator *Vet Surg* **23** 182-9

Rawlings C A, Mahaffey M B, Barsanti J A, Quandt J E, Oliver J E, Jr., Crowell W A, Downs M O, Stampley A R and Allen S W (1997) Use of partial prostatectomy for treatment of prostatic abscesses and cysts in dogs *J Am Vet Med Assoc* **211** 868-71

Riendeau D, Charleson S, Cromlish W, Mancini J A, Wong E and Guay J (1997) Comparison of the cyclooxygenase-1 inhibitory properties of nonsteroidal anti-inflammatory drugs (NSAIDs) and selective COX-2 inhibitors, using sensitive microsomal and platelet assays *Can J Physiol Pharmacol* **75** 1088-95

Satoh T, Irie A, Egawa S and Baba S (2005) In situ gene therapy for prostate cancer *Curr Gene Ther* **5** 111-9

Teske E, Naan E C, van Dijk E M, Van Garderen E and Schalken J A (2002) Canine prostate carcinoma: epidemiological evidence of an increased risk in castrated dogs *Mol Cell Endocrinol* **197** 251-5

Waters D J, et al. (1998) Workgroup 4: spontaneous prostate carcinoma in dogs and nonhuman primates *Prostate* **36** 64-7

Appendix to Chapter 4

Histological evaluation of prostate tissue damage of *in vivo* subcapsular laser prostatectomy in the normal dog

Sebastiaan A. van Nimwegen[1], Henry F. L'Eplattenier[1], Jaco J. van der Lugt[2], Jolle Kirpensteijn[1]

[1]Department of Clinical Sciences of Companion Animals, Faculty of Veterinary Medicine, Utrecht University
[2]Department of Pathobiology, Faculty of Veterinary Medicine, Utrecht University, The Netherlands.

Histology

Chapter 4 described a subcapsular partial prostatectomy in dogs as part of a treatment strategy for prostate carcinoma in dogs. Pieces of excised prostate tissue and the entire remaining prostate of normal dogs in this study were gathered postoperatively and stored in 4% buffered formaldehyde to be embedded in paraffin, sectioned and stained with hematoxylin and eosin (HE) for microscopic evaluation.

Images if prostate tissue sections are displayed in Figure 1. The acute thermal damage at the margins of laser incisions is evident as a distinct coagulation necrosis zone, containing moderate interstitial hemorrhage. This tissue damage typically extends 0.3-0.8 mm, and occasional extent up to 1.5 mm is noted. From the histological evaluation of the several sections it was concluded that thermal damage margins remained <2.0 mm. Furthermore, the urethra was intact in all sections.
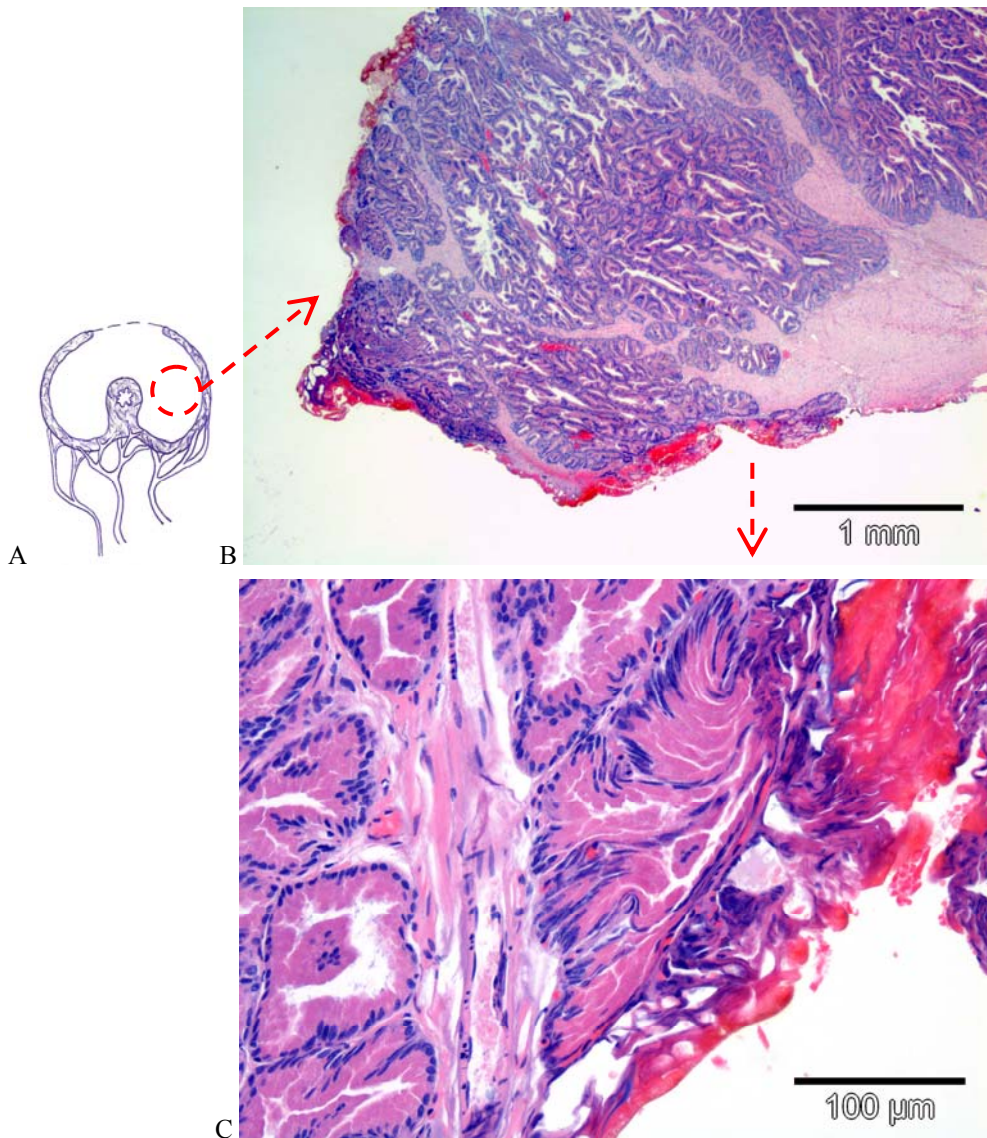
Figure 1: HE stained histological sections, showing acute thermal damage of *in vivo* Nd:YAG laser-excised prostate tissue (B and C) and the remaining prostate (E and F) after subcapsular laser prostatectomy as described in Chapter 4. During surgery, prostate parenchyma is resected leaving the capsule and urethra intact (A: cross section of the prostate after subcapsular tissue excision). Excess of ventral capsule is removed and the capsule is sutured around the urethra (D). Carbonized/caramelized tissue stains red. Thermal damage is denoted by increased dye uptake, loss of intracellular and intranuclear structure, and conformational changes of cells and nuclei.

(**Figure 1 continues on the next page**)
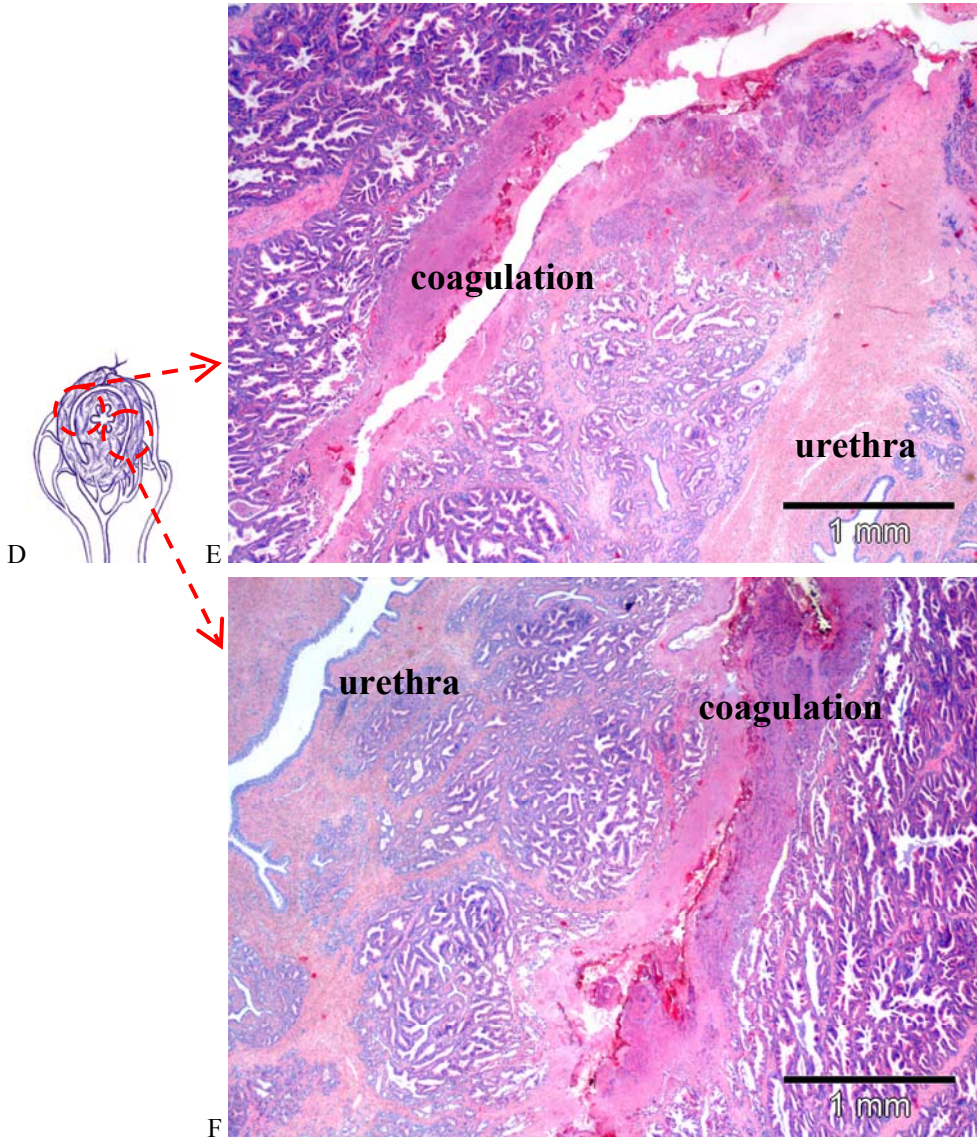
Figure 1, continued: Figure C shows the transition from carbonization and conformational cell-changes to normal tissue at the margin of laser-excised tissue from figure B. In the remaining prostate, a rim of distinct coagulation necrosis is evident at the incision margins, with moderate interstitial hemorrhage (E and F). Thermal damage at the edges of laser incisions is typically <1.0 mm (range ∼0.3-0.8 mm) and occasionally extends up to 1.5 mm in these sections (E), and was overall <2.0 mm. The urethra is intact.

Conclusion

These findings of *in vivo* laser surgery of the canine prostate are supported by the results of *in vitro* acute thermal tissue-damage investigation in *Chapter 3*. Furthermore, patients in the prostatectomy study were continent postoperatively.

It is concluded that the Nd:YAG laser is capable of relatively precise prostate tissue resection with acceptable accompanying thermal damage margins and can therefore be used for canine subcapsular partial prostatectomy, leaving prostate capsule and urethra intact.

5

Chapter 5

Neodymium:Yttrium-Aluminium-Garnet Surgical Laser Versus Bipolar Electrocoagulation For Laparoscopic Ovariectomy In Dogs.

Sebastiaan A. Van Nimwegen, DVM, Christiaan F. P. Van Swol, PhD, and Jolle Kirpensteijn, DVM, PhD, Diplomate ACVS & ECVS

[1]Department of Clinical Sciences of Companion Animals, Faculty of Veterinary Medicine, Utrecht University;
[2]Department of Clinical Physics, University Medical Center, Utrecht, The Netherlands.

Abstract

Objective- To compare use of Nd:YAG surgical laser and bipolar electrocoagulation for laparoscopic ovariectomy in dogs.

Study Design- Prospective clinical trial.

Animals - Female dogs (n = 72).

Methods- Laparoscopic ovariectomy by Nd:YAG laser (600 μm optical fiber, contact mode) in 36 dogs was compared with laparoscopic ovariectomy by bipolar electro-coagulating grasping forceps. Dogs were paired (laser, electrocoagulation) matched for breed, age, body weight, obesity, and number of heat cycles. Duration of predetermined surgery times and total surgical time were compared between groups. Occurrence of intra- and postoperative complications and their effect on surgical duration were evaluated.

Results- Laser surgery resulted in a higher incidence of intraoperative mesovarial bleeding (12 times; 9 dogs) compared with electrosurgery (4 times; 3 dogs). Use of laser caused a 2-minute delay for transection of the left ovary compared with electrosurgery. Postoperative complication rates and convalescence were similar for both groups.

Conclusions- Bipolar electrocoagulation reduced surgical time and intraoperative mesovarial bleeding compared with laser resection.

Clinical Relevance- Although the laser was effective for laparoscopic ovariectomy, bipolar electrosurgical laparoscopic ovariectomy remained the method of choice.

Introduction

Ovariectomy (OVE) is the preferred method for neutering female dogs in the Netherlands (Okkens *et al* 1997, Van Goethem *et al* 2003). Laparoscopic OVE is less invasive and has several advantages over laparotomy (Wildt *et al* 1977, Thiele *et al* 1996), including better visibility of abdominal structures, smaller abdominal incisions (better aesthetic results), less postoperative pain (Davidson *et al* 2004) and adhesion formation (Schippers *et al* 1998, Gamal *et al* 2001), and shorter convalescence (Bohm *et al* 1995, Tintara and Leetanaporn 1995).

Surgical lasers can be used in laparoscopic surgery because the laser beam can be applied by an optical fiber. Neodymium:yttrium-aluminum-garnet (Nd:YAG) surgical laser has many applications in human soft tissue surgery and is appreciated for its abilities in coagulation (by photocoagulation) and cutting of tissues (Brackett 1988, Peavy 2002, Tan

and Gilling 2003). In non contact mode (free beam) use, the 1064 nm wavelength has a penetration depth of 5-10 mm (dependent on tissue properties and power density of the beam) in most tissues (Peavy 2002), serving as a useful tool for photocoagulation. In contact mode, the laser fiber can cut through tissue by evaporating a small layer of tissue in contact with the bare fiber tip. Heat produced causes coagulation of a small layer of tissue at the cut surface, so hemorrhage is controlled. Potentially dangerous heat dissipation to surrounding tissue structures is negligible with correct contact mode use of the surgical laser because laser energy is largely absorbed and transferred into carbonization and vaporization of tissue at the fiber tip (Palmer 1993, Janda *et al* 2003).

Nd:YAG surgical laser use has been shown equally effective in coagulation of upper gastrointestinal bleeding lesions compared with bipolar electrocoagulation (BEC) (Goff 1986), and resulted in better hemostasis compared with monopolar electrosurgery in laparoscopic large bowel resection in dogs (Bohm *et al* 1994). Laparoscopic BEC-OVE has been described for dogs (Van Goethem *et al* 2003) and horses (Rodgerson *et al* 2001) and is a generally accepted technique with few complications. Use of a Nd:YAG surgical laser for laparoscopic OVE has been reported in horses (Palmer 1993) where the laser is used to coagulate (non contact mode) and dissect (contact mode) the mesovarial pedicle. The equine ovarian artery and other large vessels are clipped or stapled to control hemorrhage. Laser assisted laparoscopic OVE has not been reported in dogs.

In this prospective clinical trial, we compared laparoscopic use of a Nd:YAG surgical laser for ovariectomy (Laser-OVE) in the bitch with laparoscopic BEC-OVE (Van Goethem *et al* 2003). Duration of times for different surgical stages and total surgical time were compared as were intra- and postoperative complications.

Materials and Methods

Groups

Two laparoscopic OVE techniques were compared: Laser-OVE which was laser resection combined with BEC-hemostasis (experimental group) and BEC-OVE which was BEC combined with sharp transection (control group). Because the laser also coagulates during cutting, the total BEC time before laser resection (Laser-OVE) was kept shorter than before scissor resection (BEC-OVE).

Dogs

Dogs admitted for laparoscopic OVE, between September 2003 and May 2004, had Laser-OVE. These dogs were compared with dogs with similar profiles (pairing criteria) that had BEC-OVE, the usual ovariectomy technique before Laser-OVE was available at our clinic.

A standard questionnaire about the dog (number of heat cycles, date of last heat, presence of pseudopregnancy, general health, diet, vaccination status) was completed by the owner before surgery. Data about breed, age, bodyweight, and obesity were obtained. Obesity scores were based on a published scoring system (Impellizeri *et al* 2000). Dogs were individually paired (BEC-OVE versus Laser-OVE) by criteria such as breed, obesity, bodyweight, and age.

Surgery

All surgical procedures were performed by JK. Dogs were positioned in dorsal recumbency in a 10° Trendelenburg position for video-assisted laparoscopic OVE through 3 median portals. An open pediatric approach was used at the caudal portal (Magne and Tams 1999). A 15 mm incision was made in skin and subcutis, midway between the pubis and umbilicus, and stay sutures were placed in the cranial and caudal ends of the incision. A 10 mm trocar (Surgiport 10 mm disposable trocar with 10 cm sleeve; Auto Suture, US Surgical Corporation, Norwalk, CT, USA) was inserted through the abdominal wall while pulling the stay sutures upward, to avoid damage to viscera. After insertion of the trocar, CO_2 flow was adjusted to 1 L/min to check correct placement of the trocar, then the abdomen was insufflated (6 L/min) to an intra-abdominal pressure of 8 mmHg. A 5 mm, 0° telescope (Hopkins II, Karl Storz-Endoscopy, Vianen, The Netherlands) was inserted through the trocar and two 5 mm trocars (Surgiport 5 mm disposable trocar; Auto Suture, US Surgical Corp) were inserted under laparoscopic guidance, 1 cm caudal and 1 cm cranial to the umbilicus. After trocar insertion, the telescope was redirected to the middle portal.

The ovarian bursa was located by identifying the round ligament at the inguinal ring and following it cranially using 2 endoscopic grasping forceps (Endo Dissect 5 mm and Endo Clinch II 5 mm; US Surgical Corporation). The bursa was grasped at the bursal opening with the self-retaining forceps inserted through the cranial portal. The bipolar grasping forceps (Take-Apart Bipolar Grasping Forceps; Karl Storz-Endoscopy, The Netherlands) was inserted in the caudal portal and was used to coagulate the proper ligament and suspensory ligament.

During Laser-OVE, both ligaments were resected using a Nd:YAG laser (Medilas 40 N, MBB Medizintechnik GmbH, München, Germany) with 600 μm optical fiber (Ultraline, side-firing tip removed, Heraeus LaserSonics, Milpitas, California) in contact mode (at 10 W power setting; continuous wave). The laser fiber was inserted through the caudal portal in exchange for the bipolar forceps using a fiber application device (Laser inserter, Karl Storz-Endoscopy). OVE was performed by transection of the ovarian pedicle, leaving the ovary inside the bursa (en bloc). When larger vessels (> 2-3 mm) were encountered, the laser was exchanged for the BEC forceps to coagulate the vessels before laser resection.

The ovarian bursa was thus resected in a caudal to cranial direction by exchanging laser and bipolar forceps. If bleeding occurred, hemostasis was usually easily manageable using the bipolar coagulation forceps. The remnant of the pedicle was checked for hemorrhage by visual inspection after completion of the procedure. The bursal remnant containing the ovary was extracted from the abdomen through the caudal portal, using grasping forceps. In all dogs, the left ovary was excised first with the surgeon standing at the right side of the dog and the laparoscopic unit on the left side. The surgeon and the unit exchanged sides for removal of the right ovary. All ovaries were checked to ensure complete removal.

During BEC-OVE, endoscopic scissors (Endo Mini-Shears Short 5 mm; US Surgical Corporation) were used for resection of the ovarian pedicle following bipolar electrocoagulation instead of laser excision. If visibility decreased because of smoke production during either Laser-OVE or BEC-OVE, excess smoke was released through the insufflation port of the caudal trocar. At each portal, the abdominal wall was closed using one interrupted, monofilament, absorbable 2-0 suture. Skin and subcutis were closed with one inverted, monofilament, absorbable 4-0 suture. All dogs were administered carprofen (2mg/kg orally twice daily for 3 days).

Minor revisions of the BEC-OVE surgical approach were used in the Laser-OVE method. Two stay-sutures were used in Laser-OVE to insert the caudal trocar compared with 1 stay-suture in BEC-OVE. After Laser-OVE, the transected ovary was immediately removed from the abdomen through the caudal portal. During BEC-OVE the transected left ovary was placed next to the urinary bladder and was removed from the abdomen after completion of resection and removal of the right ovary.

Data recorded

The following defined surgical times were recorded:

OV_0: from skin-incision to resection of the left ovary (= incision + trocar insertion + searching of left ovary)

OV_1: resection of the left ovary

OV_2: turning of surgeon and equipment to other side + searching + resection of right ovary

OV_3: removal of both ovaries from abdominal cavity

Total surgical time: $OV_0 + OV_1 + OV_2 + OV_3$.

Additionally, accessibility of the ovaries, occurrence of intraoperative bleeding, and abnormalities of ovaries or uterus were recorded.

Postoperative care

Dogs were released from the hospital immediately after full recovery from anesthesia. Carprofen was prescribed for pain management until the third day postoperatively.

Follow up

Ten days after surgery, the owner of the dog was contacted by telephone and a standard questionnaire was completed, including questions concerning number of days until full recovery, the dogs' appetite, number of days on postoperative medication and the aspect of the surgery wounds.

Statistical analysis

A paired sample t-test was used to test equality of the laser- and BEC-OVE groups by means of the pairing criteria and to test for possible differences in duration of defined surgical times. An independent samples t-test and ANOVA were used to test for other (unpaired) variables, such as occurrence of intraoperative bleeding between groups and their effect on surgical time. *P* values < .05 (two-tailed) were considered significant. Results were reported as means ± SD unless indicated otherwise.

Results

Mean bodyweight (n = 72 dogs) was 24.8 ± 10.2 kg (range, 5.8 – 56.2 kg), mean age was 2.3 ± 1.7 years (range, 0.7 – 9.5 years). Mean total surgical time was 38.1 ± 9.6 minutes (range, 24.0 – 77.5 minutes). Paired dogs were of the same breed for >50 % of the pairs; others were paired by breed resemblance (height, posture).

Surgery time intervals

Total surgical time was not significantly different for the groups (39.3 ± 9.6 minutes for BEC-OVE, 36.9 ± 9.7 for Laser-OVE; Figure 1). Laser-OVE (OV_1) for the left ovary (10.9 ± 4.6 minutes) was significantly longer than BEC-OVE (8.7 ± 3.3 minutes; *P* =.015). Resection time for the right ovary (including turning of the equipment and searching the right ovary; OV_2) was not significantly different between techniques.
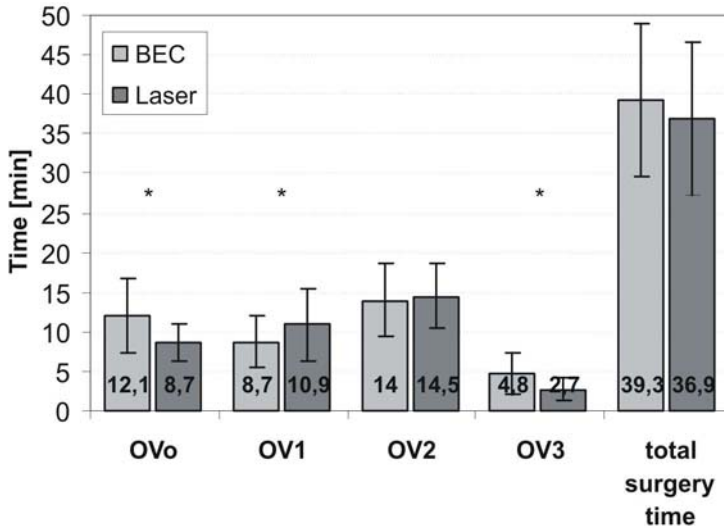
Figure 1: Means (± SD) time intervals for different surgical stages for laser- and BEC-OVE. OV_0: from skin-incision to resection of the left ovary (= incision + trocar insertion + searching of left ovary); OV_1: resection of the left ovary; OV_2: turning to other side + searching + resection of right ovary; OV_3: removal of both ovaries from abdominal cavity. * = significant difference in duration of procedure (paired sample t-test; $P < .05$). BEC, bipolar electrocoagulation; OVE, ovariectomy.

Time from skin incision to resection of the left ovary (OV_0) was significantly shorter for Laser-OVE (8.7 ± 2.3 minutes) than for BEC-OVE (12.1 ± 4.7 minutes; $P < .0005$). Removal of ovaries (OV_3) from the abdomen was significantly faster with Laser-OVE (2.7 ± 1.4 minutes) than BEC-OVE (4.8 ± 2.6; $P < .0005$).

Intra-operative hemorrhage

Laser-OVE was associated with a significantly higher occurrence of intraoperative mesovarial bleeding than BEC-OVE ($P = .034$; Figure 2). During laser surgery, 12 intraoperative mesovarial bleeding episodes occurred (8 right, 4 left) in 9 dogs (25 %) and significantly increased total surgical time by 7.9 ± 3.5 minutes (mean increase ± SEM) within the Laser-OVE group (23 %; $P = .031$; Figure 2). There was no significant difference in occurrence of hemorrhage for the left and right ovary. Four intraoperative mesovarial bleeding episodes occurred with the BEC-technique (2 right, 2 left) in 3 dogs (8.3 %); the increase in surgery time of 8.8 ± 5.7 minutes (mean ± SEM; 23 %) was not significant in the BEC-OVE group.

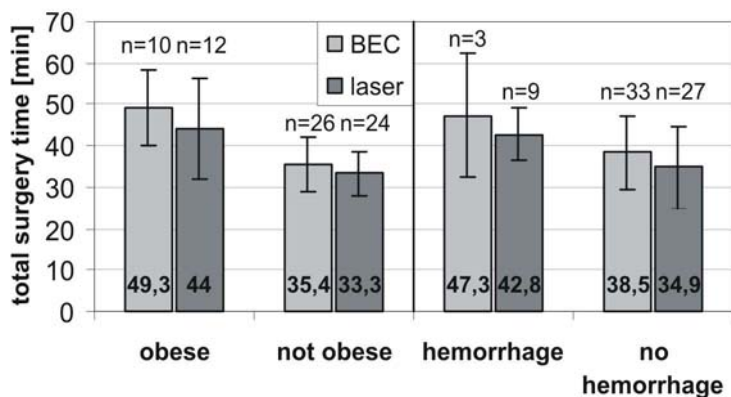**Figure 2**: Effects of obesity and hemorrhage on mean (± SD) total surgical time for both BEC-OVE and Laser-OVE. Obesity significantly increased surgical time for both techniques, intra-operative hemorrhage significantly increased surgical time with Laser-OVE, but not with BEC-OVE (independent sample t-test). BEC, bipolar electrocoagulation; OVE, ovariectomy.

Obesity
Duration of surgery for both obese and non obese dogs did not differ significantly between groups. Obesity (31 % of the dogs) increased mean surgical time by 12.0 ± 2.0 minutes (mean increase ± SEM) for both groups (increase of 35 %, $P < .0005$; Figure 2).

Postoperative variables
Recovery rate and postoperative wound complications were comparable for the groups. Dogs returned to normal activity in 1.7 ± 1.4 days after Laser-OVE and in 1.5 ± 0.6 days after BEC-OVE. Three percent of the wounds had swelling and/or discharge but none required treatment.

Discussion
Laser-OVE was comparable to BEC-OVE for most of the tested surgical variables and was safe and effective in the non parous bitch. During removal of the left ovary, Laser-OVE had a significant 20 % increase in surgical time compared with BEC-OVE; this equaled a 2 minute delay. Interestingly, a time difference was not observed for the right ovary. This finding supports the hypothesis that laser resection of the right ovary is easier than that of the left ovary because of difficulty directing the laser beam towards the left ovary and mesovarium. The left ovary is located more caudally than the right ovary and so there is a lesser angle of attack for the laser fiber. This positional difference does not affect BEC-OVE. A more caudal position for the most caudal portal should eliminate this problem;

however, a more caudal trocar position would increase the risk of trauma to the bladder or its ventral median ligament.

Measured differences in duration of approach to the abdomen and removal of ovaries were caused by mild procedural differences in the 2 techniques. For Laser-OVE, 2 stay sutures were used for insertion of the 1st trocar, while in BEC-OVE a single stay suture-was used. The 2 suture technique was a refinement of the single suture technique and resulted in a reduction in time even though an extra suture was placed. The 2nd suture allowed better stabilization of the abdominal wall to facilitate introduction of the trocar though the linea alba and improved traction to prevent laceration of underlying viscera.

The technique for ovary removal from the abdomen also varied. In the Laser-OVE, each ovary was removed directly after transection whereas in BEC-OVE, both ovaries were removed after resection of the right ovary; the left ovary was placed in the right caudodorsal quadrant of the abdomen to be retrieved later in the procedure. These 2 variations in technique resulted in a decrease in mean surgical time of approximately 6 minutes; however, with the increase in surgery time caused by the laser, total surgical time was comparable for the groups.

Using the laser as a solitary device for coagulating and cutting the ovarian pedicle was complicated because of the limited coagulation capacity of the Nd:YAG laser in contact mode (Brackett 1988, Janda *et al* 2003) and the large diameter of the ovarian pedicle within the mesovarium. Therefore, Laser-OVE had to be combined with BEC to prevent bleeding and more hemorrhage occurred during laser-resection. By comparison, the bipolar forceps were applied longer during BEC-OVE to achieve coagulation of vessels than in Laser-OVE. With laser OVE, the vessels are not clamped but photocoagulated by fiber contact whereas with BEC-OVE, the BEC forceps compress the vessel before coagulation, effectively causing a smaller vessel lumen during coagulation. Blood stream, which is assumed to act as a heat sink during photocoagulation (Sturesson *et al* 1997), is more or less impaired during BEC.

Hemorrhage will cause an increase in surgical time, because the bipolar forceps needs to be reinserted to coagulate the bleeder, but the higher occurrence of mesovarial bleeding during Laser-OVE does not explain the total difference in surgical time between groups. Occurrence of mesovarial bleeding significantly increased surgery-time by ~ 20% in both laser-OVE and both groups combined just as described in earlier studies (Van Goethem *et al* 2003). However, the increase in surgical time caused by the laser was still significant even when occurrence of mesovarial bleeding was considered. Thus, use of laser requires more surgical time and results in more intraoperative mesovarial bleeding than occurred with BEC-OVE. We also confirmed the previous observation that obesity will increase surgical time significantly compared with non obese dogs (Van Goethem *et al* 2003).

Production of smoke during contact mode laser resection reduces visibility inside the abdomen. Although some authors have reported no significant differences in visibility between laparoscopic contact laser and electrosurgery (Bohm *et al* 1994), we encountered a less clear image because of smoke production during Laser-OVE when compared with BEC-OVE.

Although Laser-OVE was more challenging, use of the laser did not have a significant advantage in laparoscopic OVE surgery compared with BEC-OVE. Further, BEC forceps were still needed to prevent mesovarial hemorrhage. Thus, from our perspective, BEC is still the method of choice for laparoscopic OVE, a decision also reinforced by the added cost and extra precautions required for laser.[1]

References

Bohm B, Milsom J W and Fazio V W (1995) Postoperative intestinal motility following conventional and laparoscopic intestinal surgery *Arch Surg* **130** 415-9

Bohm B, Milsom J W, Kitago K, Brand M and Fazio V W (1994) Monopolar electrosurgery and Nd:YAG Contact Laser in laparoscopic intestinal surgery *Surg Endosc* **8** 677-81

Brackett K A (1988) Tissue interactions of Nd:YAG lasers *Advances of Nd:YAG laser surgery* S Joffe and Y Oguro (ed) (New York: Springer-Verlag) pp 336-43

Davidson E B, Moll H D and Payton M E (2004) Comparison of laparoscopic ovariohysterectomy and ovariohysterectomy in dogs *Vet Surg* **33** 62-9

Gamal E M, Metzger P, Szabo G, Brath E, Peto K, Olah A, Kiss J, Furka I and Miko I (2001) The influence of intraoperative complications on adhesion formation during laparoscopic and conventional cholecystectomy in an animal model *Surgical Endoscopy* **15** 873-80

Goff J S (1986) Bipolar electrocoagulation versus Nd-YAG laser photocoagulation for upper gastrointestinal bleeding lesions *Dig Dis Sci* **31** 906-10

Impellizeri J A, Tetrick M A and Muir P (2000) Effect of weight reduction on clinical signs of lameness in dogs with hip osteoarthritis *J Am Vet Med Assoc* **216** 1089-91

Janda P, Sroka R, Mundweil B, Betz C S, Baumgartner R and Leunig A (2003) Comparison of thermal tissue effects induced by contact application of fiber guided laser systems *Lasers Surg Med* **33** 93-101

Magne M L and Tams T R (1999) Laparoscopy: instrumentation and technique *Small Animal Endoscopy* T R Tams (ed) (St Louis: Mosby) pp 397-408

Okkens A C, Kooistra H S and Nickel R F (1997) Comparison of long-term effects of ovariectomy versus ovariohysterectomy in bitches *J Reprod Fertil Suppl* **51** 227-31

Palmer S E (1993) Standing laparoscopic laser technique for ovariectomy in five mares *J Am Vet Med Assoc* **203** 279-83

Peavy G M (2002) Lasers and laser-tissue interaction *Vet Clin North Am Small Anim Pract* **32** 517-34, v-vi

Rodgerson D H, Belknap J K and Wilson D A (2001) Laparoscopic ovariectomy using sequential electrocoagulation and sharp transection of the equine mesovarium *Vet Surg* **30** 572-9

Schippers E, Tittel A, Ottinger A and Schumpelick V (1998) Laparoscopy versus laparotomy: comparison of adhesion-formation after bowel resection in a canine model *Digestive Surgery* **15** 145-52

Sturesson C, Liu D L, Stenram U and Andersson-Engels S (1997) Hepatic inflow occlusion increases the efficacy of interstitial laser-induced thermotherapy in rat *J Surg Res* **71** 67-72

Tan A H and Gilling P J (2003) Free-beam and contact laser soft-tissue ablation in urology *J Endourol* **17** 587-93

Thiele S, Kelch G and Frank K G (1996) [Endoscopy of body cavities and minimally invasive surgery in small animals--review] *Berl Munch Tierarztl Wochenschr* **109** 288-91

Tintara H and Leetanaporn R (1995) Cost-benefit analysis of laparoscopic adnexectomy *Int J Gynaecol Obstet* **50** 21-5

Van Goethem B E, Rosenveldt K W and Kirpensteijn J (2003) Monopolar versus bipolar electrocoagulation in canine laparoscopic ovariectomy: a nonrandomized, prospective, clinical trial *Vet Surg* **32** 464-70

Wildt D E, Kinney G M and Seager S W (1977) Laparoscopy for direct observation of internal organs of the domestic cat and dog *American Journal of Veterinary Research* **38** 1429-32

[1]American national standard for safe use of lasers in health care facilities (ANSI-Z0136.3-1996). American National Standard Institute, New York, 1996

6

Chapter 6

Comparison of Nd:YAG Surgical Laser and Remorgida Bipolar Electrosurgery Forceps for Canine Laparoscopic Ovariectomy.

Sebastiaan A. van Nimwegen, DVM, and
Jolle Kirpensteijn DVM, PhD, Diplomate ACVS & ECVS

From the Department of Clinical Sciences of Companion Animals, Faculty of Veterinary Medicine, Utrecht University, Utrecht, the Netherlands.

Abstract

Objective- To investigate and compare technique, surgical time and complications of canine laparoscopic ovariectomy using Nd:YAG surgical laser and Remorgida bipolar electrosurgery forceps.

Study Design - Randomized, prospective clinical trial.

Animals – Female dogs (n = 40) for elective ovariectomy.

Methods - Dogs had bilateral ovariectomy with one ovary randomly assigned to removal by use of Nd:YAG surgical laser with a 600 μm optical fiber in contact mode and the other ovary to removal by use of a Remorgida forceps (featuring bipolar electrocoagulation with simultaneous sharp resection). Duration of predetermined surgery intervals and complications were compared between techniques. Additionally, the effects of several intraoperative variables on surgical time were evaluated.

Results – Ovariectomy by use of Remorgida forceps required significantly less time than laser ovariectomy but intraoperative hemorrhage was not reduced. Surgical time was significantly increased in obese dogs, depending on the amount of fat in the ovarian ligament. Intraoperative hemorrhage had no significant influence on surgical time.

Conclusion - Both ovariectomy techniques were effective but the Remorgida forceps can be used as a relatively inexpensive, stand-alone device that decreases surgical time compared with Nd:YAG laser ovariectomy.

Clinical Relevance - Novel techniques, such as laser and combined bipolar electrosurgical and cutting forceps aim to reduce surgery duration, complication rates and recovery time in laparoscopic surgery.

Introduction

Ovariectomy (OVE) is less invasive compared with ovariohysterectomy; is as effective and has not been associated with an increased risk of complications (Okkens *et al* 1997, van Goethem *et al* 2006). Use of laparoscopic ovariectomy (lapOVE) has obvious advantages and was established to be a reliable and safe technique in dogs (Van Goethem *et al* 2003, Van Nimwegen *et al* 2005, Wenkel *et al* 2005), horses (Hendrickson 2006), cows (Bleul *et al* 2005), llamas (Rodgerson *et al* 1998), rhesus macaques (Matchett *et al* 2006), and humans (Pittaway *et al* 1994). To decrease intra- and postoperative complications other techniques have been investigated in dogs including bipolar electrocoagulation (BEC) (Van Goethem *et al* 2003, Van Nimwegen *et al* 2005) and Nd:YAG surgical laser (*Chapter*

5, Van Nimwegen *et al* 2005). Both techniques required 2 devices for ovarian excision: the BEC forceps needed additional endoscopic scissors, whereas the fiber-guided surgical laser required additional BEC for adequate hemostasis of larger mesovarial vessels. This added exchange of instruments increases surgical time.

The Nd:YAG surgical laser can coagulate (free beam) and resect (contact mode) tissue (Goff 1986, Bohm *et al* 1994, Brown 2000, Peavy 2002, L'Eplattenier *et al* 2006). Use of a Nd:YAG surgical laser in canine lapOVE had been compared (surgical time, intra- and postoperative complications) in a prospective clinical trial with a standard laparoscopic BEC-facilitated method (Van Nimwegen *et al* 2005). The laser performed well but had difficulty with coagulation of large vessels in the ovarian pedicle. Free beam coagulation of these vessels was impractical whereas BEC forceps facilitated excellent coagulation of the ovarian pedicle by squeezing the vessels during coagulation, reducing the functional vessel size and reducing the cooling effect of blood flow. The Remorgida forceps combines BEC with sharp resection in a single instrument and should be able to reduce instrument exchange during lapOVE. Remorgida forceps consist of a double BEC forceps with an independently-movable knife blade in the middle (Figure 1). Cutting is thus combined with tissue coagulation on both sides of the plane of incision.
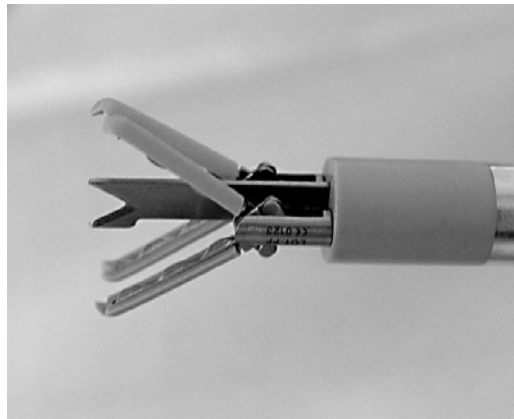
Figure 1: The Remorgida forceps, combining a double BEC forceps with an independently movable knife blade in the middle.

Studies on combined bipolar cutting devices are sparse. A combined device, similar to the Remorgida, the BiCOAG (Gyrus Medical, Minneapolis, MN) combines bipolar forceps with cutting blade and had excellent vessel sealing capabilities and simultaneous section in pigs (Santa-Cruz *et al* 2003). The PlasmaKinetic (PK) cutting forceps (Gyrus Medical) is similar, except for a different power source (using pulsed energy and measuring tissue

impedance for improved, computer controlled, coagulation) and therefore different coagulation abilities. Comparison of the PK with harmonic coagulation shears in Nissen fundoplication (Underwood *et al* 1999) and with BEC forceps (Kleppinger, Richard Wolf Instruments, Vernon Hills, IL) in hysterectomy (Ou *et al* 2004) in humans showed improved hemostasis (Ou *et al* 2004) but no improvement in surgery duration (Underwood *et al* 1999, Ou *et al* 2004). LigaSure laparoscopic forceps (Valleylab, Boulder, CO) combines computer-controlled pulsed bipolar energy with sharp resection. It has been successfully used in laparoscopic removal of granulosa cell tumors in horses (Hubert *et al* 2006) and had better and safer coagulation compared with conventional bipolar electrocoagulation in a rabbit model (Diamantis *et al* 2006). In contrast to computer-controlled BEC and surgical laser, the Remorgida device is less expensive to purchase and operate.

Our purpose was to develop a low-cost, safe, and fast technique with minimal complications for canine lapOVE. We hypothesized that the Remorgida bipolar electrosurgery forceps would enhance lapOVE by reducing surgical time and decrease occurrence of intraoperative mesovarial bleeding compared with surgical laser. The techniques were compared in normal dogs admitted for elective lapOVE by using one technique, randomly assigned, for each ovary, and evaluating the duration of selected surgical variables and occurrence of complications.

Materials & Methods

Experimental Approach

The Remorgida bipolar electrosurgery forceps was compared with the Nd:YAG surgical laser in lapOVE in a randomized prospective clinical trial. A standardized surgery and anesthesia protocol was used. Each dog had both methods and were randomly divided into 2 groups: group 1 (n = 20 dogs) had the left ovary resected using laser (Laser-OVE) and the right ovary using Remorgida (Remo-OVE) and group 2 (20) had Remo-OVE of the left ovary and Laser-OVE of the right ovary. Randomization was performed preceding the trial, and group assignment (group 1 or 2) was enclosed in an envelope for each dog to be opened by the surgeon at start of surgery.

Animals

Forty client-owned female dogs were admitted for elective lapOVE. A standard questionnaire about the dog (number of heat-cycles, date of last heat, presence of pseudopregnancy, general health, diet, vaccination status) was completed by the owner

before surgery. Breed, age, bodyweight, and obesity scores (Impellizeri *et al* 2000) were recorded on admission.

Anesthesia

After premedication with medetomidine (20 - 30 µg/kg [1.0 mg/m^2 body surface area] intravenously [IV]) anesthesia was induced with propofol (1-2 mg/kg IV to effect) and maintained with isoflurane vaporized in a mixture of oxygen and air. After connection to a circle breathing system, automatic intermittent positive pressure ventilation (IPPV) was initiated. Medetomidine (10 - 15 µg/kg IV [0.5 times premedication dose]) was administered 1 hour after the premedication dose, if applicable. Monitoring consisted of continuous electrocardiogram (ECG), gas analyzer (measuring CO_2 and isoflurane concentrations), pulse-oximetry, body temperature and ventilation pressure. Ventilation pressure was maintained <20 cmH$_2$O. Carprofen (4 mg/kg IV) and buprenorphine (20 µg/kg IV) were administered to provide additional intra and perioperative analgesia. Atipamezole (50 - 75 µg/kg intramuscularly (2.5 times premedication dose of medetomidine) was administered at the start of the recovery period.

Surgery

All surgical procedures were performed by a single, experienced surgeon. Video-assisted lapOVE was performed through 3 median portals. Dogs were positioned in dorsal recumbency in a 10° Trendelenburg position. An abdominal wall-lifting approach was used for direct (blind) trocar insertion at the caudal portal, before inducing pneumoperitoneum (Yerdel *et al* 1999, Gunenc *et al* 2005). A 15 mm incision was made in skin and subcutis, midway between the cranial edge of the os pubis and umbilicus, and stay-sutures were placed in the cranial and caudal corner of the incision. A 10 mm shielded trocar (Surgiport 10 mm disposable trocar with 10 mm sleeve; Auto Suture, United States Surgical, Norwalk, CT) was inserted through the abdominal wall while pulling the stay sutures upward, to avoid damaging abdominal structures (eg, spleen, bladder). After trocar insertion, CO_2-flow was set to 1 L/min to check correct trocar placement. The abdomen was then insufflated at 6 L/min and intra-abdominal pressure was maintained at 8 - 10 mmHg. A 5 mm, 0° telescope (Hopkins II, Karl Storz-Endoscopy, Vianen, the Netherlands) was inserted through the trocar and two 5 mm trocars (Surgiport 5 mm disposable trocar; Auto Suture, US Surgical) were inserted under laparoscopic guidance, 1 cm caudal and 1 cm cranial to the umbilicus. After trocar insertion, the telescope was redirected to the middle portal. The ovarian bursa was located by identifying the round ligament at the vaginal ring and following it cranially using 2 endoscopic grasping forceps (Endo Dissect 5 mm and Endo

Clinch II 5 mm; US Surgical). Through the cranial portal, the bursa was grasped with the self-retaining forceps, by introducing 1 jaw into the bursal opening.

Laser Technique

A bipolar grasping forceps (Take-Apart Bipolar Grasping Forceps; Karl Storz-Endoscopy) was inserted in the caudal portal and was used to coagulate the proper ligament and the suspensory ligament. Both ligaments were resected using a Nd:YAG laser (Medilas 40 N, MBB Medizintechnik GmbH, München, Germany) with 600 μm optical fiber in contact mode (10 W; continues wave). The laser-fiber was inserted through the caudal portal in exchange for the bipolar forceps using a fiber-application device (Laser inserter, Karl Storz-Endoscopy). Ovariectomy was performed by transection of the ovarian pedicle, leaving the ovary inside the bursa. When larger vessels were encountered, the laser was exchanged for the bipolar forceps to coagulate the vessels before laser resection. The ovarian bursa was resected in a caudal to cranial direction by intermittent exchange of the laser and bipolar forceps. If bleeding occurred, hemostasis was managed with the BEC forceps.

Remorgida Technique

The 10mm Remorgida double bipolar forceps (Karl Storz-Endoscopy) was inserted through the caudal portal and was used to coagulate and transect the ovarian pedicle, working from the proper ligament towards the suspensory ligament. If bleeding occurred, hemostasis was achieved by the Remorgida forceps.

In all dogs, the left ovary was excised first with the surgeon standing at the right side of the dog and the laparoscopic unit at the left side. The surgeon and the unit changed sides for right ovariectomy. After each procedure, the pedicle remnant was checked for hemorrhage and the bursal remnant containing the ovary was extracted from the abdomen using the caudal portal. All ovaries were checked for complete removal. Abdominal portals were closed by placing one interrupted suture of 2-0 polyglecaprone in the abdominal wall. An intradermal suture pattern with 4-0 polyglecaprone was used to close the skin. All dogs were administered carprofen (2mg kg^{-1} orally every 12 hours for 3 days).

Measured Variables

Recorded surgical stages, timed by stop watch were: skin-incision until trocar insertion; searching for the left ovary; resection of the left ovary; removal of left ovary from abdomen; turning of surgeon and equipment to other side; searching for the right ovary; resection of the right ovary; removal of right ovary from abdomen; total surgical time (excluding closure). Accessibility of the ovaries, occurrence of intraoperative bleeding, and

abnormalities of ovary or uterus were recorded. The amount of fat in the ovarian ligament was scored (Fat-Score [FS]) where 0 = no fat; 1= small amount of fat; 2 = moderate amount of fat; and 3 = large amount of fat.

Outcome

Ten days after surgery, the owner was contacted by telephone and a standard questionnaire used to establish time (days) until full recovery, the dog's appetite, days of postoperative medication, appearance of the surgical portals, and owner satisfaction (not satisfied, satisfied, very satisfied).

Statistical Analysis

A power analysis was performed (ß=0.90; α= 0.05, variation coefficient = 20%; estimated difference of 15%, based on a previous study) and the number of dogs needed was determined to be 40. A paired sample t-test was used to test for differences in duration of defined surgical stages of left versus right and Laser-OVE versus Remo-OVE. An independent samples t-test and ANOVA were used to test for other (unpaired) variables such as occurrence of intraoperative bleeding between groups. Multivariate linear regression was used to test for effects of significant variables on surgical time. *P*-values <.05 (2-tailed) were considered significant. Results are reported as mean ± SD unless stated otherwise.

Results

Forty dogs of various breeds (25 different breeds, 3 crossbreeds) with normal general health status were enrolled in the study. Mean age was 2.5 ± 1.8 years (range, 0.5 – 8.4) and mean body weight was 26.0 ± 13.6 kg (range, 4.7 – 63.5). Surgical duration was 0:32:47 ± 0:09:19 hours:min:s (range, 0:22:08 – 1:10:32). There were no significant differences in surgical times between left and right ovaries (Figure 2).

Laser versus Remorgida

Ovariectomy using the Remorgida device (Remo-OVE; 5:38 ± 2:32 min:s) was significantly faster compared with Laser-OVE (7:28 ± 3:11 min:s, *P*<.001; Figure 3). Further investigation revealed a significant difference between Laser-OVE (8:04 ± 3:34) and Remo-OVE (5:11 ± 2:11 min:s; *P* = .004) only existed for the left ovary (Figure 3). Difference in duration between Laser-OVE (6:52 ± 2:42 min:s) and Remo-OVE (6:04 ± 2:49 min:s; *P* = .364) for the right ovary was not significant. There were no significant

differences between the left and the right side for laser-OVE (P = .242) or for Remo-OVE (P = .275).

Qualitative differences between laser and Remorgida included a somewhat reduced visibility during laser surgery because of smoke production and a better functionality of the laser with transection of adipose tissue.
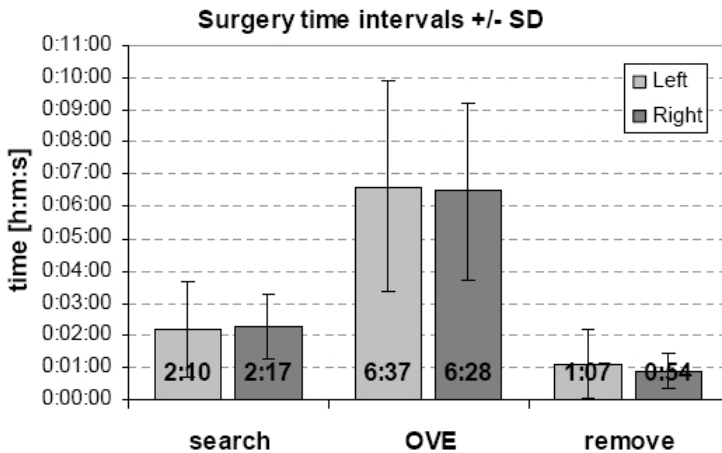

Figure 2: Searching, resection (OVE) and removal interval of the left and the right ovary. OVE, ovariectomy.
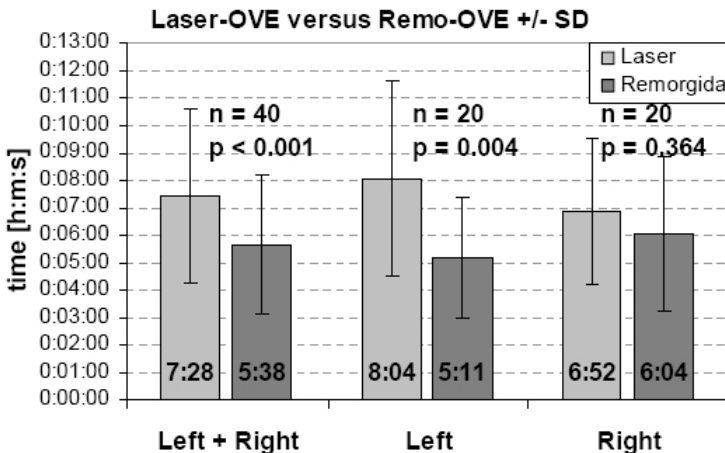

Figure 3: Laser-OVE compared with Remo-OVE. Significant difference in duration of surgical resection of the left ovary was detected. OVE, ovariectomy.

Accessibility

Difficult access to the ovary occurred 6 times: 2 times on the left (both Remo-OVE) and 4 times on the right (3 Laser-OVE, 1 Remo-OVE). It caused a significant increase in duration of the searching interval for the right ovary (2:00 ± 0:41 min:s versus 4:11 ± 0:50 min:s; P < .001), but not of the left ovary (2:05 ± 1:29 min:s versus 3:36 ± 0:20 min:s; P = .162). Accessibility had no significant effect on Laser-OVE, Remo-OVE or total surgical time and the mean duration of the searching interval did not differ between the left and the right side.

Hemorrhage

Although intraoperative hemorrhage occurred less with Laser-OVE (4) than Remo-OVE (7), the difference was not significant (P = .336). Hemorrhage had no significant effect on any surgery interval (Table 1).

| | Surgical Time (min:s) | | |
Technique	No hemorrhage	Hemorrhage	*P*-value
Laser-OVE	7:22 ± 3:17	8:17 ± 2:00	.593
	N = 36	N = 4	
Remo-OVE	5:18 ± 2:25	7:09 ± 2:38	.081
	N = 33	N =7	
Total Surgical Time	32:06 ± 9:50	34:51 ± 7:35	.426
	N = 30	N = 10	

Table 1: Effect of Intraoperative Hemorrhage on Duration of Laser-OVE, Remo-OVE, and Surgical Time.

Obesity and Fat-Score

Seventeen dogs were considered to be obese and FS was significantly increased in obese dogs (P = .004).Obesity had a significant effect on surgery duration (Table 2). A significant increase in OVE duration (P = .001) and total surgical time (P = .006) was found with increasing FS of the ovarian ligament (ANOVA; Figure 4).

Technique	Surgical Time (min:s)		Increase in Surgical Time	*P*-value
	Normal N = 23	Obese N = 17		
Laser-OVE	6:11 ± 2:06	9:12 ± 3:36	49 %	.002
Remo-OVE	4:55 ± 1:25	6:35 ± 3:20	34 %	.038
Total Surgical Time	29:58 ± 5:26	36:37 ± 11:58	22 %	.023

Table 2: Influence of Obesity on Surgical Time.
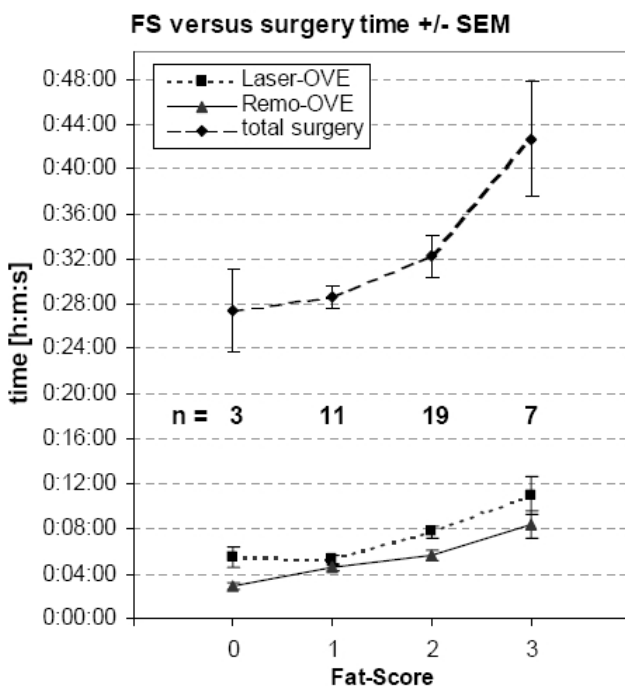
Figure 4: Fat-Score versus OVE and total surgical time (mean values ± SEM). OVE, ovariectomy.

Pseudopregnancy, uterus and ovary abnormalities, heat-cycles, age and time

Pseudopregnancy was defined by preoperative changes in behavior and/or enlarged nipples/mammary glands. Abnormalities of the uterus or ovaries were defined by intraoperative changes: mainly enlargement because of hormonal activity. Few exceptions included: a torn bursa, an ovarian cyst, and 1 case of estrus. Pseudopregnancy (16) and uterine abnormalities (8) had no significant effect on duration of any surgery interval and were not related to intraoperative bleeding or age (P = .089).

Abnormal ovaries (intraoperative; 15 ovaries in 10 dogs) resulted in a significant increase in total surgical time (38:49 ± 12:36min:s versus 30:47 ± 7:06 min:s). Abnormalities of the right ovary (n=8; 5 Remo-OVE, 3 Laser-OVE) had no significant effect on any surgery interval or variable. Abnormalities of the left ovary (n=7; 6 Laser-OVE, 1 Remo-OVE) caused a significant increase in duration of excision of the left ovary (8:51 ± 5:08 min:s versus 6:09 ± 2:35 min:s; P = .046) and caused an increase in total surgical time (40:35 ± 14:48 min:s versus 31:08 ± 6:57 min:s; P = .013). However, when determining the effect of abnormal ovaries on duration of Laser-OVE and Remo-OVE respectively, no significant difference was found. Linear regression analysis revealed that abnormal ovaries no longer had a significant effect on duration of left OVE when taking Remo-OVE versus Laser-OVE into account (P = .217 versus P = .017). Thus, the difference found for left versus right OVE with abnormal ovaries was because of the unequal distribution of Laser- and Remo-OVE in these groups.

Abnormal ovaries were not related to occurrence of intraoperative bleeding, obesity, or age. Ovary abnormalities significantly occurred in combination with abnormal uterus (P < .0005). Both abnormal uterus and ovaries were not related to pseudopregnancy (P = .531 and P = .143 respectively). Age had no effect on surgical time or complications. There was no significant learning curve for duration of Laser-OVE or Remo-OVE in time. The number of heat-cycles (mean: 3.23 ± 3.46, range: 0 – 15) did not affect surgical time.

Postoperative Variables

Postoperative appetite and activity were unchanged compared with preoperative assessment. Five of 120 wounds had signs of swelling, redness, or discharge, but none required treatment. Postoperative pain medication was administered for 2.7 ± 0.9 days (range, 0 – 3 days). Complete recovery was noted after 1.3 ± 1.1 days (range, 0.5 – 7.0 days). All owners were satisfied with the procedure and results, 15 owners were very satisfied.

Discussion

We found that the Nd:YAG surgical laser and the Remorgida bipolar forceps were both useful and safe instruments for laparoscopic OVE in dogs, without major complications. The Remorgida forceps significantly decreased surgical time compared with laser ovariectomy; however, this difference was only significant for left ovariectomy comparable with a previous report of laser lapOVE in dogs (*Chapter 5*, Van Nimwegen *et al* 2005). The most reasonable explanation for this finding is that laser resection of the left ovary is somewhat more complicated compared with the right ovary because of difficulties in

positioning of the laser fiber (Van Nimwegen *et al* 2005). The left ovary is more caudally located than the right ovary (Evans 1993), making laser resection, but not Remorgida resection, more difficult. The Remorgida forceps can easily grab the tissue to be coagulated and cut. However, the difference in duration of Laser-OVE for the left versus right ovary (8:04 ± 3:34 min:s versus 6:52 ± 2:42 min:s; n=20; *P* = .242) was not significant in contrast to a previous study (10:53 ± 4:38 min:s versus 8:40 ± 3:54 min:s; n=36; *P* < .0005) (Van Nimwegen *et al* 2005).

Contrary to our hypothesis, more intraoperative bleeding occurred with the Remorgida forceps than with the laser. This was probably resulted from increased experience with Laser-OVE (compared with a previous study (Van Nimwegen *et al* 2005)) and a higher occurrence of intraoperative bleeding with Remo-OVE than might have been expected based on a previous study using standard bipolar (BEC) forceps (Van Nimwegen *et al* 2005). In contrast to previous studies (Van Goethem *et al* 2003, Van Nimwegen *et al* 2005), intraoperative hemorrhage did not significantly affect surgical time. None of the hemorrhage episodes was considered a major complication and all were easily managed using the Remorgida or BEC forceps.

Obesity

Obesity caused an overall increase in surgical time of 22%, comparable with previous studies in dogs (Van Goethem *et al* 2003, Van Nimwegen *et al* 2005). Furthermore, FS was increased in obese dogs and surgical time increased with increasing FS, thus FS is probably the most important patient-associated variable significantly affecting surgical time. This assumption is supported by the fact that in cats obesity did not increase surgery duration because FS was not significantly related to obesity (*Chapter 7*, van Nimwegen and Kirpensteijn 2007). FS was always 0 or 1 in both obese and non-obese cats.

Instrument and Technique Familiarity

Although no learning curve was observed in our study, significant progress can be detected in surgical time when our results are compared with a previous study of laser lapOVE (*Chapter 5*, Van Nimwegen *et al* 2005). In Table 3, duration of excision of the left ovary is displayed for Laser-OVE and Bipolar OVE (BEC-OVE) in 2003 (Van Nimwegen *et al* 2005) compared with Laser-OVE and Remo-OVE in the current study (2005). With BEC-OVE, the ovarian bursa and ovary were excised using BEC forceps and endoscopic scissors. Remo-OVE significantly decreased duration of OVE compared with BEC-OVE (5:11 ± 2:11 min:s versus 8:42 ± 3:18 min:s respectively; *P* = 0 <0.001; Table 3). This is caused by the reduction of instrument exchange with the Remorgida forceps. Also, duration

of Laser-OVE has significantly decreased in the current study compared with the previous study[4]: 8:04 ± 3:34 min:s versus 10:54 ± 4:36 min:s respectively; P = .022).

2003	Laser-OVE	BEC-OVE	P = .015
(N = 36)	10:54 ± 4:36	8:42 ± 3:18	
2005	Laser-OVE	Remo-OVE	P = .004
(N = 20)	8:04 ± 3:34	5:11 ± 2:11	
	P = .022	P < .001	

Table 3: Duration (min:s) for OVE of the Left Ovary using Laser, Remorgida and BEC. Comparison of Results from the Current Study (2005) and a Previous Study (2003) (Van Nimwegen *et al* 2005).

Intraoperative Hemorrhage

Occurrence of intraoperative hemorrhage decreased from 17% to 10% for Laser-OVE (P = .338) whereas more hemorrhage occurred with Remo-OVE (18%) compared to BEC-OVE (6%; P = .042) in 2003 (Van Nimwegen *et al* 2005). Probable reasons for this are increased technical skills in laser surgery over time (learning curve) and differences in coagulation ability of the Remorgida forceps compared with BEC forceps.

Figure 5: Comparison of the working mechanisms of the Remorgida (Remo) and Bipolar electrocoagulation forceps (BEC).

Coagulation of the ovarian pedicle is probably less superior with the Remorgida device compared with BEC forceps because the ability to grab and squeeze tissue differs between the 2 forceps (Figure 5). The BEC forceps is able to grab more tissue and, even more importantly, pressure is more equally distributed over the tissue. Also, the more parallel position of the conducting jaws of the BEC forceps probably enables a more equal distribution of tissue coagulation within the forceps jaws, achieving more reliable coagulation. Another reason for better vessel coagulation may be the broader jaws of the BEC forceps compared with the Remorgida forceps, creating a broader band of tissue

coagulation, which improves vessel sealing. When cutting tissue with the Remorgida forceps, the knife blade is pushed through the tissue between the jaws of the forceps, creating some traction at the coagulated tissue which might cause laceration of coagulated vessels.

The laser produced more fume compared with the Remorgida device, which did not complicate surgery and had no remarkable effect on measured surgical variables. Pedicles containing large amounts of fat (FS=3) were more easily resected using the surgical laser compared with Remorgida. This was caused by either the increased thickness of the tissue or the altered conduction properties of fatty tissue, or both, which reduce the rate of bipolar tissue coagulation. This qualitative finding was not identified quantitatively between Remorgida or laser for higher FS. On the other hand, increased amounts of adipose tissue in the pedicle, making the tissue less absorptive for Nd:YAG energy, decreased the rate at which the laser was able to create the initial tissue carbonization, necessary for further contact mode tissue ablation (Peavy 2002, Janda *et al* 2003). This was the most important time-consuming factor during laser surgery besides extra instrument exchanges when BEC was needed for additional hemostasis of larger blood vessels.

Ovarian Access

Difficult access to the ovary significantly lengthened the searching interval of the right ovary (n = 4), which is comparable to previous findings (Van Goethem *et al* 2003), but was not observed for the left ovary, possibly because of the small occurrence of difficult access to the left ovary (n = 2). In multiparous dogs, the ovaries are generally located more caudally and ventrally (Evans 1993). How much this position is affected by age or estrus; however, has not been reported. Difficult access to the ovaries occurred only in younger animals (5 dogs; mean age, 1.0 ± 0.5 versus 2.7 ± 1.9 years; 0, 1 or 2 heat-cycles), but was not significant ($P = .064$).

Ovarian Abnormalities

Abnormalities of ovaries and uterus occurred simultaneously most of the time, indicating a shared origin, most probably hormonal in nature (eg, pseudopregnancy). This hypothesis is supported by the observation that intraoperative abnormal ovaries (and uterus) were significantly related to the time after estrus: 3.9 ± 1.4 months for normal ovaries compared with 2.5 ± 1.3 months for abnormal ovaries ($P = .006$). However, preoperative signs of pseudopregnancy were not related to intraoperative changes ($P = .531$).

We conclude that duration of laparoscopic ovariectomy is mainly determined by technique and instrumentation, the amount of fat in the ovarian ligament, and the experience of the

surgeon. By applying a high level of standardization, these factors can be separated and investigated. Although hemorrhage is best prevented using the BEC-forceps in Laser-OVE, the Remorgida forceps reduces surgical time, is not associated with an increased complication rate, produces less fume, and is used as a stand-alone device for ovariectomy. Furthermore, it is associated with lower costs and safety requirements compared with laser surgery. Thus, the Remorgida forceps is seemingly a more suitable device for canine lapOVE.

References

Bleul U, Hollenstein K and Kahn W (2005) Laparoscopic ovariectomy in standing cows *Anim Reprod Sci* **90** 193-200

Bohm B, Milsom J W, Kitago K, Brand M and Fazio V W (1994) Monopolar electrosurgery and Nd:YAG Contact Laser in laparoscopic intestinal surgery *Surg Endosc* **8** 677-81

Brown D H (2000) The versatile contact Nd:YAG laser in head and neck surgery: an in vivo and clinical analysis *Laryngoscope* **110** 854-67

Diamantis T, Kontos M, Arvelakis A, Syroukis S, Koronarchis D, Papalois A, Agapitos E, Bastounis E and Lazaris A C (2006) Comparison of monopolar electrocoagulation, bipolar electrocoagulation, Ultracision, and Ligasure *Surg Today* **36** 908-13

Evans H E (1993). Miller's Anatomy of the Dog

Philadelphia, Saunders.

Goff J S (1986) Bipolar electrocoagulation versus Nd-YAG laser photocoagulation for upper gastrointestinal bleeding lesions *Dig Dis Sci* **31** 906-10

Gunenc M Z, Yesildaglar N, Bingol B, Onalan G, Tabak S and Gokmen B (2005) The safety and efficacy of direct trocar insertion with elevation of the rectus sheath instead of the skin for pneumoperitoneum *Surg Laparosc Endosc Percutan Tech* **15** 80-1

Hendrickson D (2006) Laparoscopic cryptorchidectomy and ovariectomy in horses *Vet Clin North Am Equine Pract* **22** 777-98

Hubert J D, Burba D J and Moore R M (2006) Evaluation of a vessel-sealing device for laparoscopic granulosa cell tumor removal in standing mares *Vet Surg* **35** 324-9

Impellizeri J A, Tetrick M A and Muir P (2000) Effect of weight reduction on clinical signs of lameness in dogs with hip osteoarthritis *J Am Vet Med Assoc* **216** 1089-91

Janda P, Sroka R, Mundweil B, Betz C S, Baumgartner R and Leunig A (2003) Comparison of thermal tissue effects induced by contact application of fiber guided laser systems *Lasers Surg Med* **33** 93-101

L'Eplattenier H F, van Nimwegen S A, van Sluijs F J and Kirpensteijn J (2006) Partial prostatectomy using Nd:YAG laser for management of canine prostate carcinoma *Vet Surg* **35** 406-11

Matchett C A, Morales P R and Orkin J L (2006) Evaluation and comparative analysis of a technique for laparoscopic ovariectomy in rhesus macaques (Macaca mulatta) *J Am Assoc Lab Anim Sci* **45** 74-8

Okkens A C, Kooistra H S and Nickel R F (1997) Comparison of long-term effects of ovariectomy versus ovariohysterectomy in bitches *J Reprod Fertil Suppl* **51** 227-31

Ou C S, Joki J, Wells K, Zabriske V, Hamilton K, Tsuang M and Rowbotham R (2004) Total laparoscopic hysterectomy using multifunction grasping, coagulating, and cutting forceps *J Laparoendosc Adv Surg Tech A* **14** 67-71

Peavy G M (2002) Lasers and laser-tissue interaction *Vet Clin North Am Small Anim Pract* **32** 517-34, v-vi

Pittaway D E, Takacs P and Bauguess P (1994) Laparoscopic adnexectomy: a comparison with laparotomy *Am J Obstet Gynecol* **171** 385-9; discussion 9-91

Rodgerson D H, Baird A N, Lin H C and Pugh D G (1998) Ventral abdominal approach for laparoscopic ovariectomy in llamas *Vet Surg* **27** 331-6

Santa-Cruz R W, Auge B K, Lallas C D, Preminger G M and Polascik T J (2003) Use of bipolar laparoscopic forceps to occlude and transect the retroperitoneal vasculature: a porcine model *J Endourol* **17** 181-5

Underwood R A, Dunnegan D L and Soper N J (1999) Prospective, randomized trial of bipolar electrosurgery vs ultrasonic coagulation for division of short gastric vessels during laparoscopic Nissen fundoplication *Surg Endosc* **13** 763-8

van Goethem B, Schaefers-Okkens A and Kirpensteijn J (2006) Making a rational choice between ovariectomy and ovariohysterectomy in the dog: a discussion of the benefits of either technique *Veterinary Surgery* **35** 136-43

Van Goethem B E, Rosenveldt K W and Kirpensteijn J (2003) Monopolar versus bipolar electrocoagulation in canine laparoscopic ovariectomy: a nonrandomized, prospective, clinical trial *Vet Surg* **32** 464-70

van Nimwegen S A and Kirpensteijn J (2007) Laparoscopic ovariectomy in cats: comparison of laser and bipolar electrocoagulation *J Feline Med Surg* **9** 397-403

Van Nimwegen S A, Van Swol C F and Kirpensteijn J (2005) Neodymium:yttrium aluminum garnet surgical laser versus bipolar electrocoagulation for laparoscopic ovariectomy in dogs *Veterinary Surgery* **34** 353-60

Wenkel R, Ziemann U, Thielebein J and Prange H (2005) Laparoskopische Kastration der Hündin Darstellung neuer Verfahren zur minimal invasiven Ovariohysterektomie *Tierarztliche Praxis* **33** 177-88

Yerdel M A, et al. (1999) Direct trocar insertion versus Veress needle insertion in laparoscopic cholecystectomy *Am J Surg* **177** 247-9

7

Chapter 7

Laparoscopic ovariectomy in cats: comparison of laser and bipolar electrocoagulation

Sebastiaan A. van Nimwegen, DVM
Jolle Kirpensteijn, Prof, DVM, PhD, diplomate ACVS & ECVS

Department of Clinical Sciences of Companion Animals, Faculty of Veterinary Medicine
Utrecht University, the Netherlands.

Abstract

Fourteen mixed-breed domestic cats underwent laparoscopic ovariectomy (lapOVE) using pediatric equipment, a Nd:YAG laser and a bipolar electrocoagulation forceps. Cats were placed in 10° Trendelenburg position (head down) and insufflation pressure was kept at 4 mmHg, while surgery was performed through three midline portals. Randomly-assigned unilateral laser resection of one ovary (Laser-OVE) and bipolar electrocoagulation (BEC-OVE) of the contralateral ovary were performed. Duration of predetermined surgery intervals were recorded, as well as occurrence of intra- and post-operative complications. Both methods were successful and without complications. Duration of Laser-OVE was significantly increased compared to BEC-OVE. The right ovary was more difficult to access; however, both ovaries were easy to manipulate because of the relatively long suspensory ligament. The ovarian ligaments contained minimal amounts of fat and obesity did not influence surgery duration. Convalescence period was short (0.9 ± 0.4 days) and owner satisfaction high.

Introduction

Ovariectomy (OVE) is the standard procedure for neutering the domestic cat and dog in the Netherlands (van Goethem *et al* 2006). The canine laparoscopic OVE (lapOVE) is a well-documented procedure (Van Goethem *et al* 2003, Van Nimwegen *et al* 2005, Wenkel *et al* 2005) that is routinely performed at specialized clinics. Research in dogs, pigs and humans indicates that laparoscopic procedures are superior to open surgery due to reduced morbidity caused by less incisional trauma, wound complications, adhesion formation (Schippers *et al* 1998, Gamal *et al* 2001), peri- and postoperative pain (Devitt *et al* 2005, Hancock *et al* 2005) and physical stress response (Marcovich *et al* 2001, Matsumoto *et al* 2005). Furthermore, laparoscopy is associated with better aesthetic results and increased visibility of abdominal structures (Wildt *et al* 1977). The shorter convalescence period (Barkun *et al* 1992, Bohm *et al* 1995) has resulted in improved cost-effectiveness in human medicine (Vilos and Alshimmiri 1995).

Often a mini-laparotomy (key hole) technique is used to perform OVE in the cat. In this procedure, the ovaries may be exteriorized (by some surgeons) in a blind fashion, using a spay hook and ligated extra-abdominally. The amount of intra abdominal trauma caused by the blind technique does not lead to major complications and is suggested to be minor, but has not been investigated. The lapOVE technique should allow a more controlled excision of the ovaries under direct visualization causing minimal trauma when specialized

laparoscopic equipment is used. Laparoscopic-assisted cryptorchidectomy has been described in cats (Vannozzi *et al* 2002, Miller *et al* 2004) and, in addition to our own experiences with feline laparoscopic cryptorchidectomy (unpublished data), has shown that laparoscopy is feasible in cats. To the authors' knowledge, neither laparoscopic-assisted nor laparoscopic OVE have been described in the domestic cat.

Multiple techniques of canine lapOVE have been published. Laser dissection (Van Nimwegen *et al* 2005) and bipolar electrocoagulation (BEC) (Van Goethem *et al* 2003) are most commonly used at the authors' institution. Laser can be applied in laparoscopic surgery, because the beam passes along a flexible optical fiber. This fiber-guided laser beam can be used to coagulate (non-contact mode) and to cut tissue (contact mode). Cutting, and especially coagulating ability, depends on the type of laser used; being wavelength-dependant (Peavy 2002). The Nd:YAG laser wavelength of 1064 nm shows relatively deep tissue penetration, being absorbed by tissue constituents but not by water and can be used in several procedures requiring deep tissue coagulation. In contact mode, the fiber tip is used in contact with tissue, which is comparable to the use of an electrical (monopolar) knife. The high energy density of the diverging laser beam at the tip leads to rapid vaporization of the tissue while at the same time the heat produced coagulates small blood vessels in the cut surface (Janda *et al* 2003).

Currently, the use of bipolar electrocoagulation forceps is considered superior in canine lapOVE because of excellent coagulation of mesovarial vessels and short duration of surgery (*Chapters 5 and 6*). In dogs, the Nd:YAG laser is associated with more intra-operative hemorrhage. It was unable to coagulate the larger vessels in the ovarian pedicle and could therefore not be used as a stand-alone device for ovary excision. The laser technique required additional use of bipolar electrocoagulation, which resulted in increased surgery duration (Van Nimwegen *et al* 2005). Neither of these techniques has been described in cats.

The aim of this study was to prove that lapOVE is possible in cats and is a relatively simple method, despite the small size of the feline abdomen. Additionally, the use of surgical laser dissection was compared to bipolar electrocoagulation in a prospective clinical trial.

Methods

Ethics and owner consent

All procedures were approved by the Ethics Committee of the University of Utrecht and conducted in a manner consistent with Dutch law concerning care and use of animals. Approval of owners was obtained prior to surgery in all cats.

Animals

Both techniques were performed and refined in a pilot study in 4 healthy, client-owned, intact, female cats. After the pilot study, 14 healthy client-owned female cats, presented for elective OVE entered the lapOVE clinical trial comparing the two methods. A standard questionnaire was completed by the owner concerning the patient's age, breed, general health status, diet, previous estrus cycles and pregnancies. All cats underwent a full physical examination. Bodyweight was measured and obesity was scored, ranging from 1 (thin) to 5 (obese), to subjectively differentiate obese from non-obese cats. The cats were randomly assigned to two groups. Group 1 cats had a laser dissection (Laser-OVE) performed of the left ovary and bipolar electrocoagulation (BEC-OVE) of the right ovary. Group 2 cats had a BEC-OVE performed of the left ovary and Laser-OVE of the right ovary. The cats served as their own controls in comparing the two techniques. Only cats with normal anatomy of the uterus and ovaries during laparoscopy were allowed to participate in the study. As this was a routine surgical procedure on normal cats, no selection bias was present.

Anesthesia

All cats received general anesthesia according to a standard protocol. The cats were sedated using medetomidine (Domitor; Pfizer), 40 µg/kg IM. After placement of a catheter in the cephalic vein, the cats were induced using propofol (Propovet; Abbott Laboratories Ltd.), 1 to 2 mg/kg IV, administered to effect preceding tracheal intubation. Anesthesia was maintained using isoflurane (IsoFlo; Abbot Laboratories Ltd.) in a mixture of oxygen/air by means of mechanical IPPV ventilation. Additional analgesia was accomplished by administering carprofen (Rimadyl; Pfizer), 4 mg/kg IV, single dose. Monitoring consisted of continuous ECG, gas analyser (measuring CO_2 and isoflurane concentrations), pulse-oximetry and body temperature measurements using an esophageal probe. Sedation was reversed using atipamezole (Antisedan; Pfizer), 100 µg/kg IM.

Surgery

All surgery was performed by the same surgeon (JK). Before surgery, the urinary bladder was emptied manually, to decrease the chance of puncture during trocar insertion and increase the visibility during laparoscopy. The surgical field was prepared aseptically after clipping the hair between the nipples from sternum to os pubis. Patients were positioned in dorsal recumbency in a 10° Trendelenburg position (head down) for video-assisted laparoscopic surgery through three midline portals as described for the dog (Van Nimwegen *et al* 2005). A variation of the standard closed trocar technique was used for the

first trocar, without the use of a Veress needle. The first trocar was placed just caudal to the umbilicus. A 4 mm skin incision was made and the subcutis was carefully prepared using scissors, revealing the linea alba. After suture placement in the linea, the abdominal wall was pulled upward. Two stay-sutures were placed at the cranial and caudal border of the skin incision, penetrating skin, subcutis, abdominal wall and peritoneum. The first suture in the linea was removed and the two stay-sutures were used to pull up the ventral abdominal wall while inserting the primary camera trocar (4.5 mm diameter sheath, 6 cm length; Karl Storz-Endoscopy, Vianen, the Netherlands) avoiding trauma to visceral organs. Insufflation with CO_2 was started at 1 l/min to check for proper trocar placement. Insufflation was then set to 6 l/min and intra-abdominal pressure was kept at 4 mmHg. A 4 mm diameter 0° rigid telescope (18 cm length, Hopkins II; Karl Storz-Endoscopy) was inserted and the abdominal space was inspected. The second and third trocar (3.5 mm diameter sheath, 5 cm length; Karl Storz-Endoscopy) were inserted under laparoscopic guidance through a 3 mm skin incision midway between os pubis and umbilicus and midway between umbilicus and xyphoid. Care was taken not to traumatize the ventral ligament of the urinary bladder. Surgery always started with the left ovary with the surgeon and assistant on the right side of the cat. The ovary was located using either the uterus or teres ligament that originated from the inguinal canal. The uterus was grasped using a 3 mm diameter pediatric grasping forceps (20 cm length, Click-Line; Karl Storz-Endoscopy) through the cranial portal and a 3 mm diameter pediatric self-retaining grasping forceps (20 cm length, Click-Line; Karl Storz-Endoscopy) through the caudal portal. The uterus was followed cranially until the ovary was visualized. The ovary was grasped and lifted upward using the self-retaining grasping forceps through the cranial portal (Figure 1).
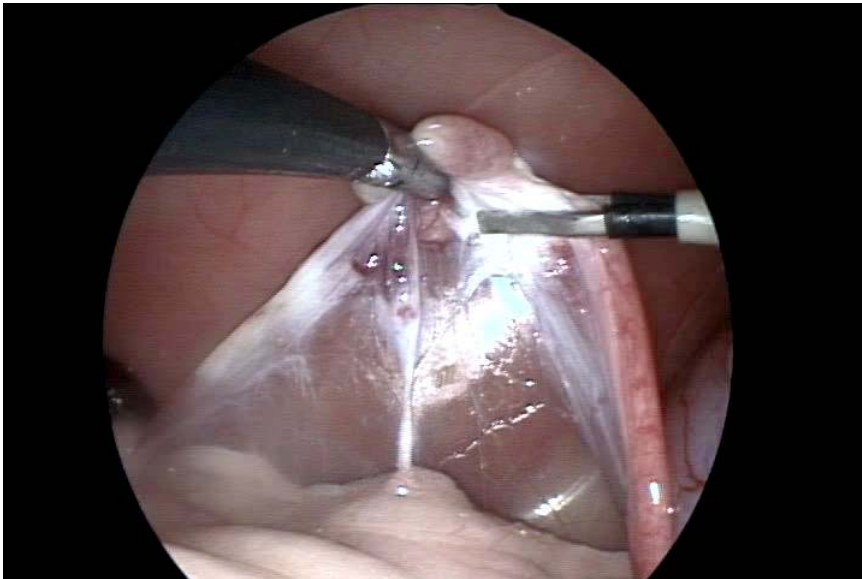
Figure 1: BEC-OVE. The left ovary is grasped and held upward by the self-retaining grasping forceps (left). The proper ligament is being coagulated using the bipolar electrocoagulating forceps (right). Tissues from left to right: Suspensory ligament, pedicle vessels, proper ligament and uterus.

During BEC-OVE, the proper ligament, the suspensory ligament and the ovarian pedicle were coagulated using a 3 mm diameter bipolar electrocoagulating forceps (Take-Apart; Karl Storz-Endoscopy) through the caudal portal (Figure 1). These structures were then cut using 3 mm diameter endoscopic scissors (20 cm length, Click-Line; Karl Storz-Endoscopy) (Figure 2). During the Laser-OVE, major blood vessels of the ovarian pedicle were coagulated using the BEC-forceps. The laser fiber (600 μm diameter optical fiber, Ultraline (side-firing tip removed); Heraeus LaserSonics, Milpitas, CA) connected to a Nd:YAG surgical laser (Medilas 40 N; MBB Medizintechnik GmbH, München, Germany) was inserted through the caudal portal. The ovary was resected by cutting the proper ligament, pedicle and suspensory ligament respectively, using the laser fiber in contact-mode with 10 W continuous wave laser power (Figure 3).
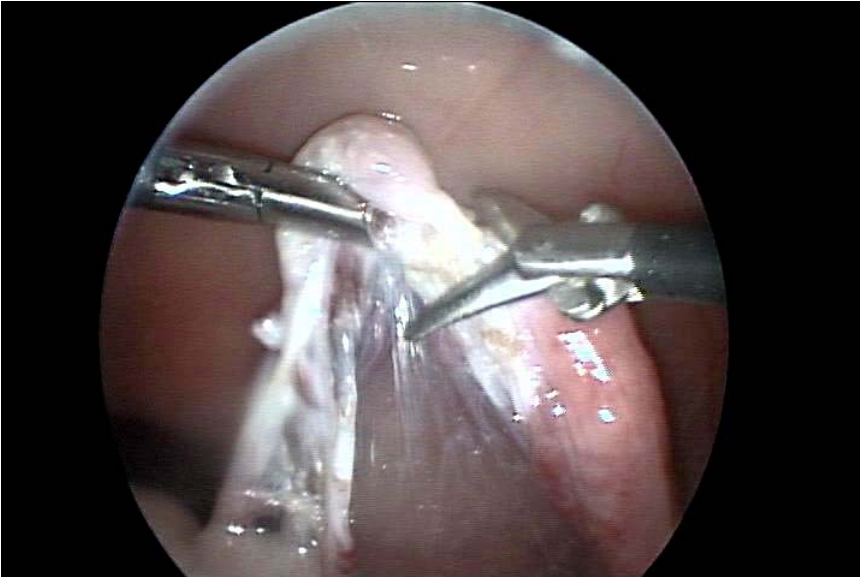
Figure 2: The bursa and ovary are excised using endoscopic scissors (right). The grasping forceps holds the ovary (left). At this stage the proper ligament is cut.

In both techniques, iatrogenic hemorrhage was controlled using the BEC-forceps. Care was taken to remove the complete ovary, excising at least 10 mm of non-ovarial tissue around the ovary. After complete resection, the ovary was removed from the abdomen through the caudal portal, after removal of the trocar sheath. After reinsertion of the caudal trocar, the surgeon and assistant turned to the other side of the operating table and the same procedure was performed for the right ovary using the laser method instead of BEC (group 2) or vice-versa (group 1). The excised tissue was checked to ensure that both ovaries had been removed in entirety. A routine, exploratory laparoscopy was performed of the abdomen, excess CO_2 was removed and each portal was closed in a routine fashion with one 4-0 inverted, absorbable, monofilament suture (Monocryl; Ethicon, Amersfoort, the Netherlands).

Postoperative care and follow-up

Patients were released from the hospital immediately after recovery. Ketoprofen (Ketofen, Fort Dodge) was prescribed for pain management (1 mg/kg orally once a day for three days). The owners were contacted 7-10 days after surgery using a standard follow-up questionnaire concerning time taken for complete recovery, appetite (decreased, same, increased), activity (decreased, same ,increased), number of days on pain medication,

evaluation of the surgery wounds, satisfaction (unsatisfied, neutral, satisfied, very satisfied), whether they would recommend the laparoscopic treatment to other owners and whether they would choose lapOVE again in the future instead of a regular laparotomy. Cases of minor wound swelling, redness and/or discharge were considered wound complications.

Experimental data

During surgery the following time points were recorded:

First skin incision:	t_0
Insertion first trocar:	t_1
Start searching for the left ovary:	t_2
Start excision of the left ovary:	t_3
End excision of the left ovary:	t_4
End removal of the left ovary:	t_5
Start searching for the right ovary:	t_6
Start excision of the right ovary:	t_7
End excision of the right ovary:	t_8
End removal of the right ovary:	t_9

Other recorded intra-operative parameters were accessibility of the ovaries, occurrence of hemorrhage during surgery, abnormalities of ovaries or uterus, the amount of fat in the ovarian ligament (fat score: 0 (no fat), 1 (moderate amount of fat), 2 (large amount of fat)) and loss of vision because of smoke production or insufficient insufflation.

Data analysis

Paired data (laser versus BEC and left versus right) were tested for equality using Student's t-test for paired samples. Influences of obesity, hemorrhage and access-difficulty on surgery duration were evaluated using one-way ANOVA tests. Differences were assumed significant if $p<0.05$, two-tailed. Results are reported as means ± SD.

Results

Patients were all healthy, mixed-breed, domestic shorthair cats. It was not necessary to exclude any of the cats from the study because of ovarial or uterine abnormalities. Mean age was 1.5 ± 1.9 years (range, $0.3 - 7.6$ years). Mean bodyweight was 2.8 ± 0.5 kg (range, $2.3 - 3.8$ kg). The distension of the feline abdomen was relatively extensive at lower pressures. An intra-abdominal pressure of 4 mmHg was enough to create enough abdominal distension for an adequate surgical working space and good laparoscopic visibility. The distension did not cause any problems with maintaining the anesthetic plane. Production of

smoke impairing visibility during surgery was minimal. None of the ovarian ligaments contained much fat, even in obese cats. This made the excision of the ovaries relatively easy. The relatively long suspensory and mesovarial ligaments allowed easy manipulation of the ovary. Rather large depositions of fat were found at the mid-ventral abdominal wall, in the falciform ligament, especially in obese cats.
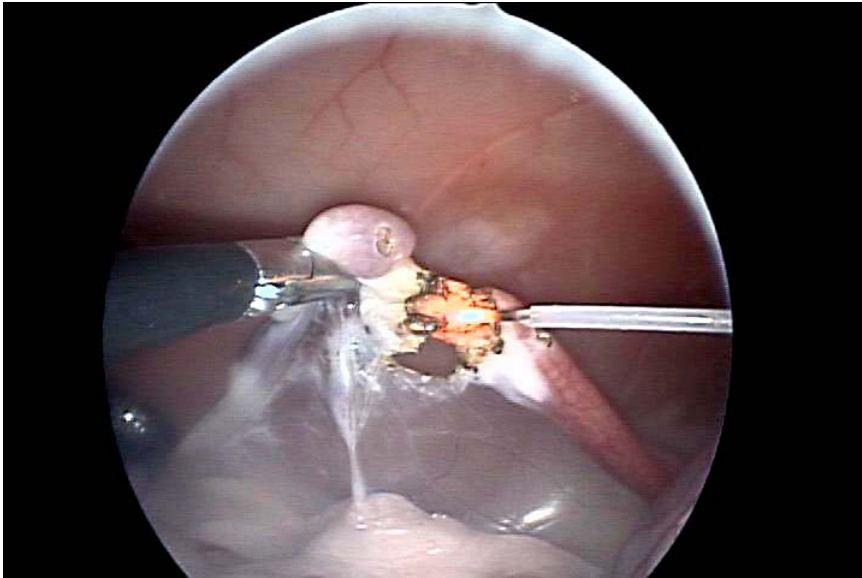
Figure 3: Laser-OVE. The bursa and ovary are excised using Nd:YAG laser irradiation through a 600 μm diameter optical fiber (right). At this stage the proper ligament is cut using the laser fiber in contact mode.

Surgery time intervals

The time points recorded during surgery were used to reconstruct the duration of selected time intervals (for instance, searching left ovary = $t_3 - t_2$). The time intervals were compared for the left side versus the right side and excision (OVE) time was also compared for Laser-OVE versus BEC-OVE (Figure 4).

There were no significant differences in surgery time intervals between the left versus the right side. The increased duration of OVE of the right ovary (3:54 ± 2:52 minutes) compared to the left ovary (2:37 ± 1:16 minutes), was not significant (p=0.135). Laser resection of the ovary (Laser-OVE, 4:09 ± 2:50 minutes) took significantly longer compared to the bipolar technique (BEC-OVE, 2:23 ± 1:01 minutes, p=0.032). Mean overall surgery duration was 30:01 ± 5:58 minutes (range, 19:41 – 40:02 minutes).

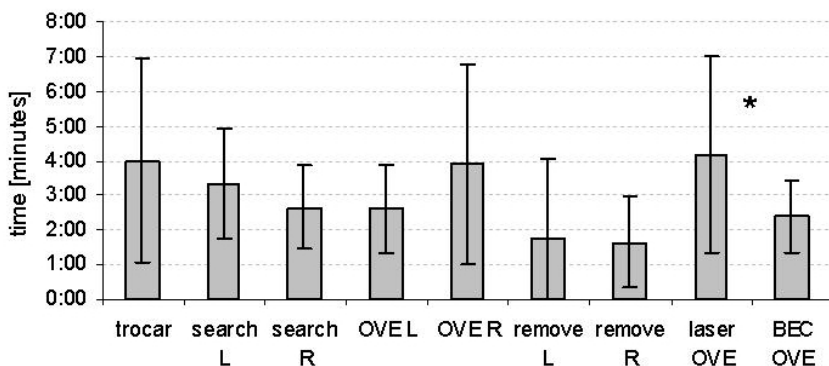**Figure 4**: Surgery time intervals ± SD for placement of the first trocar, searching, resection (OVE) and removal of the ovary from the abdomen, laser resection (Laser-OVE) and bipolar resection (BEC-OVE) of the ovary (R: Right, L: Left; * indicates significant difference).

Obesity, accessibility, hemorrhage

Five of 14 cats were considered obese. Obesity was not correlated with a higher fat score of the ovary and ligaments. Neither obesity nor fat score had a significant effect on duration of any surgery interval. The left ovary was generally more easily accessible than the right ovary, although both ovaries were easily manipulated when grasped by forceps. Notable difficulty accessing the ovary occurred in 3 cats, all concerning the right ovary. Difficult access significantly lengthened duration in searching for the right ovary in these three cats compared to cats that had an ovary that was easily accessible (3:59 ± 1:05 versus 2:17 ± 1:00 minutes, p=0.025). There was no overall difference in mean duration of searching, however, for the left ovary compared to the right ovary (Figure 4). Difficult access had no significant effect on other surgery intervals. Occurrence of hemorrhage was not a problem in BEC-OVE or Laser-OVE. Only one notable bleeding occurred with BEC-OVE, which was managed properly using the BEC-forceps and had no obvious effect on surgery duration.

Postoperative variables

Mean period for complete recovery was 0.9 ± 0.4 days (range, 0.5 – 2 days) and all cat owners were very satisfied with the results. Ketoprofen was given 2.9 ± 0.3 days (range, 2 – 3 days). Postoperative appetite was unchanged compared to eating behavior of the cats before surgery. Postoperative activity did vary from cats becoming sweeter and calmer (3 cats), no change (9 cats) to increased activity (2 cats). A wound complication occurred in 1 of 42 wounds in which the suture did not properly hold the edges together. Surgical intervention was not required, and the wound healed without further complications. All cat

owners reported that they would choose the laparoscopic approach over laparotomy again in future cases of OVE, and that they would recommend it to other cat owners.

Discussion

Fourteen cats received laparoscopic ovariectomy through 3 midline portals, comparing the use of laser and bipolar electrocoagulation. An intra-abdominal CO_2 pressure of 4 mmHg was sufficient to create a comprehensive surgical space compared to 10 to 12 mmHg noted in other publications (Vannozzi *et al* 2002, Miller *et al* 2004). This is an encouraging finding, considering that pneumoperitoneum is responsible for many negative hemodynamic effects (Bailey and Pablo 1999), and could be the main factor causing surgical stress in laparoscopic procedures (Marcovich *et al* 2001). An intra-abdominal pressure of 8 to 12 mmHg is considered safe in dogs (Ishizaki *et al* 1993), with no major hemodynamic derangements. Such safety limits have not been determined for cats, but we expect them to be lower for cats compared to dogs. The 4 mmHg CO_2 pressure allows full visibility of all essential abdominal organs, mainly caused by the flexibility of the feline abdominal wall. In order to reduce the risk of injuring the urinary bladder, the position of the first trocar was more cranial compared to the technique used in dogs and it was necessary to empty the urinary bladder manually prior to surgery to reduce the risk of bladder injury and to create an appropriate surgical space. The stay suture technique for trocar placement was also modified, by placing the sutures through and through to enable sufficient tension during trocar insertion. Because of a less tight fit of the trocar in the abdominal wall, more effort had to be made to keep the trocars in place during surgery compared to laparoscopy in dogs. There was also more difficulty directing the laser fiber towards the ovary, because an additional laser-guide could not be used with the pediatric trocars. Fiber movements had to be guided by the trocar, leading to a relatively large degree of flexibility.

In all the cats, including the obese ones, there was a relatively small amount of fat deposited in the ligaments supporting the ovary and uterus. Only one cat had a pedicle fat score of 1, the rest had a fat score of 0. In contrast, obese dogs always had pedicle fat scores of 2 or 3 in previous studies (Van Goethem *et al* 2003, Van Nimwegen *et al* 2005) (*Chapters 5 and 6*). This probably explains why duration of lapOVE was not affected by obesity in cats, whereas in dogs obesity significantly increased surgery duration by 35% (Van Nimwegen *et al* 2005). The minimal amount of fat in the ligaments improved surgical access. More fat was located against the abdominal wall in obese cats, mainly in the mid-ventral region including the falciform ligament. In the cat, initial access to the right ovary was more demanding compared to the left ovary with a distinct access difficulty occurring three times on the right side, causing a significant increase in duration of searching for the

right ovary compared to normal access of the right ovary. No significant difference, however, was found in searching time or resection time overall between the right and the left ovary. Furthermore, after grasping the ovary and if necessary, creating more working space by gently uncovering the ovary and pedicle from viscera, both ovaries could easily be retracted and manipulated for surgery. Laser resection was combined with BEC-forceps for proper haemostasis, instead of using the surgical laser as a stand-alone device for OVE. Using the laser in non-contact mode to coagulate blood vessels running in the pedicle had been achieved in a pilot case. However, the authors were not confident that no damage could be done to surrounding tissues by the diverging (non-contact) laser beam and the BEC-forceps were chosen for their safer, more rapid and localized method of coagulation. Apart from the extra instrument exchange (laser versus BEC-forceps), most of the increased duration of Laser-OVE compared to BEC-OVE is probably caused by a distinct delay that occurred during each first attempt to use the laser fiber in contact mode. When a clean laser fiber is used for contact mode surgery, some char-formation has to occur at the fiber tip, in order to catalyze further tissue carbonization and vaporization during surgery. The speed at which this initial tissue char is formed is largely dependent on laser absorption characteristics of the tissue (Janda *et al* 2003). Formation of this initial layer of charred tissue may take a relatively long time, compared to the time needed for ovary excision. Apparently, absorption of Nd:YAG irradiation is relatively weak in the pale-colored tissue of the feline pedicle and initial charring is somewhat delayed. The amount of smoke produced during either laser or bipolar OVE did not remarkably decrease visibility during feline lapOVE as compared to lapOVE in dogs (Van Nimwegen *et al* 2005), probably because of the much smaller dimensions of the feline ovary and the reduced amount of lipoid tissue.

Duration of lapOVE is probably not reduced compared to OVE or ovariohysterectomy by means of laparotomy, although this was not the scope of the research reported here. Equipment setup and initial laparoscopic abdominal access require more effort compared to a plain laparotomy. Additionally, equipment requirements are more demanding for laparoscopic procedures including the need for laparoscopy unit, insufflator, bipolar electrocoagulation unit, extra help during surgery, and the need for mechanical ventilation. On the other hand, besides the decrease in trauma to the patient, excision of the ovaries is probably faster because of improved accessibility and visibility and the absence for the need of ligatures. Additionally, the improved visibility greatly enhances detection and control of pedicle hemorrhage and allows a quick scan of the abdomen for subclinical abnormalities. LapOVE is most likely not going to replace normal ovariectomy in the cat but the minimal invasive technique is appreciated by cat owners and can be offered as a successful alternative to the standard OVE.

This study shows the feasibility of feline lapOVE. The authors did not encounter major difficulties or complications during or after surgery. In fact, low-pressure pneumoperitoneum, easy manipulation of the ovaries and a minimal amount of fat in the ovarian ligament facilitated excellent surgical access and outcome. Furthermore, convalescence time was short and owner satisfaction was high. The use of laser, although effective, did not significantly enhance the procedure or outcomes.

References

Bailey J E and Pablo L S (1999) Anesthetic and Physiologic Coinsiderations for Veterinary Endosurgery *Veterinary Endosurgery* ed L J Freeman (St. Louis, MO: Mosby) pp 24-43

Barkun J S, Barkun A N, Sampalis J S, Fried G, Taylor B, Wexler M J, Goresky C A and Meakins J L (1992) Randomised controlled trial of laparoscopic versus mini cholecystectomy. The McGill Gallstone Treatment Group *Lancet* **340** 1116-25

Bohm B, Milsom J W and Fazio V W (1995) Postoperative intestinal motility following conventional and laparoscopic intestinal surgery *Archives of Surgery* **130** 415-24

Devitt C M, Cox R E and Hailey J J (2005) Duration, complications, stress, and pain of open ovariohysterectomy versus a simple method of laparoscopic-assisted ovariohysterectomy in dogs *Journal of the American Veterinary Medical Association* **227** 921-8

Gamal E M, Metzger P, Szabo G, Brath E, Peto K, Olah A, Kiss J, Furka I and Miko I (2001) The influence of intraoperative complications on adhesion formation during laparoscopic and conventional cholecystectomy in an animal model *Surgical Endoscopy* **15** 873-80

Hancock R B, Lanz O I, Waldron D R, Duncan R B, Broadstone R V and Hendrix P K (2005) Comparison of postoperative pain after ovariohysterectomy by harmonic scalpel-assisted laparoscopy compared with median celiotomy and ligation in dogs *Veterinary Surgery* **34** 273-82

Ishizaki Y, Bandai Y, Shimomura K, Abe H, Ohtomo Y and Idezuki Y (1993) Safe intraabdominal pressure of carbon dioxide pneumoperitoneum during laparoscopic surgery *Surgery* **114** 549-54

Janda P, Sroka R, Mundweil B, Betz C S, Baumgartner R and Leunig A (2003) Comparison of thermal tissue effects induced by contact application of fiber guided laser systems *Lasers in Surgery and Medicine* **33** 93-101

Marcovich R, Williams A L, Seifman B D and Wolf J S, Jr. (2001) A canine model to assess the biochemical stress response to laparoscopic and open surgery *Journal of Endourology* **15** 1005-13

Matsumoto E D, Margulis V, Tunc L, Taylor G D, Duchene D, Johnson D B, Pearle M S and Cadeddu J A (2005) Cytokine response to surgical stress: comparison of pure laparoscopic, hand-assisted laparoscopic, and open nephrectomy *Journal of Endourology* **19** 1140-5

Miller N A, Van Lue S J and Rawlings C A (2004) Use of laparoscopic-assisted cryptorchidectomy in dogs and cats *Journal of the American Veterinary Medical Association* **224** 875-83

Peavy G M (2002) Lasers and laser-tissue interaction *Veterinary Clinics of North America. Small Animal Practice* **32** 517-34

Schippers E, Tittel A, Ottinger A and Schumpelick V (1998) Laparoscopy versus laparotomy: comparison of adhesion-formation after bowel resection in a canine model *Digestive Surgery* **15** 145-52

van Goethem B, Schaefers-Okkens A and Kirpensteijn J (2006) Making a rational choice between ovariectomy and ovariohysterectomy in the dog: a discussion of the benefits of either technique *Veterinary Surgery* **35** 136-43

Van Goethem B E, Rosenveldt K W and Kirpensteijn J (2003) Monopolar versus bipolar electrocoagulation in canine laparoscopic ovariectomy: a nonrandomized, prospective, clinical trial *Veterinary Surgery* **32** 464-70

Van Nimwegen S A, Van Swol C F and Kirpensteijn J (2005) Neodymium:yttrium aluminum garnet surgical laser versus bipolar electrocoagulation for laparoscopic ovariectomy in dogs *Veterinary Surgery* **34** 353-60

Vannozzi I, Benetti C and Rota A (2002) Laparoscopic cryptorchidectomy in a cat *Journal of Feline Medicine and Surgery* **4** 201-4

Vilos G A and Alshimmiri M M (1995) Cost-benefit analysis of laparoscopic versus laparotomy salpingo-oophorectomy for benign tubo-ovarian disease *Journal of the American Association of Gynecologic Laparoscopists* **2** 299-303

Wenkel R, Ziemann U, Thielebein J and Prange H (2005) Laparoskopische Kastration der Hündin Darstellung neuer Verfahren zur minimal invasiven Ovariohysterektomie *Tierarztliche Praxis* **33** 177-88

Wildt D E, Kinney G M and Seager S W (1977) Laparoscopy for direct observation of internal organs of the domestic cat and dog *American Journal of Veterinary Research* **38** 1429-32

Appendix to Chapter 7

Images of laparoscopic ovariectomy in cats

Cranial abdomen

Right caudal abdomen, showing uterus, intestine and bladder

Left caudal abdomen, left horn of the uterus

Left ovary

Bipolar electrocoagulation of the ovarian pedicle

Laser excision of the left ovary

8

Chapter 8

Summarizing discussion and conclusion

Summarizing discussion

Nd:YAG laser-tissue interaction was investigated *in vitro*, prior to *in vivo* clinical application of the laser in prostate surgery and laparoscopy in dogs and cats. *Ex vivo* canine prostate tissue was used to investigate laser-induced temeprature and damage distribution, circumventing difficulties and uncertainties of theoretical modeling of light and temperature distribution in tissue, considering the wide variation in published experimentally-determined optical properties of canine prostate tissue (**Chapter 1**, *Table 2*). Although prostate tissue (both human and canine) is one of the most extensively studied and modeled tissues concerning laser-induced temperature and damage behavior, specific Arrhenius parameters or acute damage threshold temperatures were never determined for the canine prostate. Recently, Arrhenius parameters for human benigne prostatic hyperplasia (BPH) tissue have been determined (Bhowmick *et al* 2004). The only experimentally-determined Arrhenius parameters for normal prostate tissue are not of canine origin (i.e. rat prostate (Skinner *et al* 2000), see also *Chapter 1, Section 4.2*). Thermal damage models for prostate tissue mostly use Arrhenius parameters of other tissueus, such as skin. One study compared calculated necrosis extent in prostate thermotherapy using Arrhenius parameters of pig skin (Henriques *et al* 1947) and of BPH tissue (Bhowmick *et al* 2004) and obtained similar results for the two (Huidobro *et al* 2004). The relations between temperature and exposure time for these Arrhenius parameters are displayed in *Chapter 1, Figure 8*. The most likely explanation for obtaining similar results is that exposure times in the order of 10 minutes were used, since the graphs cross in that time range. In fact, most Arrhenius damage relations seem to predict similar threshold temperatures in the 10-20 minute range (*Chapter 1, Figure 8*). This explains why Arrhenius parameters of different tissues could be used successfully in prostate as well as liver models for LITT (Prapavat *et al* 1996, Bolmsjo *et al* 1998, Sturesson 1998, Huidobro *et al* 2004). The question can be raised how much significance the Arrhenius parameters have in these tissue-damage models of > 10 minutes exposure. Several studies of prostate LITT with MRI temperature monitoring used an iso-effect thermal dose calculation (an approximation to the Arrhenius accumulated damage integral) to determine damage margins. The calculations yield a thermal damage threshold of 50-52°C , which correlates well with histologically determined damage margins (Peters *et al* 2000, Diederich *et al* 2004, Nau *et al* 2005, Pauly *et al* 2006), using exposure times of typically 10-20 minutes. It is clear from *Figure 8 in Chapter 1*, that for shorter exposure time, thresholds will not be the same for different tissues, and consequently, models may be expected to predict

different outcomes. The modelling of temperature-induced tissue damage is an emerging and developing field of science, and although the Arrhenius theory is useful to describe the process of thermal tissue damage, future research will learn if a sound biophysical/chemical interpretation of the Arrhenius integral is possible.

The schlieren technique, as described in *Chapter 2*, was useful to interpret qualitative differences between contact and non-contact laser exposure. Relative extensive effects may occur in depth of the tissue when using the free beam. This fact has to be considered by surgeons working with near infrared lasers. The use of the schlieren technique as a model to study the effects of laser energy in tissue was proposed. Fitting the model to histological data (*Chapter 3 Appendix*) yields promising results, indicating that calibration of the model for prostate tissue may be possible. Further investigations and calibration, using thermometry in the schlieren gel, are needed to clarify whether the gel model may serve as a quantitative means for studying laser-tissue interaction in prostate tissue.

Damage extent underneath the carbonized surface in *Chapter 3* is comparable to findings of various contact laser exposure times in other tissues (*Chapter 1, Table 5*). In contact mode, the damage region underneath the exposed surface was largely time-independent (*Chapter 3, Table 2*). It is assumed that at the crater bottom, the rapid vaporization of tissue consumes a significant amount of energy and therefore acts as an important heat-sink, creating a steep temperature gradient and preventing deeper thermal damage (Verdaasdonk *et al* 1990). Non-contact laser exposure created more extensive tissue coagulation, depending on exposure time and laser power.

Chapter 3 provides a description of static acute damage threshold temperature for short duration laser exposure, not depending on exposure duration within this short time interval (<30 s). This is supported by the Arrhenius damage theory, and by the experimentally-determined damage threshold temperature for canine prostate tissue. The experimentally-determined short-term damage threshold temperature can not be used to obtain Arrhenius parameters for the canine prostate, since tissue damage needs to be measured over longer exposure times to obtain an acceptable accuracy of the kinetic parameters (Pearce and Thomsen 1995, Diller and Pearce 1999).

The subcapsular partial prostatectomy technique described in *Chapter 4* succeeded in preserving postoperative urinary continence, except for 2 dogs in which severe preoperative dysuria and stranguria persisted postoperatively. One dog had severe complications of a systemic kind, possibly of paraneoplastic origin. These 3 cases point out that preoperative staging of the disease may be important for clinical outcome and prognosis. In other cases treatment resulted in adequate palliation or even resolved clinical signs. A recent study randomly compared total prostatectomy (TP, n=10) with subcapsular partial prostatectomy (SPP, n=11), as described by Robertson and Bojrab (1984), for prostate carcinoma in dogs

(Vlasin *et al* 2006). Survival of the SPP group (112 ± 63 days (mean ± sd)) is comparable with the results of our study, and was dramatically better than that of TP (survival: 20 ± 11 days). Likewise, SPP was palliative and no significant urinary incontinence or other complications were present after surgery. In contrast, TP resulted in severe postoperative complications in 3 dogs and there was considerable morbidity in all other dogs (urinary incontinence, stranguria, dyschezia). Exact data about individual complication rates were not given, and therefore it is not clear whether these complications represent a failure of the technique. However, these results support the conclusion of *Chapter 4* that SPP can be used as a palliative treatment of PCA.

As for Nd:YAG laser surgery, the histological findings in normal dogs (*Chaper 4, Appendix*) and clinical findings in PCA patients were consistent with the damage margins as determined in *Chapter 3*: typically < 1 mm thermal damage in contact mode tissue resection, and occasionally deeper necrosis in free beam laser use for hemostasis and probably also from increased exposure time at some points during surgery, denoting the importance of a dedicated surgical technique. Furthermore, the urethra and prostate capsule were spared, indicating that Nd:YAG laser surgery is capable of precise surgery in prostate parenchyma with adequate hemostasis, with the known exception of vessels > 2 mm in diameter. Recently, a pilot study was performed in 5 men with prostate carcinoma in which the neurovascular bundles were dissected from the prostate using a Nd:YAG laser in contact mode in laparoscopic radical prostatectomy (Gianduzzo *et al* 2007). The neurovascular bundles were subsequently excised for histological investigation, which showed a mean maximal depth of thermal necrosis of 615 μm (range: 182-1400 μm). Mean surgery time and blood loss seemed to be less compared to conventional laparoscopic prostatectomies and ease of surgery and hemostasis were promising (Gianduzzo *et al* 2007). These findings confirm that the Nd:YAG laser is useful for delicate tissue dissection during nerve-sparing prostatectomy.

Nd:YAG laser-assisted laparoscopic ovariectomy (lapOVE) in dogs and cats, as described in *Chapters 5, 6 and 7* was successful. An excellent working space could be created using relatively low intra-abdominal pressures, giving a better view and access to the abdominal organs and a better control of pedicle bleeding compared to the common approach by open celiotomy. Besides the required exchange of instruments when blood vessels of > 2 mm in diameter were encountered during laser ovariectomy, an additional cause of increased surgery duration of the Nd:YAG laser compared to bipolar electrosurgical techniques was the time needed for initial charring of the fiber tip, especially in cats and in dogs with a high FatScore of the ovarian pedicle. Since a clean tip was used in every new surgery for the removal of only one ovary (*Chapters 6 and 7*), this initial charring time is an important cause of increased OVE duration. If the laser would be used for procedures of longer

duration, this effect would probably diminish. In **Chapter 5**, the laser was useful but had no essential benefits over the lapOVE procedure with the standard bipolar electro surgery (BEC) forceps and scissors. The Remorgida forceps, a relatively cost-effective dual purpose device, further shortened surgery duration and increased the ease of surgery, although the coagulation ability was somewhat less compared to the BEC method, as discussed in **Chapter 6**. As the lapOVE technique in dogs was further optimized and established as a reliable routine technique (*chapters 5 and 6*), the next step was evaluation in a smaller species: the cat (**chapter 7**). LapOVE in cats requires a more delicate approach (i.e. smaller size instruments and careful intra-abdominal pressure management). The Nd:YAG laser performed very well in laparoscopic ovariectomy in cats and pneumoperitoneum was maintained at 4 mmHg CO_2 pressure. The overall technique and outcome were very satisfying.

Devices that produce rapid and reliable hemostasis are an important prerequisite for laparoscopic surgery. The Nd:YAG surgical laser has no significant advantage over bipolar techniques in lapOVE in dogs and cats. An important reason for this is that the procedure lends itself for a 'grasping forceps-approach': The pedicle structure can easily be grabbed and coagulated with the same instrument. Furthermore, it is concluded that bipolar devices are superior in vessel sealing in laparoscopy and are an invaluable tool in minimally invasive procedures. The Remorgida forceps compared favorably to the other techniques in dogs in terms of surgery duration and ease of use (because of its dual function) and can serve as a relatively low-cost high-end solution in lapOVE. A rather thorough discussion on the use of the bipolar forceps in lapOVE and its advantages was presented in **Chapter 6**. An additional comment is that recently several studies have reported that bipolar vessel sealing accomplishes arterial bursting pressures comparable to those after te use of vascular clips or ligatures, which can be more than twice the bursting-pressure values of monopolar electrocautery and ultrasonic devices (Harold *et al* 2003, Bubenik *et al* 2005, Klingler *et al* 2006, Vassiliades *et al* 2007). Furthermore, bipolar devices are capable of sealing larger diameter vessels and provide better hemostasis. It seems that when it comes to large vessel sealing, the relatively sophisticated (and more expensive) pulsed, impedance-controlled laparoscopic bipolar devices with simultaneous sharp excision (high-tech variations of the Remorgida technique) are becoming increasingly popular (Takada *et al* 2005, Entezari *et al* 2007, Eroglu *et al* 2007, Guerrieri *et al* 2007, Hruby *et al* 2007, Mayhew and Brown 2007, Tepetes *et al* 2007, Wallwiener *et al* 2007).

In contrast to our findings for the ovarian pedicle, (laparoscopic) surgery of larger structures that can not be readily grabbed to be resected but have to be incised in a 'knife-like' manner, may benefit from the use of the Nd:YAG laser, as was observed in prostate surgery (*Chapter 4*). This also applies to ovarian pedicles with high FatScore, in which

laser dissection was easier than the use of Remorgida in *Chapter 6*. The laser was very useful to dissect large ovarian pedicles and adipose tissue seemed to melt away, exposing the blood vessels to be coagulated using the bipolar forceps. Furthermore, combined with BEC or other vessel sealing device for larger vessels, the laser can be of value in laparoscopic surgery, improving overall hemostasis and ease of surgery and reducing thermal damage spread. This is also advocated by others (Johnson *et al* 1992, Jeganathan 2003, Hecher *et al* 2006, Diehl and Hecher 2007, Gianduzzo *et al* 2007), although research in this area is sparse (Lanzafame 2001).

Conclusion

The fiber-guided Nd:YAG laser can be used for tissue coagulation as well as incisional surgery. The dynamic color schlieren technique visualizes temperature distribution of non-contact and contact Nd:YAG laser irradiation in a polyacrylamide tissue model. It clearly denotes the difference in temperature distribution between contact and non-contact laser exposure. A polyacrylamide schlieren gel, containing 9 mg/ml $CuSO_4$, can be used to model the shape of Nd:YAG laser-induced temperature distribution for canine prostate tissue for up to 20 s exposure. The schlieren temperature-distribution images coincide well with histological findings of non-contact laser-induced thermal damage in *ex vivo* canine prostate tissue, in which the 6th schlieren line coincides with the histological damage margin.

Temperature measurements during laser exposure of tissue need to be corrected for an artefact caused by direct heating of the thermocouple probes.

The Arrhenius parameters of burn wounds in pig skin (Henriques 1947) are not suitable to describe thermal damage after less than 20 s in canine prostate tissue. Furthermore, existing Arrhenius parameters are only valid for the temperature range and duration in which they were determined.

Acute thermal tissue damage is considered to be governed by a constant threshold temperature during short exposure (<<1 min). Under this assumption, threshold temperature is independent of duration in short term heating. An acute damage threshold temperature was determined *in vitro* for canine prostate tissue (T=69 $\pm$ 6 ^{o}C). The extent of tissue damage during contact mode surgery is generally 0.9 $\pm$ 0.6 mm or less underneath the surface, but the non-contact technique can produce deeper thermal coagulation, depending on laser power and exposure time.

In dogs with PCA, partial prostatectomy facilitated by Nd:YAG laser dissection and accompanied by adjuvant treatment can be considered as a palliative treatment that can provide resolution of clinical signs for at least several months postoperatively. Furthermore, urinary continence was preserved. Histological findings of *in vivo* laser surgery of the canine prostate were consistent with results of *in vitro* acute thermal tissue-damage investigation. It is concluded that the Nd:YAG laser is capable of relatively precise prostate tissue resection with acceptable thermal damage margins of < 1 mm. The laser can therefore be used for canine subcapsular partial prostatectomy, leaving prostate capsule and urethra intact and preserving urinary continence.

Duration of lapOVE is mainly determined by technique and instrumentation, the amount of fat in the ovarian ligament, and the experience of the surgeon. Although Laser-OVE is challenging, the use of laser did not have a significant advantage over BEC-OVE in laparoscopic OVE. The main reason for this is that blood vessels of > 2 mm in diameter can not be properly coagulated with the laser, and BEC forceps are still needed to prevent mesovarial hemorrhage. Although hemorrhage is best prevented using the BEC-forceps in Laser-OVE, the Remorgida forceps reduces surgical time, is not associated with an increased complication rate, produces less fume, and can be used as a stand-alone device in ovariectomy. Furthermore, it is associated with lower costs and safety requirements compared with laser surgery. Thus, the Remorgida forceps is seemingly a more suitable device for canine lapOVE. However, the laser technique combined with BEC resulted in less hemorrhage and under certain circumstances (i.e. large pedicles containing much adipose tissue) the laser performed better than Remorgida forceps. In all lapOVE studies, laser surgery took more time (~2 min) than bipolar electrosurgery. In the dog, laser excision was typically slower for the left ovary compared to BEC. Obesity significantly increases surgery duration in dogs, but not in cats because of the small amount of adipose tissue in the ovarian ligament of cats.

The Nd:YAG laser performed well in feline lapOVE. No major difficulties or complications were encountered during or after surgery. In fact, low-pressure pneumoperitoneum, easy manipulation of the ovaries and a minimal amount of fat in the ovarian ligament facilitated excellent surgical access and outcome. Furthermore, convalescence time was short and owner satisfaction was high. The laser was effective but did not significantly improve the feline lapOVE procedure or outcomes.

The overall conclusion is that the Nd:YAG laser is useful for precise open and laparoscopic soft tissue incisional surgery, with minimal accompanying thermal tissue damage and adequate hemostasis, except for blood vessels of > 2 mm in diameter which are best coagulated using bipolar forceps.

Samenvatting

De interactie tussen Nd:YAG laser en weefsel werd onderzocht *in vitro*, voorafgaand aan *in vivo* gebruik van de laser bij prostaat chirurgie en laparoscopie van de hond en kat. De verdeling van door laser geïnduceerde temperatuurstijging en schade werd onderzocht in *ex vivo* prostaatweefsel van de hond. Hiermee werden de moeilijkheden en onzekerheden van theoretische modellering van licht en warmte omzeild, met betrekking tot de grote variatie in experimenteel bepaalde optische eigenschappen van prostaatweefsel van de hond (***Hoofdstuk 1**, Tabel 2*). Ondanks dat prostaatweefsel (zowel van de mens als van de hond) een van de meest bestudeerde en gemodelleerde weefsels is met betrekking tot door laser geïnduceerde temperatuur- en schadeverdeling, zijn er nooit specifieke Arrheniusparameters of een acute schadetemperatuur bepaald bij de hondenprostaat. Recentelijk zijn Arrheniusparameters bepaald van humaan prostaatweefsel afkomstig van mannen met benigne prostaathyperplasie (BPH) (Bhowmick *et al* 2004). De enige experimenteel bepaalde Arrheniusparameters bij normaal prostaatweefsel zijn niet van hondenorigine maar van de rat ((Skinner et al 2000), zie ook *Hoofdstuk 1, Sectie 4.2*). Modellen voor temperatuur-geïnduceerde schade van prostaatweefsel maken meestal gebruik van Arrheniusparameters van andere weefsels, zoals de huid. Een onderzoek vergeleek de berekende prostaatweefselschade door thermotherapie met Arrheniusparameters van varkenshuid (Henriques 1947) en van BPH-weefsel (Bhowmick *et al* 2004); er werden vergelijkbare reultaten verkregen (Huidobro *et al* 2004). De relaties tussen temperatuur en tijd van deze Arrheniusparameters zijn weergegeven in *Hoofdstuk 1, Figuur 8*. De meest waarschijnlijke verklaring voor het verkrijgen van vergelijkbare resultaten is dat de toegepaste duur van blootstelling aan verhoogde temperatuur in de orde van grootte van 10 minutes was, aangezien de grafieken van deze Arrheniusparameters elkaar snijden rond deze tijdsduur (*Hoofdstuk 1, Figuur 8*). Bovendien lijken de meeste Arrheniusrelaties vergelijkbare schadetemperaturen te voorspellen in het gebied van 10-20 minuten (*Hoofdstuk 1, Figuur 8*). Dit verklaart dat Arrheniusparameters van verschillende weefsels met succes konden worden gebruikt in modellen van door laser geïnduceerde thermotherapie (LITT) voor zowel prostaat- als leverweefsel (Prapavat *et al* 1996, Bolmsjo *et al* 1998, Sturesson 1998, Huidobro *et al* 2004). Dit roept de vraag op hoeveel invloed de Arrheniusparameters hebben in deze weefselschademodellen bij een blootstelling van >10 minuten. Op vergelijkbare wijze wordt in verschillende prostaat-LITT studies met MRI thermometrie gebruik gemaakt van een iso-effect thermische dosisberekening (een benadering van de Arrhenius-weefselschadeintegraal) om de schadegrenzen te bepalen. Deze berekening levert een schadegrenstemperatuur op van 50-52°C, die goed overeenkomt

met histologische bevindingen (Peters *et al* 2000, Diederich *et al* 2004, Nau *et al* 2005, Pauly *et al* 2006), bij een typische blootstellingsduur van 10-20 minuten. Het moge duidelijk zijn uit *Figuur 8 in Hoofdstuk 1* dat bij kortere blootstellingsduur de schadegrenstemperaturen van verschillende weefsels zullen verschillen en modellen zullen dan ook naar verwachting verschillende uitkomsten geven. De modellering van temperatuur-geïnduceerde weefselschade is een jonge en in ontwikkeling zijnde tak van wetenschap en ondanks dat de Arrheniustheorie waardevol is om het proces van thermische weefselschade te beschrijven, zal toekomstig onderzoek moeten uitwijzen of er daadwerkelijk een valide biofysische/chemische interpretatie van mogelijk is.

De schlierentechniek, zoals beschreven in **Hoofdstuk 2**, was nuttig om kwalitatieve verschillen tussen contact- en non-contact laserbehandeling te kunnen interpreteren. Relatief uitgebreide effecten kunnen optreden in de diepte in weefsels tijdens non-contact laserbehandeling. Chirurgen die gebruik maken van lasers met golflengtes die richting infrarood gaan (800-1100 nm) moeten hiermee rekening houden. De schlierentechniek werd geïntroduceerd als model om door laser geïnduceerde effecten in weefsel te bestuderen. Vergelijking van het model met histologische bevindingen (*Hoofdstuk 3, Appendix*) leverde veelbelovende resultaten op en gaf aan dat calibratie van het model voor weefsel mogelijk is. Verder onderzoek en calibratie, met behulp van temperatuurmetingen in de gel, zal nodig zijn om te bepalen of het gel-model daadwerkelijk in kwantitatieve zin gebruikt kan worden.

De uitbreiding van weefselschade onder het gecarboniseerde weefseloppervlak in **Hoofdstuk 3** is vergelijkbaar met de bevindingen bij blootstelling aan contact-mode gedurende verschillende tijdsduren in diverse weefsels (*Hoofdstuk 1, Tabel 5*). Het weefselschadegebied onder het behandelde weefseloppervlak tijdens contact-mode laserbestraling is grotendeels tijdsonafhankelijk (*Hoofdstuk 3, Tabel 2*). Aangenomen wordt, dat de snelle vaporisatie van weefsel op de bodem van de gevormde krater een significant deel van de laserenergie verbruikt en daardoor als belangrijke warmteafvoer fungeert, daarbij een steile temperatuurgradiënt creërend die diepere weefselschade voorkomt (Verdaasdonk *et al* 1990). Non-contact laserbestraling veroorzaakte uitgebreidere weefselcoagulatie, afhankelijk van tijdsduur en laservermogen.

Hoofdstuk 3 geeft een beschrijving van een constante grenstemperatuur voor het ontstaan van acute weefselschade bij korte lasertijden. Deze grenstemperatuur is niet afhankelijk van blootstellingstijd binnen dit korte interval (<30 s). Dit wordt ondersteund door de Arrhenius weefselschadetheorie en door de experimenteel verkregen resultaten van de grenstemperatuur voor acute schade in prostaatweefsel van de hond. De resultaten bij korte lasertijden kunnen niet gebruikt worden om Arheniusparameters voor hondenprostaatweefsel te berekenen omdat voor het verkrijgen van parameters met

acceptabele significantie metingen over een veel groter tijdsinterval nodig zijn (Pearce en Thomsen 1995, Diller and Pearce 1999).

De subkapsulaire partiële prostatectomie-techniek beschreven in ***Hoofdstuk 4*** resulteerde in behoud van urinecontinentie na operatie, behalve bij 2 honden waarbij een aanzienlijke preoperatieve dysurie en strangurie persisteerden na operatie. Eén hond had ernstige complicaties van systemische aard, mogelijk van paraneoplastische oorsprong. Deze 3 gevallen wijzen op het mogelijk belang van een goede preoperatieve stagering van de ziekte met betrekking tot te verwachten klinische resultaten en prognose. Een recent gerandomiseerd onderzoek vergeleek totale prostatectomie (TP, n=10) met subkapsulaire partiële prostatectomie (SPP, n=11), zoals beschreven door Robertson en Bojrab (1984), bij honden met prostaatcarcinoom (Vlasin *et al* 2006). De overleving van de SPP-groep (112 ± 63 dagen (gemiddelde ± sd)) is vergelijkbaar met de resultaten uit onze studie en was veel beter dan die na TP (overleving: 20 ± 11 dagen). Ook vergelijkbaar met onze resultaten was het palliatieve effect van SPP en het ontbreken van significante urine incontinentie of andere complicaties postoperatief. Anderzijds resulteerde TP in ernstige postoperatieve complicaties in 3 honden en aanzienlijke morbiditeit is alle andere honden (urine incontinentie, strangurie, dyschezia). Exacte data van individuele complicaties werden niet gegeven waardoor het niet duidelijk is in hoeverre de genoemde complicaties veroorzaakt kunnen zijn door een falende techniek. Desalniettemin ondersteunen de resultaten van dit onderzoek de conclusie van *Hoofdstuk 4* dat SPP kan fungeren als een waardevolle palliatieve therapie voor prostaatcarcinoom.

Aangaande Nd:YAG laserchirurgie zijn de histologische bevindingen in proefhonden (*Hoofdstuk 4, Appendix*) en de klinische bevindingen bij patienten met prostaatcarcinoom vergelijkbaar met de weefselschadegrenzen zoals bepaald in *Hoofdstuk 3*: in het algemeen < 1 mm thermische schade door contact-mode weefselresectie en soms diepere necrose, veroorzaakt door non-contact gebruik voor hemostasis en waarschijnlijk ook door incidenteel langere blootstellingstijd tijdens chirurgie, daarmee het belang aangevend van een optimale chirurgische techniek. Daarnaast werden de urethra en het prostaatkapsel gespaard. Dit wijst erop dat de Nd:YAG laser precieze chirurgie van prostaatparenchym mogelijk maakt met daarbij goede hemostase, met uitzondering van bloedvaten met een diameter van > 2 mm. Recentelijk is er een pilot onderzoek gedaan waarin bij 5 mannen met prostaatcarcinoom de neurovasculaire bundel door middel van contact mode Nd:YAG laserdissectie van de prostaat werd gescheiden tijdens laparoscopische radicale prostatectomie (Gianduzzo *et al* 2007). De neurovasculaire bundels werden daaropvolgend verwijderd en histologisch onderzocht, waarbij een gemiddelde maximale thermische necrosediepte van 615μm werd gevonden (range: 182-1400 μm). Gemiddelde operatietijd en bloedverlies leken minder te zijn vergeleken bij de conventionele laparoscopische

prostatectomie en het gebruiksgemak en hemostase waren veelbelovend (Gianduzzo *et al* 2007). Dat de Nd:YAG laser nuttig is voor delicate weefseldissectie bij zenuwsparende prostatectomie wordt door deze bevindingen ondersteund.

De Nd:YAG laser werd met succes gebruikt voor laparoscopische ovariectomie (lapOVE) bij honden en katten, zoals beschreven in *Hoofdstukken 5, 6 en 7*. Er kon een uitstekend werkveld worden gecreëerd met relatief lage intraabdominale CO_2-drukken, waarbij een beter zicht en toegang tot de buikorganen en een betere controle op bloedingen werden gerealiseerd vergeleken met de algemeen toegepaste benadering via open celiotomie. Naast de benodigde extra uitwisseling van instrumenten ten behoeve van bloedvaten met een diameter van > 2 mm, was er nog een oorzaak voor verlengde operatietijd met laser in vergelijking met de bipolaire elektrocoagulatie(BEC)-technieken: de tijd die nodig was voor de initiële zwarting van de fibertip, met name bij katten en bij honden met veel vet in het mesovarium. Omdat er bij de verwijdering van ieder ovarium met een schone tip werd gestart (*Hoofdstukken 6 en 7*) is de initiele carbonisatietijd een belangrijke tijdverslindende factor tijdens ovariectomie. Bij gebruik van de laser voor langduriger procedures zou dit vertragende effect waarschijnlijk verdwijnen. De laser was goed bruikbaar maar had geen essentiële voordelen bij lapOVE ten opzichte van de BEC-methode en de endoscopische schaar in *Hoofdstuk 5*. De relatief goedkope Remorgida-tang met dubbele functie zorgde voor een verdere verkorting van de operatieduur en had een groter gebruiksgemak, waarbij de kwaliteit van coagulatie echter minder goed was dan die van de standaard BEC-tang, zoals besproken werd in *Hoofdstuk 6*. Terwijl de lapOVE-techniek in honden verder geoptimaliseerd werd tot een betrouwbare routine techniek, was de volgende stap de evaluatie van deze techniek in een kleinere diersoort: de kat (*Hoofdstuk 7*). LapOVE in katten vereist een meer delicate aanpak (zoals het gebruik van kleinere instrumenten en een goed gecontroleerde intraabdominale druk). De Nd:YAG laser was heel goed bruikbaar bij de lapOVE bij de kat en het pneumoperitoneum kon worden gehandhaafd met een druk van 4 mmHg. De algehele techniek en resultaten stelden zeer tevreden.

Instrumenten die snel en betrouwbaar weefsel en vaten kunnen coaguleren zijn een belangrijke voorwaarde voor laparoscopische chirurgie. De Nd:YAG laser toonde geen belangrijke voordelen ten opzichte van bipolaire technieken bij lapOVE bij honden en katten. Een belangrijke reden hiervoor is dat de betreffende procedure zich heel goed leent voor het gebruik van een 'paktang': Het mesovarium met haar bloedvaten kan gemakkelijk worden beetgepakt om te worden gecoaguleerd. Daarnaast moet worden geconcludeerd dat bipolaire instrumenten superieur zijn met betrekking tot het afsluiten van vaten in de laparoscopie en daarom zeer waardevol zijn voor de minimaal invasieve chirurgie. De Remorgida-tang was sneller en makkelijker in gebruik (door de dubbele functie) en kan gezien worden als een relatief goedkope high-end oplossing voor lapOVE. Een vrij

uitgebreide discussie over het gebruik van de bipolaire tangen en hun voordelen bij lapOVE werd gevoerd in ***Hoofdstuk 6***. Als aanvulling hierop kan genoemd worden dat verschillende recente studies melden dat bipolair afgesloten arteriën even hoge intraluminale hydrostatische drukken aankunnen als vaten die zijn afgesloten met vaat-clips of ligaturen. Deze drukken zijn meer dan twee keer zo hoog als bij vaten die afgesloten zijn met behulp van monopolaire elektrocoagulatie of ultrasone instrumenten (Harold *et al* 2003, Bubenik *et al* 2005, Klingler *et al* 2006, Vassiliades *et al* 2007). Daarnaast zijn bipolaire tangen in staat om grotere vaten dicht te coaguleren en betere hemostase te bieden. Als het gaat om het afsluiten van relatief grote vaten lijkt het zo te zijn dat de geavanceerde (en duurdere) gepulste, impedance-controlled laparoscopische bipolaire instrumenten met de mogelijkheid tot simultane scherpe incisie (high-end variaties op de Remorgida techniek) in populariteit toenemen (Takada *et al* 2005, Entezari *et al* 2007, Eroglu *et al* 2007, Guerrieri *et al* 2007, Hruby *et al* 2007, Mayhew and Brown 2007, Tepetes *et al* 2007, Wallwiener *et al* 2007).

In tegenstelling tot onze bevindingen bij het mesovarium kan (laparoscopische) chirurgie van grotere structuren die niet goed gegrepen kunnen worden met een paktang maar in- of uitgesneden dienen te worden, baat hebben bij het gebruik van de Nd:YAG laser, zoals dat het geval is bij de subkapsulaire partiële prostatectomie in *Hoofdstuk 4*. Dit geldt ook voor mesovaria die veel vetweefsel bevatten (hoge FatScore). Hierbij was laserdissectie gemakkelijker dan het gebruik van de Remorgida-tang (*Hoofdstuk 6*). De laser was erg nuttig bij de dissectie van grote (vette) mesovaria, waarbij het vet leek weg te smelten waardoor de vaten zichtbaar werden die daarna met een bipolaire tang gecoaguleerd konden worden. Bovendien kan de laser, in combinatie met een bipolair instrument voor grotere vaten, waardevol zijn voor laparoscopische chirurgie, waardoor de algehele hemostase en chirurgische techniek wordt verbeterd en ongewenste verspreiding van thermische schade kan worden beperkt. Dit wordt ook door anderen beschreven (Johnson *et al* 1992, Jeganathan 2003, Hecher *et al* 2006, Diehl and Hecher 2007, Gianduzzo *et al* 2007), zij het dat er weinig onderzoek plaatsvindt in deze richting (Lanzafame 2001).

Conclusie

De Nd:YAG laser met flexibele fiber kan gebruikt worden voor zowel weefselcoagulatie als voor weefseldissectie. De dynamische kleuren-schlierentechniek kan de temperatuurverdeling van non-contact en contact-mode laserbestraling in een

polyacrylamide weefselmodel zichtbaar maken. Daarbij komt het verschil in temperatuurverdeling tussen contact- en non-contact laserblootstelling zeer duidelijk tot uiting. Een polyacrylamide schlierengel met daarin 9 mg/ml $CuSO_4$ opgelost, kan worden gebruikt om de vorm van de door Nd:YAG laser geïnduceerde temperatuurverdeling voor prostaatweefsel van de hond te modelleren tot een blootstelling van 20 s. De schlierenbeelden van door non-contact laser geïnduceerde temperatuurverdeling in de gel komen goed overeen met histologische bevindingen van laserschade in *ex vivo* prostaatweefsel, waarbij de 6[e] schlierenlijn de histologische schadegrens benadert.

Temperatuurmetingen tijdens laserbestraling van weefsel bevatten een artefact dat wordt veroorzaakt door directe beïnvloeding van de thermokoppel meetsensoren door de laser. Voor dit artefact moet worden gecorrigeerd.

De Arrheniusparameters voor brandwonden in varkenshuid (Henriques 1947) kunnen niet worden gebruikt om temperatuur-geïnduceerde schade tot 20 s in prostaatweefsel van de hond te beschrijven. Bovendien zijn Arrheniusparameters alleen bruikbaar in het temperatuur- en tijdsgebied waarin ze bepaald zijn.

Acute thermische weefselschade wordt bepaald door een constante grenstemperatuur tijdens korte laserblootstelling (tot 30 s). Onder deze aanname (korte laserduur) is de grenstemperatuur voor weefselschade onafhankelijk van expositietijd. Een grenstemperatuur voor acute weefselschade werd bepaald in *ex vivo* honden prostaatweefsel ($T=69 \pm 6^{o}C$). Tijdens contact-mode laserbehandeling zal de uitbreiding van de weefselschade in de diepte 0.9 ± 0.6 mm of minder zijn, terwijl de weefselschade door non-contact behandeling dieper zal zijn, afhankelijk van laservermogen en tijdsduur.

Bij honden met prostaatcarcinoom kan een partiële prostatectomie door middel van laserdissectie, vergezeld van een adjuvant therapie, worden gezien als een palliatieve therapie die de verschijnselen kan bedwingen gedurende meerdere maanden na de operatie. Histologische bevindingen van *in vivo* laserchirurgie van de hondenprostaat waren vergelijkbaar met resultaten van *ex vivo* acute thermische schade in prostaatweefsel. Nd:YAG laser kan worden gebruikt voor relatief preciese prostaatweefseldissectie met acceptabele bijkomende thermische schademarges van < 1 mm. De laser is daardoor geschikt voor een subkapsulaire partiële prostatectomie bij de hond waarbij urethra en kapsel worden gespaard en urinecontinentie behouden blijft.

De operatieduur van lapOVE wordt voornamelijk bepaald door de gebruikte techniek en instrumentarium, de hoeveelheid vet in het mesovarium en de ervarenheid van de chirurg. Laserchirurgie droeg niet bij aan een significante verbetering van lapOVE ten opzichte van bipolaire elektrochirurgie. De belangrijkste orzaak hiervoor is dat grote bloedvaten (diameter > 2 mm) niet goed gecoaguleerd kunnen worden met de laser, waardoor bipolaire coagulatie nodig blijft ter preventie van mesovariële bloedingen. Behalve dat bloedingen

het beste kunnen worden voorkomen met behulp van een BEC-tang tijdens laser-OVE, zorgt de Remorgida-tang voor een verkorting van de operatieduur, is niet geassocieerd met meer complicaties, veroorzaakt minder rook en kan gebruikt worden als op zichzelf staand instrument voor ovariectomie. Daarnaast is de Remorgida-tang goedkoper in aanschaf en niet geassocieerd met extra veiligheidseisen zoals die voor laserchirurgie gelden. Daarom lijkt de Remorgida-tang een geschikter instrument voor lapOVE bij de hond. Aan de andere kant zorgt de laser gecombineerd met BEC voor minder bloedingen en in bepaalde omstandigheden (zoals grote mesovaria met veel vetweefsel) is de laser beter bruikbaar dan de Remorgida-tang. In alle lapOVE-studies was laserchirurgie iets trager (~2 min) dan bipolaire elektrochirurgie. Bij de hond blijkt de laser met name trager te zijn dan de bipolaire techniek bij de dissectie van het linker ovarium. Obesitas veroorzaakt een significante verlenging van de operatieduur bij honden, maar niet bij katten omdat die in tegenstelling tot de hond weinig vetweefsel in het mesovarium hebben.

De Nd:YAG laser was heel geschikt voor lapOVE bij de kat. Er werden geen moeilijkheden ondervonden tijdens of na de operatie. Bovendien zorgden een lage intraabdominale druk, gemakkelijke manipulatie van de ovaria en een minimale hoeveelheid vetweefsel in de mesovaria voor een optimale chirurgische toegang en resultaten. Daarnaast was de herstelperiode kort en waren de patiënt-eigenaren zeer tevreden met het resultaat. De laser was effectief maar leidde niet tot een significante verbetering van lapOVE bij de kat.

Geconcludeerd kan worden dat de Nd:YAG laser geschikt is voor preciese open en laparoscopische weke delen chirurgie met minimale thermische weefselschade en adequate hemostase, behalve bij vaten van > 2 mm in diameter. Deze kunnen het best worden gecoaguleerd met bipolaire tang.

References

Bhowmick P, Coad J E, Bhowmick S, Pryor J L, Larson T, de la Rosette J and Bischofs J C (2004) In vitro assessment of the efficacy of thermal therapy in human benign prostatic hyperplasia. *Int J Hyperthermia* **4** 421-39

Bolmsjo M, Sturesson C, Wagrell L, Andersson-Engels S and Mattiasson A (1998) Optimizing transurethral microwave thermotherapy: a model for studying power, blood flow, temperature variations and tissue destruction *Br J Urol* **81** 811-6

Bubenik L J, Hosgood G and Vasanjee S C (2005) Bursting tension of medium and large canine arteries sealed with ultrasonic energy or suture ligation *Vet Surg* **34** 289-93

Diederich C J, Stafford R J, Nau W H, Burdette E C, Price R E and Hazle J D (2004) Transurethral ultrasound applicators with directional heating patterns for prostate

thermal therapy: in vivo evaluation using magnetic resonance thermometry *Med Phys* **31** 405-13

Diehl W and Hecher K (2007) Selective cord coagulation in acardiac twins *Semin Fetal Neonatal Med* **12** 458-63

Diller K R and Pearce J A (1999) Issues in modeling thermal alterations in tissues *Ann N Y Acad Sci* **888** 153-64

Entezari K, Hoffmann P, Goris M, Peltier A and Van Velthoven R (2007) A review of currently available vessel sealing systems *Minim Invasive Ther Allied Technol* **16** 52-7

Eroglu A, Turkyilmaz A, Aydin Y, Erdem A F, Tokur M and Karaoglanoglu N (2007) The use of the LigaSure Vessel Sealing System in esophageal cancer surgery *Ann Thorac Surg* **84** 2076-9

Gianduzzo T R, Chang C M, El-Shazly M, Mustajab A, Moon D A and Eden C G (2007) Laser nerve-sparing laparoscopic radical prostatectomy: a feasibility study *BJU Int* **99** 875-9

Guerrieri M, Crosta F, De Sanctis A, Baldarelli M, Lezoche G and Campagnacci R (2007) Use of the electrothermal bipolar vessel system (EBVS) in laparoscopic adrenalectomy: a prospective study *Surg Endosc*

Harold K L, Pollinger H, Matthews B D, Kercher K W, Sing R F and Heniford B T (2003) Comparison of ultrasonic energy, bipolar thermal energy, and vascular clips for the hemostasis of small-, medium-, and large-sized arteries *Surg Endosc* **17** 1228-30

Hecher K, Lewi L, Gratacos E, Huber A, Ville Y and Deprest J (2006) Twin reversed arterial perfusion: fetoscopic laser coagulation of placental anastomoses or the umbilical cord *Ultrasound Obstet Gynecol* **28** 688-91

Henriques F C (1947) Studies of thermal injury V: The predictability and significance of thermally induced rate processes leading to irreversible epidermal injury. *Arch Pathol* **43** 489-502

Hruby G W, Marruffo F C, Durak E, Collins S M, Pierorazio P, Humphrey P A, Mansukhani M M and Landman J (2007) Evaluation of surgical energy devices for vessel sealing and peripheral energy spread in a porcine model *J Urol* **178** 2689-93

Huidobro C, Bolmsjo M, Larson T, de la Rosette J, Wagrell L, Schelin S, Gorecki T and Mattiasson A (2004) Evaluation of microwave thermotherapy with histopathology, magnetic resonance imaging and temperature mapping *J Urol* **171** 672-8

Jeganathan V (2003). Laser in Laparoscopic Cholecystectomy [abstract]. 15th World Congress International Society for Laser Surgery and Medicine (ISLSM), 14th Congress International Nd:YAG Laser Society, and 14th Annual Meeting

Deutsche Gesellschaft für Lasermedizin (DGLMe.V.), Munich, Germany, *Medical Laser Application* **18** 148

Johnson D E, Cromeens D M and Price R E (1992) Use of the holmium:YAG laser in urology *Lasers Surg Med* **12** 353-63

Klingler C H, Remzi M, Marberger M and Janetschek G (2006) Haemostasis in laparoscopy *Eur Urol* **50** 948-56; discussion 56-7

Lanzafame R J (2001) Laser use and research in gastroenterology, gynecology, and general surgery: a status report *J Clin Laser Med Surg* **19** 133-40

Mayhew P D and Brown D C (2007) Comparison of three techniques for ovarian pedicle hemostasis during laparoscopic-assisted ovariohysterectomy *Vet Surg* **36** 541-7

Nau W H, Diederich C J, Ross A B, Butts K, Rieke V, Bouley D M, Gill H, Daniel B and Sommer G (2005) MRI-guided interstitial ultrasound thermal therapy of the prostate: a feasibility study in the canine model *Med Phys* **32** 733-43

Pauly K B, Diederich C J, Rieke V, Bouley D, Chen J, Nau W H, Ross A B, Kinsey A M and Sommer G (2006) Magnetic resonance-guided high-intensity ultrasound ablation of the prostate *Top Magn Reson Imaging* **17** 195-207

Pearce J and Thomsen S (1995) Rate process analysis of thermal damage *Optical-Thermal Response of Laser-Irradiated Tissue* ed A J Welch and M J C van Gemert (New York: Plenum) pp 562-606

Peters R D, Chan E, Trachtenberg J, Jothy S, Kapusta L, Kucharczyk W and Henkelman R M (2000) Magnetic resonance thermometry for predicting thermal damage: an application of interstitial laser coagulation in an in vivo canine prostate model *Magn Reson Med* **44** 873-83

Prapavat V, Roggan A, Walter J, Beuthan J, Klingbeil U and Muller G (1996) In vitro studies and computer simulations to assess the use of a diode laser (850 nm) for laser-induced thermotherapy (LITT) *Lasers Surg Med* **18** 22-33

Robertson J J and Bojrab M J (1984) Subtotal Intracapsular Prostatectomy - Results in Normal Dogs. *Vet Surg* **13** 6-10

Skinner M G, Everts S, Reid A D, Vitkin I A, Lilge L and Sherar M D (2000) Changes in optical properties of ex vivo rat prostate due to heating *Phys Med Biol* **45** 1375-86

Sturesson C (1998) Interstitial laser-induced thermotherapy: influence of carbonization on lesion size *Lasers Surg Med* **22** 51-7

Takada M, Ichihara T and Kuroda Y (2005) Comparative study of electrothermal bipolar vessel sealer and ultrasonic coagulating shears in laparoscopic colectomy *Surg Endosc* **19** 226-8

Tepetes K, Christodoulidis G, Spyridakis E M and Chatzitheofilou C (2007) Tissue preserving hepatectomy by a vessel sealing device *J Surg Oncol*

Vassiliades T A, Jr., Cosgriff N, Denham A, Olson J and Maul D H (2007) Superiority of using bipolar radiofrequency energy for internal mammary artery harvesting *Ann Thorac Surg* **83** 1508-12

Verdaasdonk R M, Borst C and van Gemert M J (1990) Explosive onset of continuous wave laser tissue ablation *Phys Med Biol* **35** 1129-44

Vlasin M, Rauser P, Fichtel T and Necas A (2006) Subtotal intracapsular prostatectomy as a useful treatment for advanced-stage prostatic malignancies *J Small Anim Pract* **47** 512-6

Wallwiener C, Wallwiener M, Neunhoeffer E, Menger M, Isaacson K and Zubke W (2007) Intelligent, impedance-regulated, pulsed coagulation in a porcine renal artery model *Fertil Steril* **88** 206-11

Dankwoord

Ik zou iedereen willen bedanken die heeft bijgedragen aan het tot stand komen van dit proefschrift. Een aantal personen wil ik in het bijzonder bedanken:

Jolle Kirpensteijn, promotor en dagelijks begeleider. Beste Jolle, toen ik voor het eerst bij je aanklopte, op zoek naar een onderwerp voor een Excellent Tracé project, had ik nooit kunnen bedenken dat dit uiteindelijk het gevolg zou zijn. Het is aan jou te danken dat ik dit proefschrift kon schrijven. Je toonde vertrouwen in mijn werk en onze samenwerking was aangenaam en klaarblijkelijk vruchtbaar. Ook jouw vooruitstrevende manier van werken en opgewekte en positieve instelling waren voor mij leerzaam. Al met al ben ik je zeer dankbaar voor alles wat je mij hebt aangereikt en voor je goede zorgen de afgelopen jaren als begeleider en als persoon. Ik zie dan ook de komende jaren als specialist in opleiding met vreugde tegemoet!

Alex Rem, copromotor, klinisch fysicus in opleiding aan het UMC. Beste Alex, ik wil je bedanken voor je inzet en belangstelling en je waardevolle inbreng in het proefschrift. Jij was een onmisbare hulp voor mij bij het bestuderen en doorgronden van onderwerpen met betrekking tot laserinteractie met weefsel en de theoretische achtergronden daarvan en het gebruik van de schlieren opstelling. Verder hoop ik dat onze samenwerking, die ik als heel prettig ervaar, ook in de toekomst nog tot mooie resultaten zal leiden.

Freek van Sluijs, promotor. Beste Freek, bedankt voor je uitermate aandachtig en kritisch doornemen van het hele proefschrift, je nuttige opmerkingen en notities en je inzet en coördinatie bij de afronding van de promotie. Daarnaast bedank ik je voor je vertrouwen in het lopende onderzoek al die tijd en de plezierige samenwerking.

Henry l'Eplattenier, begeleider tijdens het Excellent Tracé en mede-auteur. Beste Henry, bedankt voor alle hulp en inzet en de fijne tijd op de OK. Jouw enthousiasme en kennis en kunde van nieuwe technieken en high-tech chirurgie zijn zeer motiverend voor mij geweest. Ik wens je alvast veel succes met jouw proefschrift!

Ruud Verdaasdonk, hoofd afdeling Klinisch Fysisca van het UMC. Beste Ruud, onze samenwerking heeft mij veel opgeleverd. Van het initiële gebruik van de laser tot mogelijkheden met betrekking tot het onderzoek naar laser-weefsel interactie en het schlieren model. Het heeft mij in staat gesteld mijn wetenschappelijke interesses in het

onderzoek te combineren: high-tech (dier)geneeskunde en chirurgie met een fysische benadering. Verder waren jouw ideeën en opmerkingen vaak aanleiding voor mij om mij verder in de stof te verdiepen en reden om interessante nieuwe dingen uit te proberen en te onderzoeken.

Jaco van der Lugt, veterinair patholoog aan de Faculteit Diergeeskunde. Beste Jaco, ik wil je bedanken voor je hulp bij de evaluatie van laserschade in prostaatweefsel.

Hugo van Oostrom en Tim Zeedijk, mijn paranymfen en goede vrienden, bedankt voor jullie steun tijdens mijn promotie.

Mijn familie en vrienden wil ik bedanken voor hun begrip voor mijn drukke werkzaamheden de afgelopen jaren.

Verder wil ik iedereen bedanken voor ondersteuning van van mijn werkzaamheden:
Harry de Groot (technische ondersteuning van de experimenten); Louis van den Boom, Johan van Amerongen (voor de hulp bij het verkrijgen van prostaatweefsel via pathologie); Arjan de Jager, Christiaan van Swol (UMC Klinische Fysica); Anette van Drie (voor het vervaardigen van prostaatcoupes); Marylene Paes, Carolien Kolijn, Ron van Wandelen en Rob Sap (voor hulp en ondersteuning experimenten op de OK); Rick Mansveld (thermokoppel assemblage, instrumenten werkplaats UMC); Otto van de Beek (FBU instrumenten werkplaats); En alle anderen die niet bij naam genoemd zijn.

Curriculum Vitae

The author was born in Eindhoven, The Netherlands, on August 18th 1977. After attending the 'Vrije School Brabant' in Eindhoven, he finished secondary school one year later (VWO crash course) in 1996. He lived in Leuven for one year to study medicine at the Catholic University of Louvain (1996-1997) but changed his course and studied applied physics at the Eindhoven University of Technology for the next two years (1997-1999). He changed his course again and started his study in veterinary medicine at the Faculty of Veterinary Medicine of the Utrecht University and graduaded in 2006. In 2003-2004 he participated in an Excellent Tracé research program and studied the use of the Nd:YAG laser in prostate surgery and laparoscopic procedures in dogs at the Department of Clinical Sciences of Companion Animals which would be the start of his PhD project resulting in this thesis. The studies on laser-tissue interaction were performed with the help of the Department of Clinical Physics, University Medical Center, Utrecht University. The author completed an internship in companion animal medicine in 2006-2007 and started a residency in small animal surgery in January 2008 at the Department of Clinical Sciences of Companion Animals, Faculty of Veterinary Medicine, Utrecht University.

List of publications

S.A. van Nimwegen, C.F.P. van Swol, J. Kirpensteijn. *Neodymium:Yttrium Aluminum Garnet Surgical Laser Versus Bipolar Electrocoagulation for Laparoscopic Ovariectomy in Dogs.* Veterinary Surgery 34:1–5, 2005

H.F. L'Eplattenier, S.A. van Nimwegen, F.J. van Sluijs, J. Kirpensteijn. Partial prostatectomy using a Nd:YAG laser for management of canine prostate carcinoma. Veterinary Surgery 35(4):406-411, 2006

H.F. L'Eplattenier, B. Klem, E. Teske, F.J. van Sluijs, S.A. van Nimwegen, J. Kirpensteijn. *Preliminary results of intraoperative photodynamic therapy with 5-aminolevulinic acid in dogs with prostate carcinoma.* The Veterinary Journal, accepted September 2007

S.A. van Nimwegen, J. Kirpensteijn. *Comparison of Nd:YAG Surgical Laser and Remorgida Bipolar Electrosurgery Forceps for Canine Laparoscopic Ovariectomy.* Veterinary Surgery 36:533-540, 2007

S.A. van Nimwegen, J. Kirpensteijn. *Laparoscopic ovariectomy in cats: comparison of laser and bipolar electrocoagulation.* Journal of Feline Medicine and Surgery 9:397-403, 2007

Abbreviations

Ablation – Removal of tissue by heat (carbonization/vaporization), not resection.

BEC – Bipolar ElectroCoagulation

CW – Continuous Wave (laser)

Hb – Hemoglobin

HE – Hematoxylin & Eosin

LapOVE – laparoscopic Ovariectomy

LITT – Laser Interstitial ThermoTherapy/Laser Induced ThermoTherapy

NA – Numeric Aperture

Nd:YAG – Neodymium:Yttrium-Aluminium-Garnet

OVE – ovariectomy

Power density – delivered laser power per unit of area (W/m^2)

Remorgida (Remo) – Remorgida bipolar forceps, featuring simultaneous sharp incision

sd – standard deviation

Ω - tissue damage parameter (see Chapter 1, Section 4)

δ – penetration depth

λ – wavelength (nm)

Φ – fluence rate (W/cm^2)

μ – attenuation coefficient (a: absorption, s: scattering, s': reduced scattering, eff: effective)

f – frequency (s^{-1})

g – anisotropy factor (see Chapter 1, Section 2)